NASA TECHNICAL MEMORANDUM

NASA TM X- 71974

COPY NO.

NASA TM X-71974

LOW-SPEED AERODYNAMIC CHARACTERISTICS OF A HYPERSONIC RESEARCH AIRPLANE CONCEPT HAVING A 70° SWEPT DELTA WING

By

Theodore R. Creel, Jr. and Jim A. Penland

August 1974

NATIONAL AERONAUTICS AND SPACE ADMINISTRATION

LANGLEY RESEARCH CENTER, HAMPTON, VIRGINIA 23665

1. Report No.	2. Government Accession No.	3. Recipient's Catalog No.
NASA TM X-71974		

4. Title and Subtitle	5. Report Date
LOW-SPEED AERODYNAMIC CHARACTERISTICS OF A HYPERSONIC RESEARCH AIRPLANE CONCEPT HAVING A 70° SWEPT DELTA WING	August 1974
	6. Performing Organization Code

7. Author(s)	8. Performing Organization Report No.
Theodore R. Creel, Jr. and Jim A. Penland	
	10. Work Unit No.

9. Performing Organization Name and Address	11. Contract or Grant No.
Aerodynamics and Heat Transfer Section NASA-Langley Research Center Hampton, VA 23666	
	13. Type of Report and Period Covered
12. Sponsoring Agency Name and Address	Technical Memorandum
National Aeronautics and Space Administration Washington, D. C. 20546	14. Sponsoring Agency Code

15. Supplementary Notes

Special technical information release, not planned for formal NASA publication.

16. Abstract

An experimental investigation of the low-speed static longitudinal, lateral and directional stability characteristics of a hypersonic research airplane concept having a 70° swept delta wing was conducted in a low-speed tunnel with a 12-foot (3.66 meter) octagonal test section at the Langley Research Center. Aircraft component variations included: fuselage shape modifications, tip fins, center vertical fin, wing camber, and wing planform. This investigation was conducted at a dynamic pressure of 262.4 Pa (5.48 psf), a Mach number of 0.06, and a Reynolds number of 2.24×10^6, based on body length. Tests were conducted through an angle-of-attack range of 0° to 30° with elevon deflections from +5.0° to -30.0°.

The complete configuration exhibited positive static longitudinal, lateral and directional stability up to angles of attack of at least 20° and was trimmable to lift coefficients of at least 0.70 with elevon deflections of -30°.

17. Key Words (Suggested by Author(s)) (STAR category underlined)	18. Distribution Statement
Hypersonic Aircraft Low-speed stability Lift	Unclassified - Limited

19. Security Classif. (of this report)	20. Security Classif. (of this page)	21. No. of Pages	22. Price*
Unclassified	Unclassified	76	$4.00

*Available from { The National Technical Information Service, Springfield, Virginia 22151 / STIF/NASA Scientific and Technical Information Facility, P.O. Box 33, College Park, MD 20740

LOW-SPEED AERODYNAMIC CHARACTERISTICS OF A HYPERSONIC RESEARCH AIRPLANE CONCEPT HAVING A 70° SWEPT DELTA WING

by
Theodore R. Creel, Jr. and Jim A. Penland

SUMMARY

An experimental investigation of the low-speed static longitudinal, lateral and directional stability characteristics of a hypersonic research airplane concept having a 70° swept delta wing was conducted in a low-speed tunnel with a 12-foot (3.66 meter) octagonal test section at the Langley Research Center. Aircraft component variations included: fuselage shape modifications, tip fins, center vertical fin, wing camber, and wing planform. This investigation was conducted at a dynamic pressure of 262.4 Pa (5.48 psf), a Mach number of 0.06, and a Reynolds number of 2.24×10^6, based on body length. Tests were conducted through an angle-of-attack range of 0° to 30° with elevon deflections from +5.0° to -30.0°.

The complete configuration exhibited positive static longitudinal, lateral and directional stability up to angles of attack of at least 20° and was trimmable to lift coefficients of at least 0.70 with elevon deflections of -30°.

INTRODUCTION

Airbreathing hypersonic aircraft flying at speeds in excess of Mach 3 and utilizing liquid hydrogen fuel are potentially attractive for use as long-range military attack or defense weapons, low-cost spacecraft launch vehicles, and economic high-speed civilian transportation systems (ref. 1). Technology development is underway to exploit the large energy content of liquid hydrogen fuel with new high-speed power plants and to capitalize on its low pollution effects and high heat-sink capacity (ref. 2). The development of new structures to support the increased air loads under high temperature conditions and to contain the cryogenic liquid fuel is underway as well as a broad program to find optimum aerodynamic shapes. The many systems of liquid hydrogen-fueled aircraft must be proven out and the reliability of the aircraft throughout the speed range must be demonstrated before large-scale funding and construction is begun.

Experience has shown that a research airplane is the most economical method of accomplishing these tasks. The present aircraft configuration is one phase of an extensive study to define the most promising hypersonic research aircraft concept (refs. 3-8). The purpose of this paper is to provide the low-speed aerodynamic characteristics of this large fuselage, delta-wing design to support in-depth system studies that are presently underway.

SYMBOLS

A_r	reference area of wing including fuselage intercept
b	wing span
c.g.	design center of gravity, moment reference
C_D	drag-force coefficient, $F_D'/q_\infty A_r$
C_L	lift-force coefficient, $F_L/q_\infty A_r$
C_{L_α}	rate of change of lift-force coefficient with angle of attack, per deg.
C_l	rolling-moment coefficient, $M_X/q_\infty A_r b$
C_{l_β}	rate of change of rolling-moment coefficient with angle of sideslip, per deg.
C_m	pitching-moment coefficient, $M_Y/q_\infty A_r$
C_{m_o}	pitching-moment coefficient at $\alpha = 0°$
C_{m_α}	rate of change of pitching-moment coefficient with angle of attack, per deg.
$\frac{\partial C_m}{\partial C_L}$	rate of change of pitching-moment coefficient with lift coefficient, longitudinal stability
C_n	yawing-moment coefficient, $M_Z/q_\infty A_r b$
C_{n_β}	rate of change of yawing-moment coefficient with angle of sideslip, per deg.
C_Y	side-force coefficient, $F_Y/q_\infty A_r$
C_{Y_β}	rate of change of side-force coefficient with angle of sideslip, per deg.
F_A	axial force along X-axis; positive direction, -X
F_D'	$F_N \sin\alpha + F_A \cos\alpha$ (=D)

F_L	$F_N \cos \alpha - F_A \sin \alpha$ (= L)
F_N	normal force along Z-axis; positive direction, -Z
F_Y	side force along Y-axis; positive direction, +Y
ℓ	length of model body
L/D	lift-drag ratio, C_L/C_D
M_X, M_Y, M_Z	moments, about X-, Y-, and Z-axes
q_∞	free-stream dynamic pressure
X, Y, Z	reference axes
α	angle of attack, deg.
β	angle of sideslip, deg.
δ	angle of control deflection, deg., positive with trailing edge down

Subscripts:

e	both elevon controls
s	stability axis system
t	trimmed

Model nomenclature:

B	body
E	scramjet engine
F_D	forward delta wing
V_T	tip fins
V_{c1}	center vertical tail, subsonic
V_{c2}	center vertical tail, hypersonic
W_1	wing, positive camber
W_2	wing, negative camber

Subscripts for B, body

1	high profile nose, large base fuselage
2	low profile nose, large base fuselage
3	high profile nose, small base fuselage

low profile nose, small base fuselage

MODELS

The 0.058-scale test model of a winged hypersonic research aircraft is shown (fig. 1) installed in a low-speed tunnel with a 12-foot (3.66 meter) octagonal test section at the Langley Research Center. The model was of modular design, as shown in figure 2, which allowed the build-up of four variations of the basic model (fig. 3) from two nose shapes, two fuselage base shapes, a forward delta, a positively cambered wing leading edge, a negatively cambered wing leading edge and wing tip fins. The model design rationale was primarily based on the stability and control requirements at the design hypersonic cruise Mach number range of 8 to 10. The two nose profiles are the result of different packaging arrangements. The scalloped base shape was designed to accommodate four rocket motors, one on top and three along the bottom of the fuselage base; however, on a small 0.021-scale hypersonic wind tunnel model the scale base proved to be too small to allow installation of a sting-mounted strain gage force balance. The base was, therefore, modified to the large semi-circular shape to accept the force balance, and was tested on the present large 0.058-scale model. The combination of the two nose and two base shapes made possible the four basic fuselage shapes of the present tests (see symbols list for designation). The forward delta was included in the design to help decrease the rearward shift of the aerodynamic center with Mach number. The negatively cambered wing was theoretically shown to markedly increase the C_{m_0} at hypersonic speeds. Wing tip fins were designed with toe-in and located outboard of the fuselage wake to assure directional stability at hypersonic speeds and were interchanged with center vertical tails for the present tests. A streamlined subsonic center vertical tail and a hypersonic wedge-shaped center vertical tail were tested (fig. 3(b)) to assess the difference in directional stability and the effects on trim as compared with the tip fins. Elevons could be deflected from +5° to -30°. A model scramjet engine was also used to complete the model build-up (fig. 3(c)). The models were constructed of fiberglass and wood with all parts screw-attached and dowel-located on the basic wing-fuselage section. The balance was attached to a steel plate inside the wing-fuselage section. The geometric details of the models are shown in figure 3 and tabulated in table I.

APPARATUS AND TESTS

The tests were conducted in a low-speed tunnel with a 12-foot (3.66 meter) octagonal test section at the Langley Research Center at 20.6 m/sec (67.7 ft/sec), a Mach number of 0.06, a Reynolds number of 2.24×10^6, based on body length, and a dynamic pressure of 262.4 Pa (5.48 psf). A six-component strain-gage balance was installed inside the model fuselage. Force and moment data were measured through an angle-of-attack range of 0° to 30° and angles of sideslip of 0° and 5°. All joints and hinge line cracks

were sealed with plastic tape prior to each test run. Base pressure corrections were not made. Moments were reduced about a design center of gravity located 1.30 percent of the body length below the centerline and at a longitudinal station equal to 64.5 percent of the body length. The longitudinal stability data are referred to the stability-axis system and the lateral-directional stability data are referred to the body-axis system, as shown in figure 4.

Due to the very low test Reynolds number of this investigation and the relatively high turbulence factor of the tunnel flow it is not recommended that the drag data be extrapolated to flight Reynolds number. Lift-curve slopes, moments and drag increments due to component variations, however, are considered valid.

INDEX TO DATA FIGURES

Figure

Lateral and directional stability parameters of:

Models: B_1, B_1W_1, $B_1W_1V_T$, $B_1W_1V_{c1}$, $B_1W_1V_{c1}F_D$, $B_1W_1V_{c2}F_D$, $B_1W_1V_TF_D$, $B_1W_1V_TF_DE$ . . . . . 19(a)

Models: B_2, B_2W_1, $B_2W_1V_T$, $B_2W_1V_{c1}$, $B_2W_1V_TE$ . . . . . 19(b)

Models: B_3, B_3W_1, $B_3W_1V_T$, $B_3W_1V_{c1}$, $B_3W_1V_TF_DE$ . . . . . 19(c)

Models: B_4, B_4W_1, $B_4W_1V_T$, $B_4W_1V_{c1}$, $B_4W_1V_TE$ . . . . . 19(d)

RESULTS AND DISCUSSION

Configuration build-up.- The untrimmed longitudinal characteristics of each of the body configurations, alone and with various wing, fin, and engine components attached, are presented in figures 5 to 8. A comparison of the curves of lift coefficient in figures 5(a) to 8(a) shows that configurations equipped with tip fins (V_T) have higher values of lift coefficient (C_L) through the low angle-of-attack range up to about $\alpha \approx 20°$, than those configurations without tip fins or with the center vertical tail (V_{c1}). At angles of attack higher than 20° the opposite appears to be the case, i.e., the configurations without the tip fins and/or with the center vertical tail, have the higher values of lift. This can be understood by considering that the tip fins provide end plate effects at the lower angles of attack, but at the higher angles of attack the toe-in (7.5°) of tip fins contributes to the low pressures over the top surface of the wing and therefore probably to earlier separation or stall.

The addition of the forward delta (F_D) had only a small effect on the lift at the lower angles of attack, but at $\alpha > 20°$ the lift was increased. The installation of the engine module generally decreased the lift as expected due to the increased increment of axial force.

A study of the drag and lift-drag ratio, figures 5(b) to 8(b), shows that generally the B_1W_1 and $B_1W_1V_{c1}$ configurations have the highest values of lift-drag ratio and that the addition of the tip fins, the forward delta, or the engine, all decrease the L/D. This trend, due to tip fin addition, is in variance with results of reference 8 and it appears that the increased drag increment of the tip fins, having a geometric toe-in of 7.5° (2.5° greater than the model of ref. 8), more than offsets the increased lift discussed above.

The longitudinal stability is presented in figures 5(c) to 8(c) and 5(d) to 8(d) in the form of pitching-moment coefficient versus angle of attack and lift coefficient, respectively. All winged configurations exhibit positive longitudinal stability with the body-wing-tip fin models showing the highest degree of stability. The addition of the engine (figures 6(c), 7(c), 8(c), 6(d), 7(d) and 8(d)) did not significantly change the stability except at the highest angles of attack, but did provide a positive increment of pitching moment to all models tested throughout the angle-of-attack range, probably due to increased separation downstream of the engine. The winged models with tip fins exhibited a lower degree of stability due, in part, to loss in lift on the aft portion of the wing in the vicinity of tips due to tip losses. Throughout the angle-of-attack range the forward delta installation decreased the stability to the greatest extent, as might be expected, due to its location forward of the center of gravity.

Trim characteristics. - A total of eight model configurations were tested with various elevon deflections from +5° to -30°, figures 9 to 16. Of these, six were complete airplane configurations, figures 9 to 14, and these were analyzed to determine the aerodynamic trim characteristics presented in figures 17 and 18. Trim data were obtained not only from the faired data curves but also from interpolated results from cross plots of the data and are shown as dashed lines in figures 9 to 14. The trim lift and drag characteristics for the three tip-fin configurations are shown in figure 17(a). The $B_1W_1V_T$ model is shown to have the highest trim lift-drag ratio, but the lowest trim lift range of the models shown. The addition of the forward delta ($B_1W_1V_TF_D$) slightly decreased the trim lift/drag ratio, but made it possible to trim the model to a trim lift coefficient of 0.9, corresponding to an angle of attack of 30° with an elevon deflection of only 18°. The addition of the scramjet engine ($B_1W_1V_TF_DE$) decreased the trim lift/drag ratio considerably, but only decreased the trim lift coefficient to 0.83 at an angle of attack of 25°. Figure 17(b) shows the three tip-fin models to be statically stable longitudinally, but with the stability decreasing to zero at the highest trim lift coefficients. The lift-curve slope also decreased at the higher trim lift coefficients.

The trim lift and drag characteristics for the three center vertical tail test models are presented in figure 18(a). The $B_1W_1V_{C1}$ model is shown to have the highest trim lift-drag ratio of the center vertical models, and also a higher trim lift/drag ratio than that shown for $B_1W_1V_1$ in figure 17(a). A similar trend between trimmed tip-fin and center-tail models was shown in reference 8 to be due to the higher trim drag requirements of the tip-fin models. This higher trim drag occurs as a result of the end plate effect of the tip-fin which tends to improve the overall lift of the wing and increases the nose-down pitching moment due to the aft location of the improved lift; therefore the larger elevon deflections are required for trim. This is substantiated by a comparison of the tip-fin models of figure 17(a) and the center-tail models of figure 18(a) in the region near maximum trimmed lift-drag ratio, which shows that the center-vertical-tail models required 2° to 4°

less elevon deflection for trim. Conversely, at the higher trim lift coefficients (~ 0.9) the tip-fin models trimmed with 3° to 4° less elevon deflection than did the center-tail models. Figure 18(b) shows the trimmed center vertical-tail models to be statically stable longitudinally throughout the 30° angle-of-attack test range, which included trim lift coefficients up to 0.95.

Static Lateral and Directional Stability

The lateral and directional stability of the test configurations with variations due to the addition of various components are presented in figures 19(a) through 19(d), one graph for each body shape.

All bodies alone are shown to have neutral dihedral effect and to be unstable directionally up to about $\alpha = 20°$, with B_3 and B_4 becoming directionally stable at higher angles of attack. The addition of the wing had a negligible effect on the directional stability of all bodies, but the positive dihedral effect was increased, i.e., C_{l_β} was increased negatively, particularly at the lower angles of attack. The addition of either of the vertical tails, V_T, V_{c1}, or V_{c2}, increased the directional stability with the center-tail showing about twice the effectiveness of the tip fins, probably due to decreased tip losses. The wedge airfoil center vertical tail (V_{c2}) was superior to the conventional airfoil (V_{c1}) at angles of attack above 20°. The configuration planform change, by the addition of the forward delta (F_D), generally increased the directional stability. The positive dihedral effect was increased by the addition of either the vertical tails, V_T, V_{c1}, V_{c2} or the forward delta F_D. This is probably due to the location of the majority of vertical tail area above the design center of gravity and the high leading-edge sweep of the forward delta. The addition of the engine module had little effect on the directional stability or the dihedral effect.

CONCLUSIONS

An analysis of the experimental aerodynamic data for a hypersonic research airplane test configuration with various component arrangements at low subsonic speeds and a Reynolds number of 2.24×10^6, based on fuselage length, leads to the following conclusions:

1. The model, when tested with tip fins, had higher values of untrimmed lift coefficient and a higher level of longitudinal stability than when tested either without tip fins or with the center vertical tail at angles of attack less than 20° due to reduction in tip losses.

2. The addition of the forward delta increased the lift as expected, particularly at angles of attack greater than 20°, and decreased the

longitudinal stability due to its forward location ahead of the center of gravity.

3. The addition of the engine module increased the drag, decreased the lift, and provided a positive increment of pitching moment at all angles of attack, probably due to increased separation over the aircraft lower surface downstream of the engine.

4. Pitch-up was exhibited to some degree by all models at angles of attack higher than 20°. Pitch-up was relieved somewhat by use of the center vertical-tails.

5. Complete model arrangements were statically stable longitudinally and were trimmable to lift coefficients of at least 0.70 with elevon deflections up to -30°.

6. Models equipped with the forward delta were trimmable to lift coefficients of about 0.75 at angles of attack of only about 24° with only -20° elevon deflection.

7. Complete model configurations were statically stable directionally and exhibited positive dihedral effect over the test angle-of-attack range.

8. The addition of the forward delta increased the directional stability and increased the positive dihedral effect.

9. The engine addition had a negligible effect on the directional stability and dihedral effect.

REFERENCES

1. Nagel, A. L. and Becker, J. V.: Key Technology for Airbreathing Hypersonic Aircraft. AIAA Paper No. 73-58, Jan. 8-10, Washington, D.C.

2. Escher, W. J. D.: Prospects for Hydrogen as a Fuel for Transportation Systems and for Electrical Power Generation. Oak Ridge National Laboratory, ORNL-TM-4305, Sept. 1972.

3. Anon: Hypersonic Research Facilities Study, Part I - Research Requirement and Ground Facility Synthesis. Vol. II, NASA CR 115323, Oct. 1970.

4. Anon: Hypersonic Research Facilities Study. Phase I - Preliminary Studies. Vol. II, Pt. 2, Flight Vehicle Synthesis. MDC A0013, Contract No. NAS2-5458, McDonnel Aircraft Co., Oct. 1970. (Also available as NASA CR-114324, Oct. 1970.)

5. Anon: Hypersonic Research Facilities Study. Phase II - Parametric Studies. Vol. III, Pt. 2 - Flight Vehicle Synthesis. NASA CR 114326, Oct. 1970.

6. Anon: Hypersonic Research Facilities Study. Phase II - Final Studies. Vol. IV, Pt. 1 - Flight Research Facilities. NASA CR 114327, Oct. 1970.

7. Clark, L. E.: Hypersonic Aerodynamic Characteristics of an All-Body Research Aircraft Configuration. NASA TN D-7358, December 1973.

8. Penland, J. A., Creel, T. R., Jr., and Howard, F. G.: Experimental Low-Speed and Calculated High-Speed Aerodynamic Characteristics of a Hypersonic Research Airplane Concept Having a 65° Swept Delta Wing. NASA TN D-7633, 1974.

TABLE I. - GEOMETRIC CHARACTERISTICS OF MODEL

WING:	
Area, reference, includes fuselage intercept sq. m (sq. in.)	0.3399 (526.85)
Area, exposed, sq. m (sq. in.)	.1827 (283.19)
Area, wetted, sq. m (sq. in.)	.3654 (566.38)
Span, m (in.)	.6076 (23.92)
Aspect ratio	1.086
Root chord, fuselage centerline, m (in.)	.988 (38.9)
Tip chord, m (in.)	.238 (9.372)
Mean aerodynamic chord, m (in.)	.6895 (27.15)
Sweep-back angles, deg.	
Leading edge	70.0
25 percent chord-line	64.0
Trailing edge	0
Taper ratio	.241
Dihedral angle, deg. (airfoil mean-line)	-3.64°
Incidence angle, deg.	0
Airfoil section, (see fig. 3)	
Airfoil thickness ratio	
exposed root	.05
tip	.06
Leading edge radius, m (in.)	
fuselage line chord	7.94×10^{-4} (0.03125)
tip	7.94×10^{-4} (0.03125)
Area elevon, both sq. m (sq. in.)	.0362 (56.148)
FORWARD DELTA:	
Area exposed (outside of fuselage, forward of wing leading edge)	0.0172 (26.608)
Leading-edge sweep	80.0°

TABLE I.-Continued.

TIP FIN:	
Area total, each sq. m (sq. in.)	0.0294 (45.62)
Span, m (in.)	.1933 (7.61)
Aspect ratio	1.27
Taper ratio	.334
Root chord, m (in.)	.243 (9.58)
Tip chord, m (in.)	.0813 (3.2)
Mean aerodynamic chord, m (in.)	.1758 (6.92)
Sweepback angles, deg.	
Leading edge, top	55.0
Leading edge, bottom	71.0
	22.0
Tow-in angle, deg.	7.5
Airfoil section, sharp trailing edge	
Leading-edge radius, m (in.)	7.94×10^{-4} (0.03125)
Rudder:	
Area, sq. m (sq. in.)	.00429 (6.65)
Chord, constant, m (in.)	.0414 (1.63)
SUBSONIC CENTER FIN:	
Area, exposed, sq. m (sq. in.)	0.581 (90.067)
Span, exposed, m (in.)	.2403 (9.46)
Aspect ratio of exposed area	.9936
Taper ratio	.349
Root chord, fuselage surface line, m (in.)	.358 (14.11)
Tip chord, m (in.)	.1252 (4.93)
Mean aerodynamic chord of exposed area, m (in.)	.261 (10.26)
Sweepback angles, deg.	
Leading edge	55.0
Trailing edge	24.6

TABLE I. - Continued.

SUBSONIC CENTER FIN (continued):	
Airfoil section, double wedge	
Thickness ratio	
tip	0.077
root	.074
Leading-edge radius, m (in.)	7.94×10^{-4} (0.03125)
HYPERSONIC CENTER FIN:	
Area, exposed, sq. m (sq. in.)	.0581 (90.067)
Span, exposed, m (in.)	.2403 (9.46)
Aspect ratio of exposed area	.9936
Taper ratio	.349
Root chord, fuselage surface line, m (in.)	.358 (14.11)
Tip chord, m (in.)	.1252 (4.93)
Mean aerodynamic chord of exposed area, m (in.)	.261 (10.26)
Sweepback angles, deg.	
Leading edge	55.0
Trailing edge	24.6
Airfoil section, single wedge	
Thickness ratio	
tip	.1197
root	.1056
Leading-edge radius, m (in.)	7.94×10^{-4}(0.03125)
FUSELAGE: (All four configurations.)	
Length, m (in.)	1.4224 (56)
Maximum height, m (in.)	.1979 (7.79)
Maximum width, m (in.)	.204 (8.04)
Fineness ratio of equivalent round body	6.822

TABLE I. - Concluded.

Base area:	
Small base, sq. m (sq. in.)	0.0155 (24.03)
Large base, sq. m (sq. in.)	.01885 (29.214)
Wetted area, sq. m (sq. in.)	.355 (550.3)
COMPLETE MODEL:	
Area planform, sq. m (sq. in.)	.4044 (626.88)
Aspect ratio of planform	.913

NASA
L-73-4933

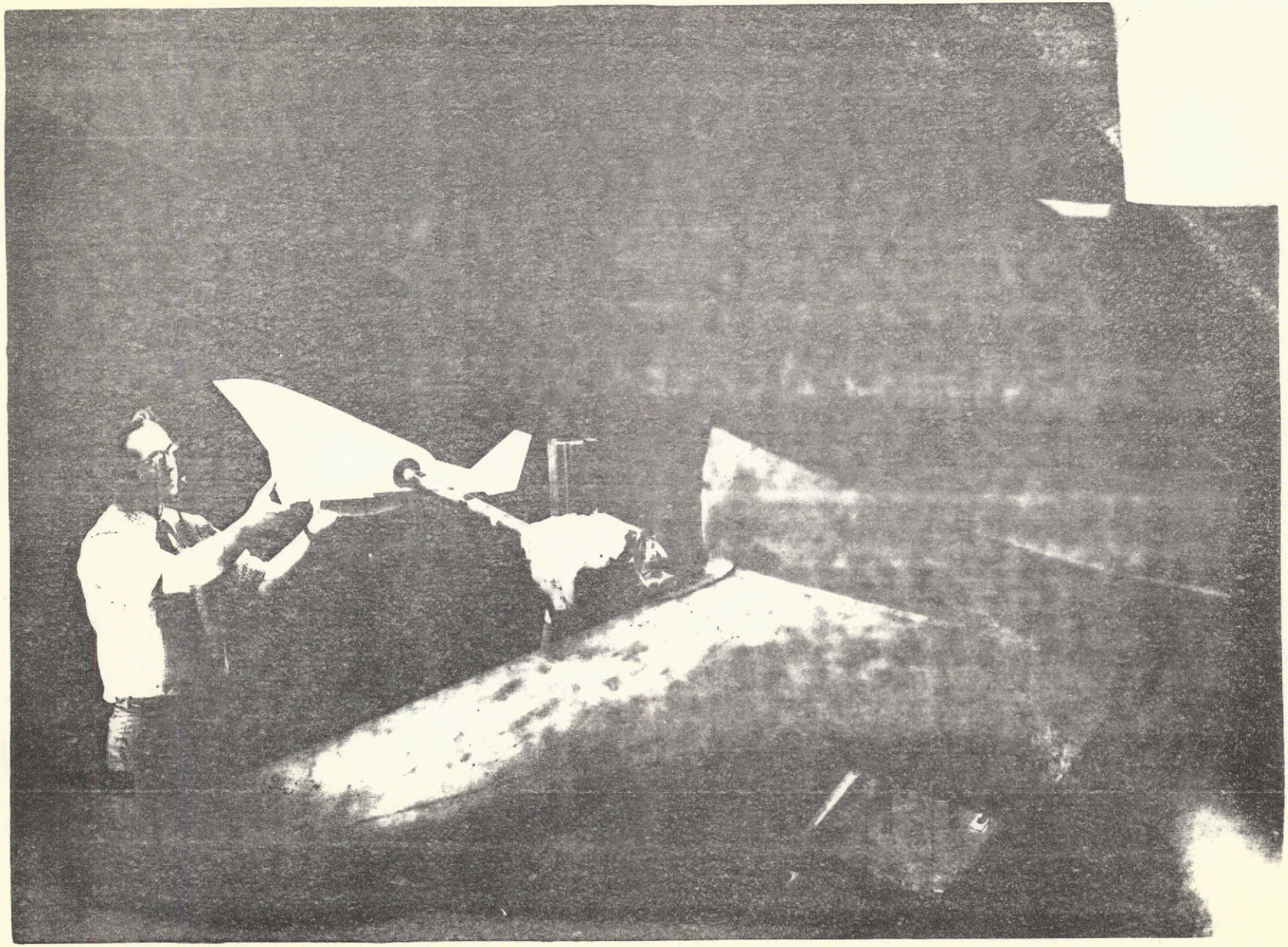

Figure 1. - Photograph of model installed in tunnel.

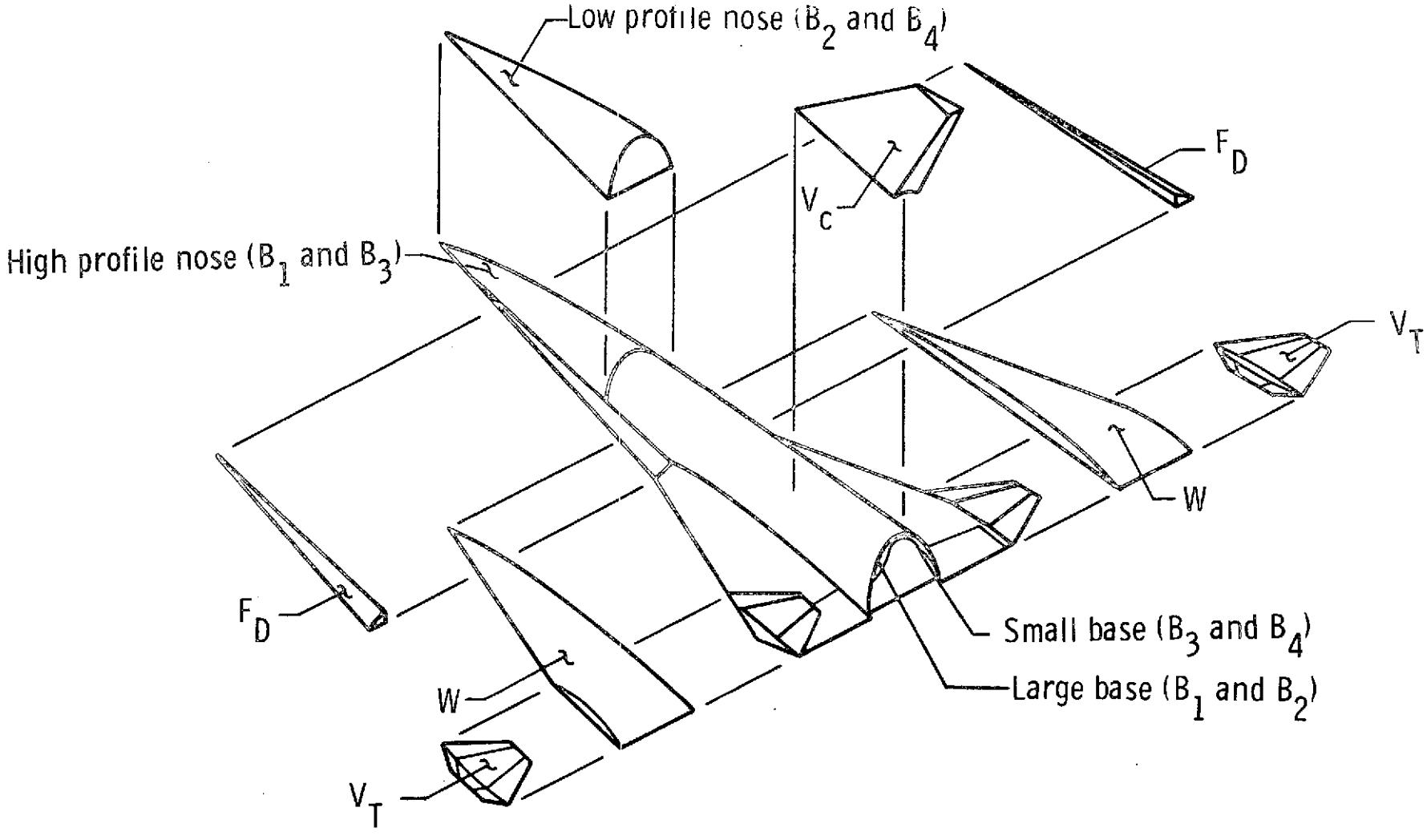

Figure 2.- Sketch of model used, showing interchangable parts.

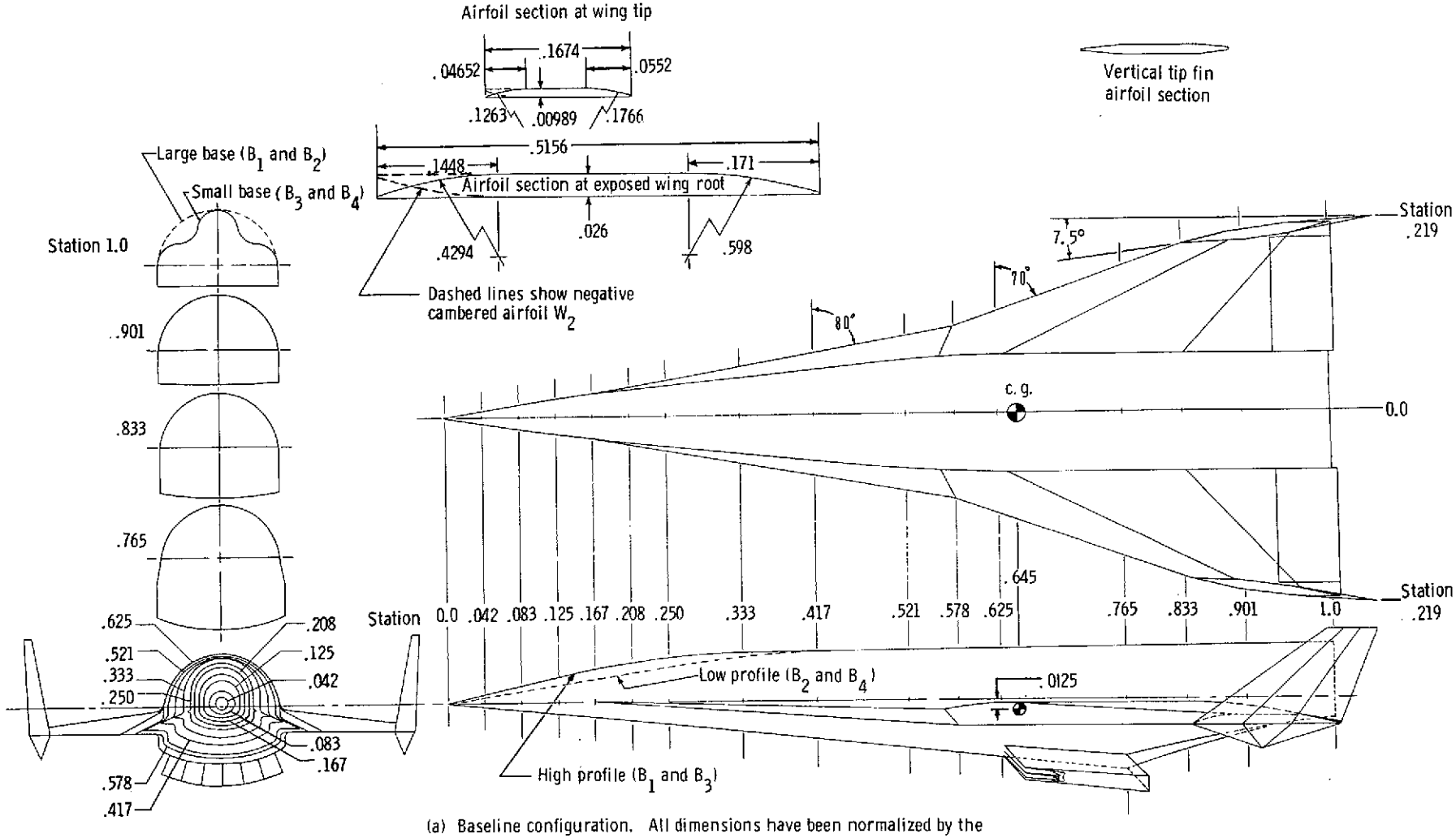

(a) Baseline configuration. All dimensions have been normalized by the body length (ℓ = 142.24 cm).

Figure 3. - Model general dimensions.

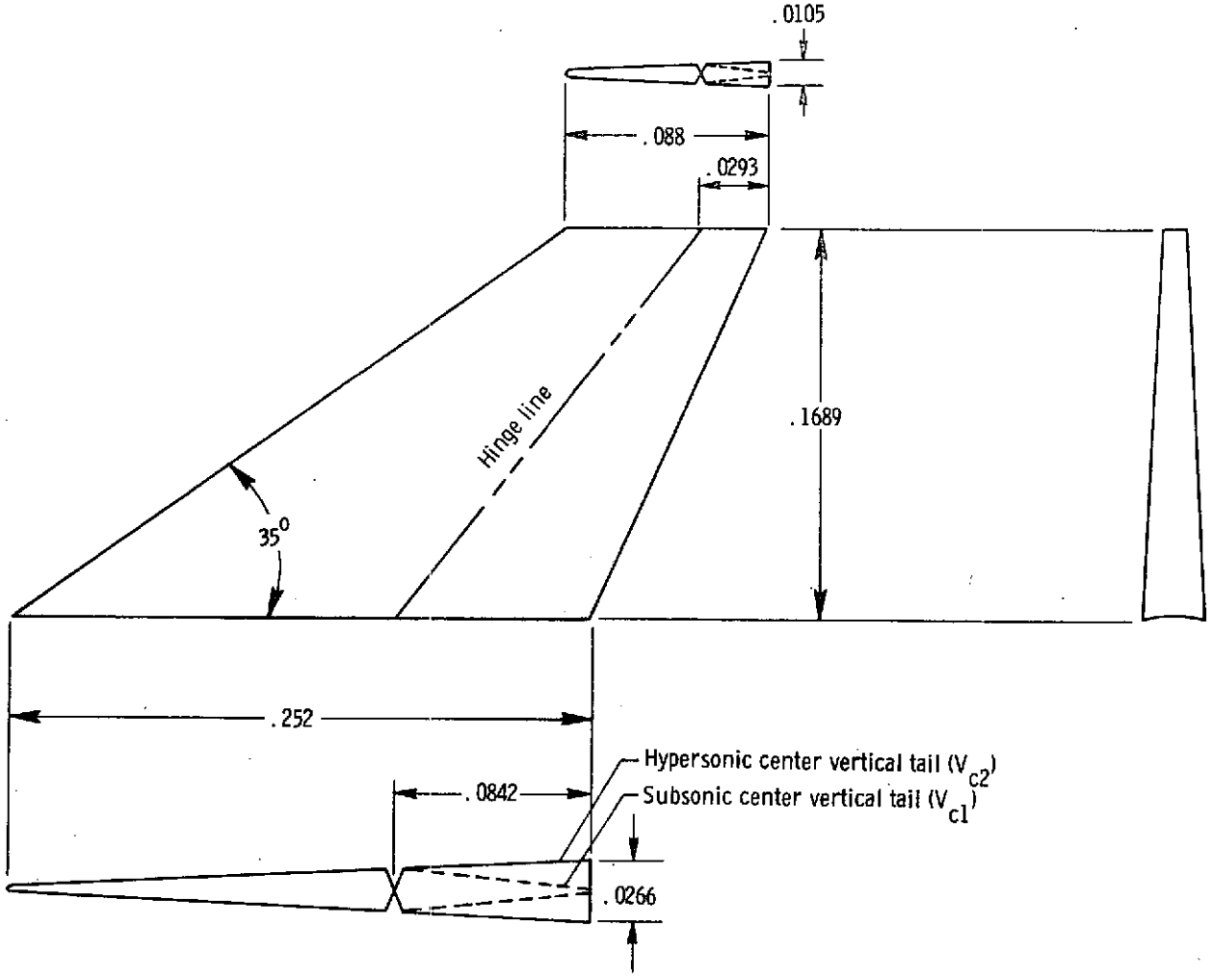

(b) Center vertical tails. All dimensions have been normalized by the body length (ℓ = 142.24 cm).

Figure 3. - Continued.

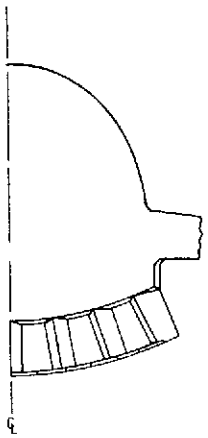

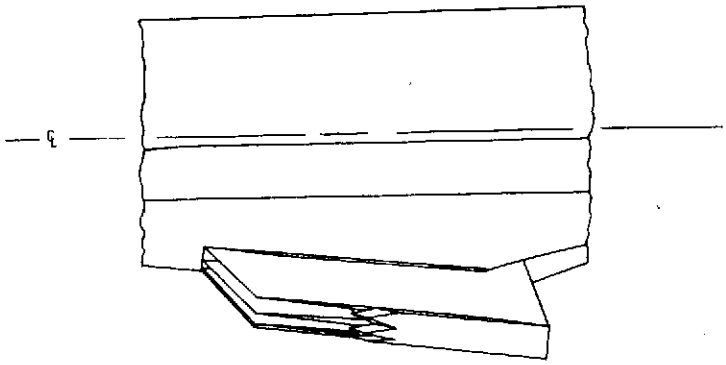

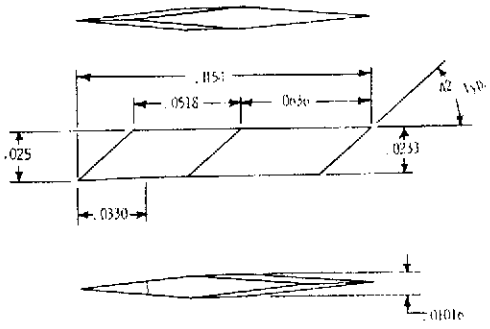

Inside splitter plate

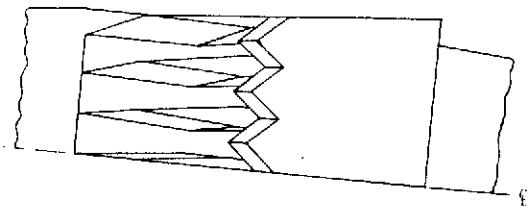

Bottom view of scramjet engine with cowl on

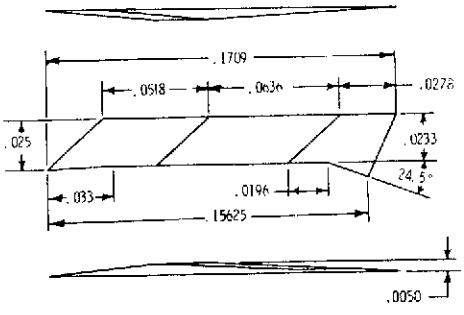

left outside plate

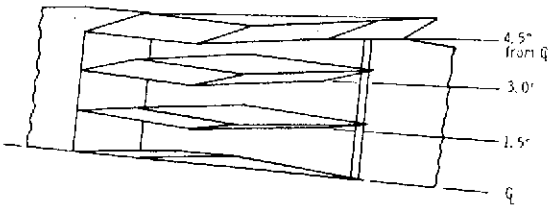

Bottom view of scramjet engine with cowl removed

(c) Scramjet engine. All dimensions have been normalized by the body length (L = 142.24 cm).

Figure 3.- Concluded.

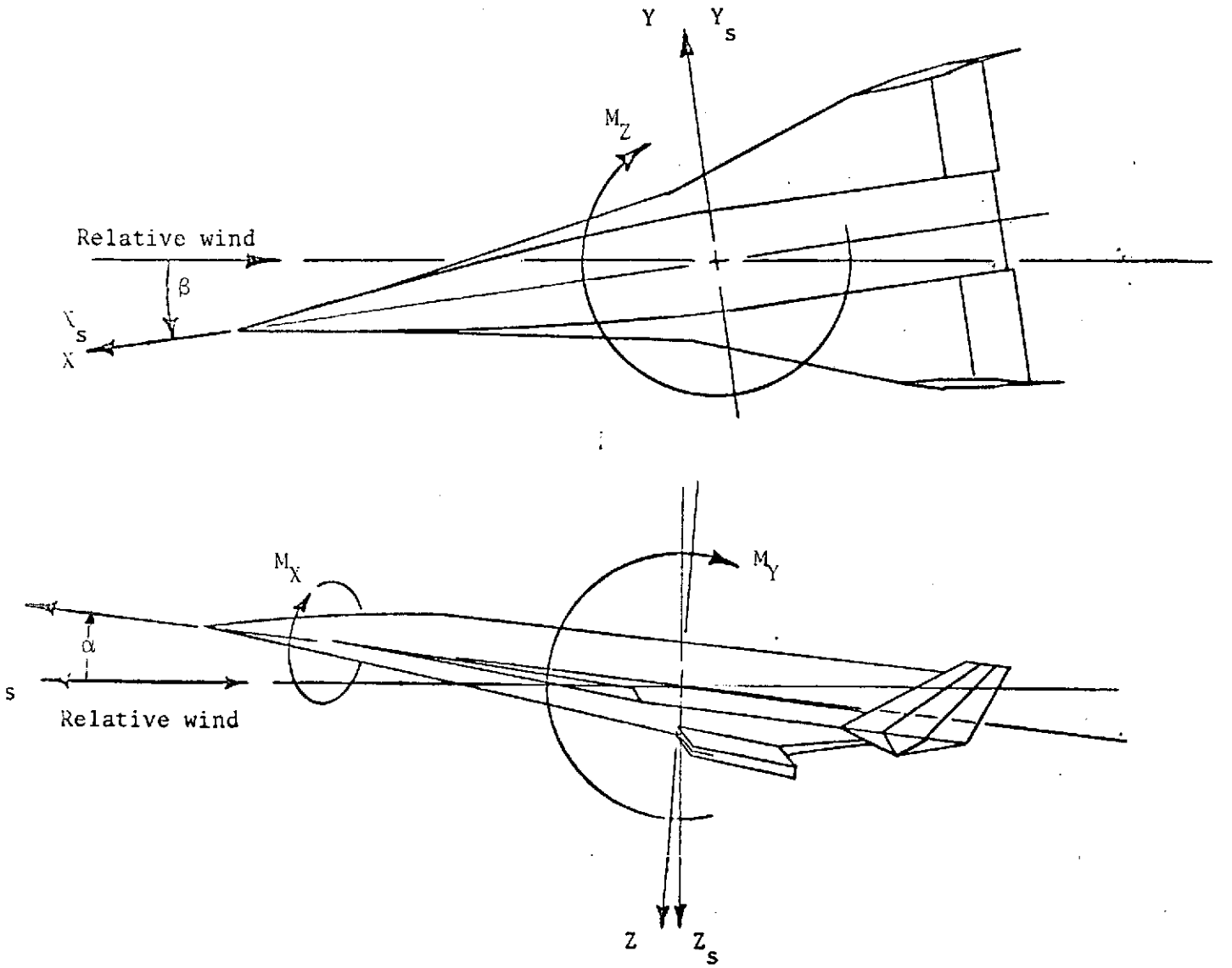

FIGURE 4 .- SYSTEMS OF REFERENCE AXES: ARROWS INDICATE POSITIVE DIRECTIONS

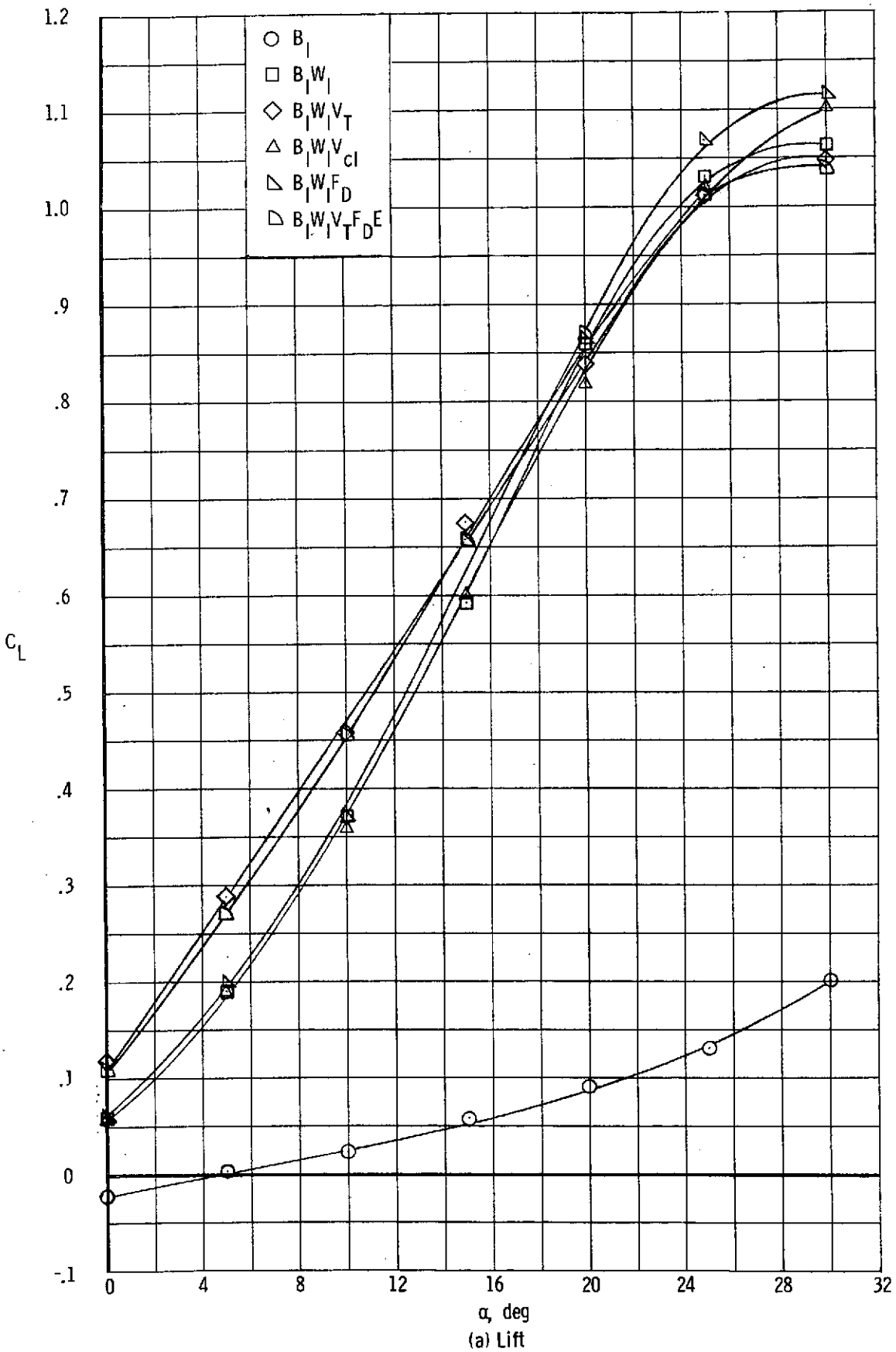

(a) Lift

Figure 5. - Longitudinal characteristics of Body 1 with various components.

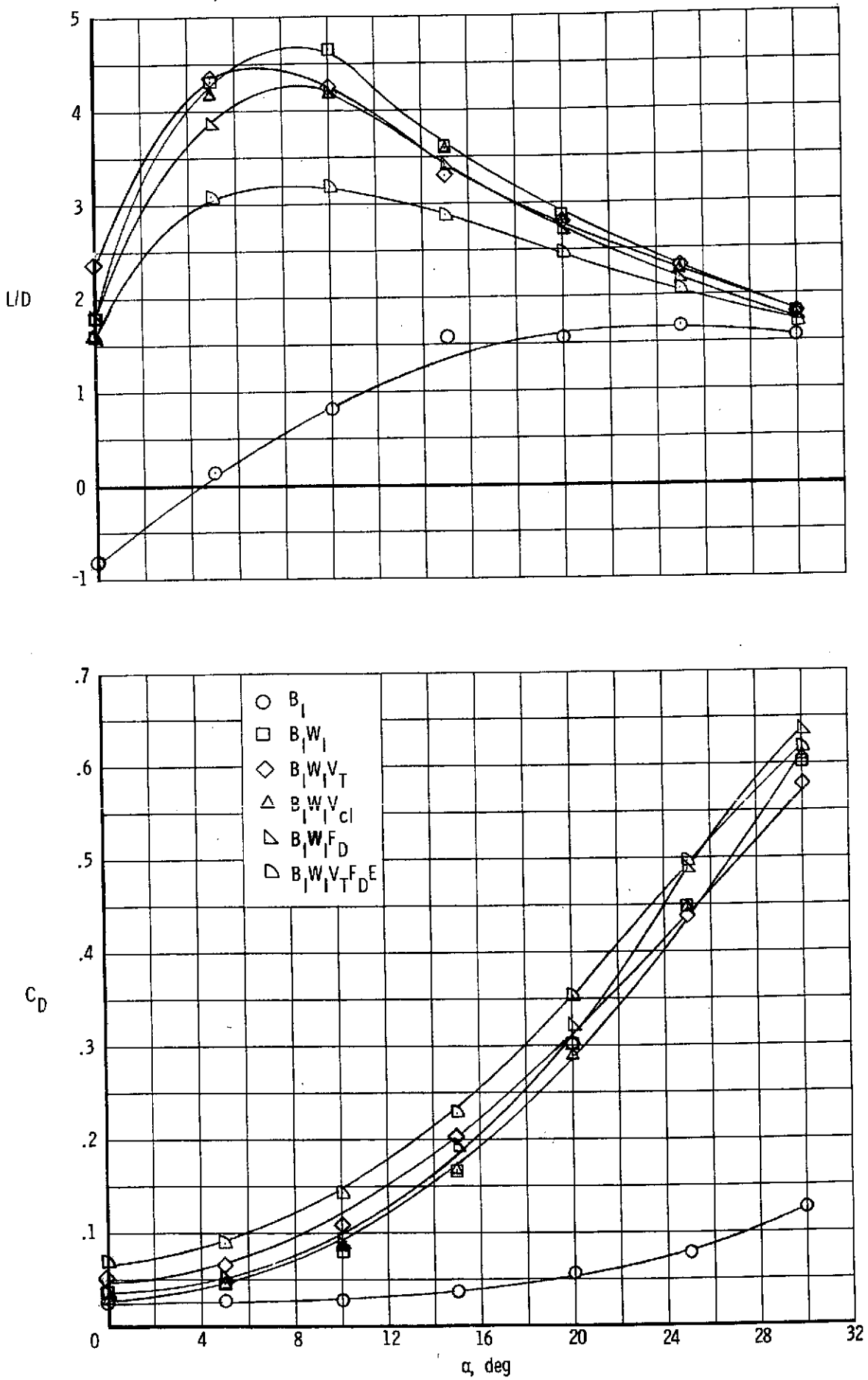

(b) Drag and lift drag

Figure 5. - Continued.

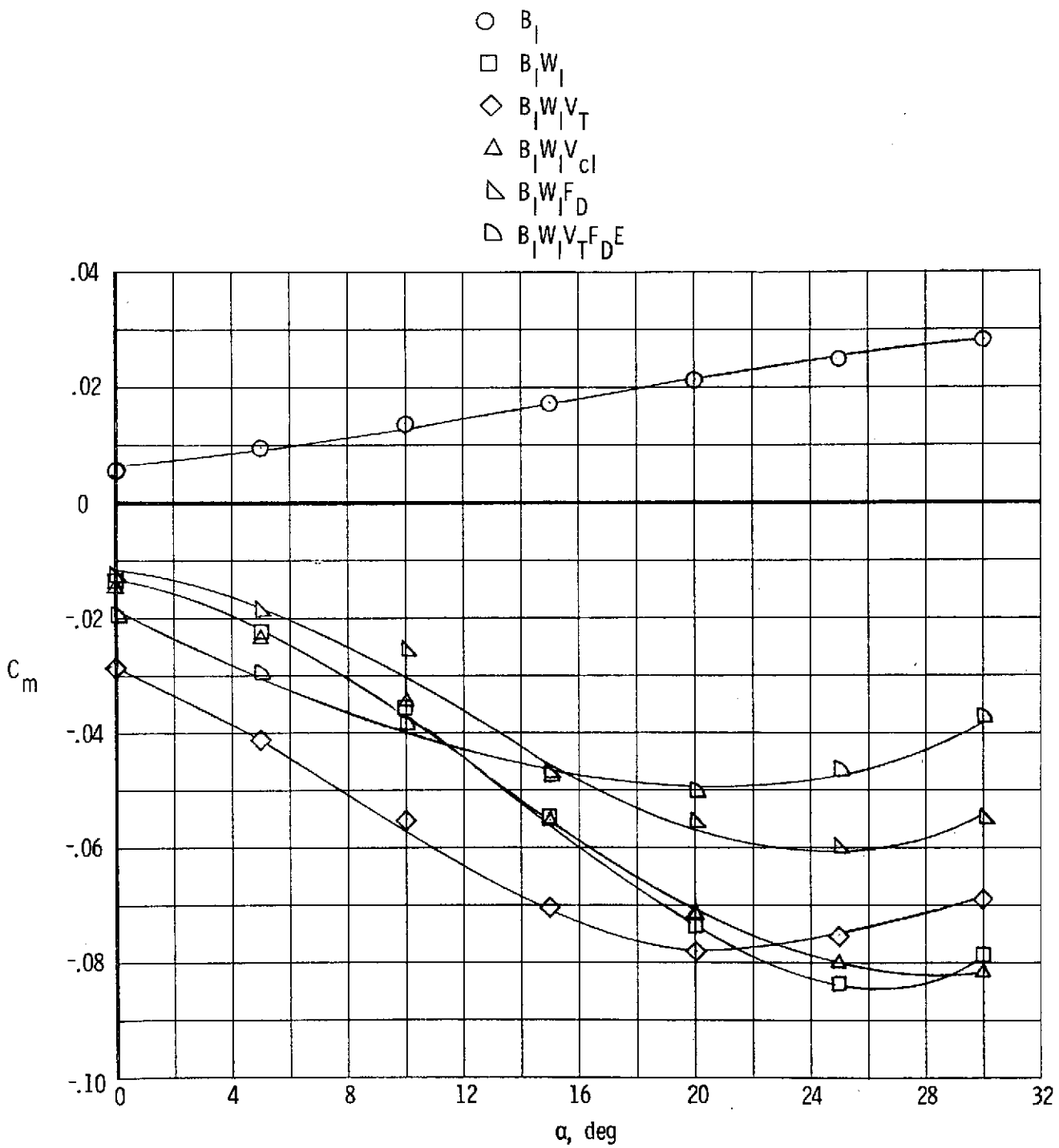

(c) Pitch

Figure 5. - Continued.

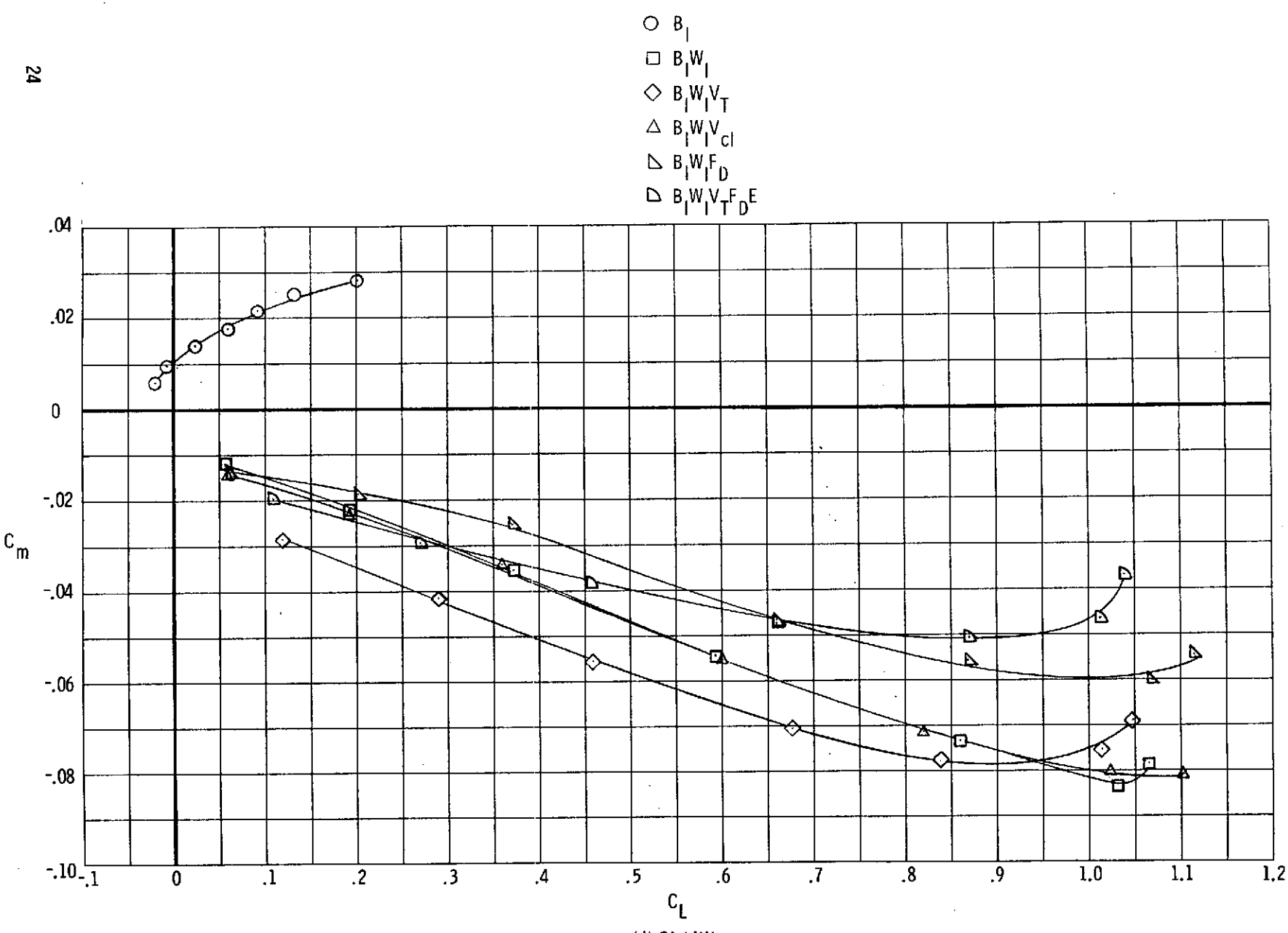

(d) Stability

Figure 5. - Concluded.

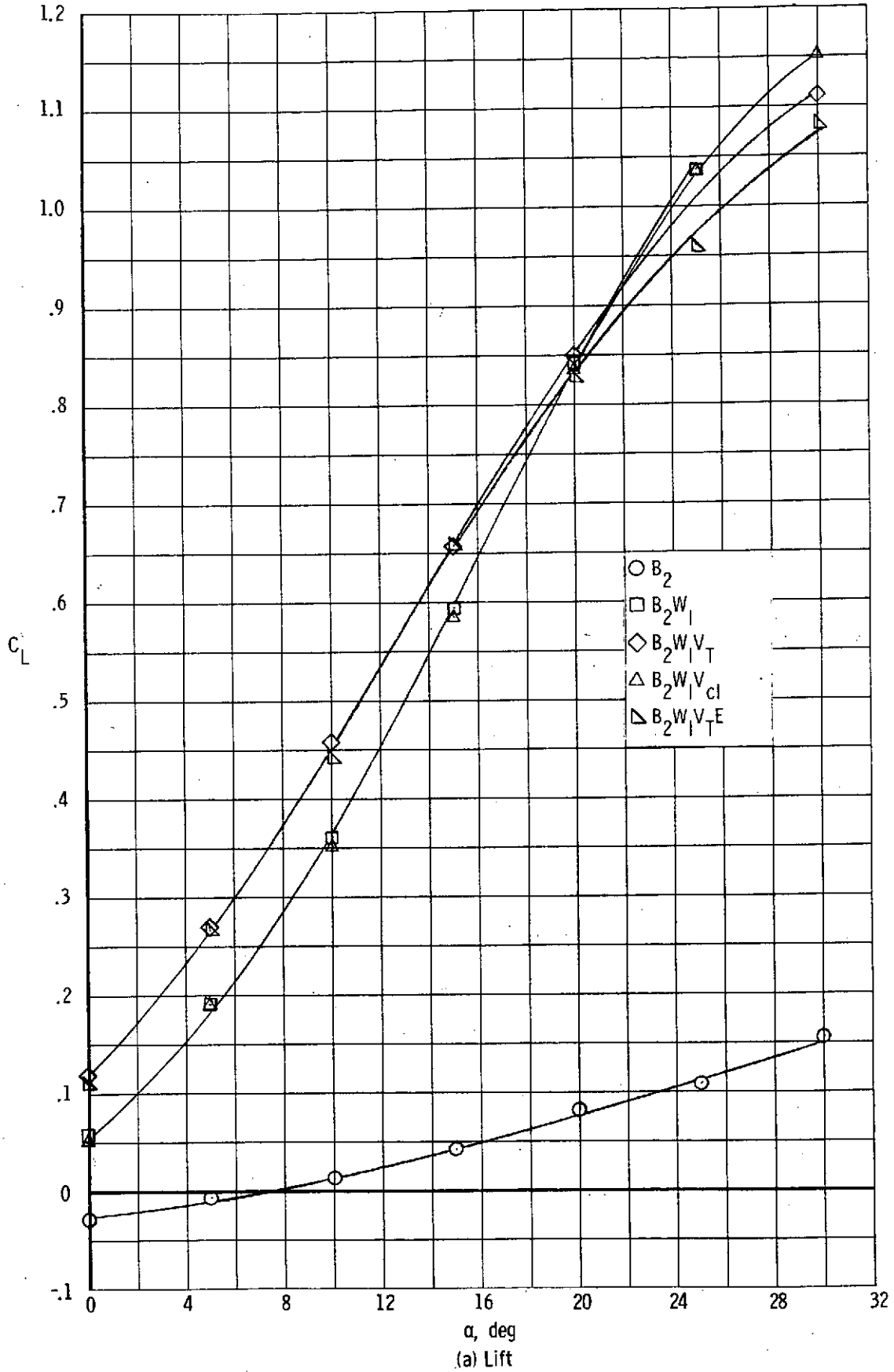

(a) Lift

Figure 6. - Longitudinal characteristics of Body 2 with various components.

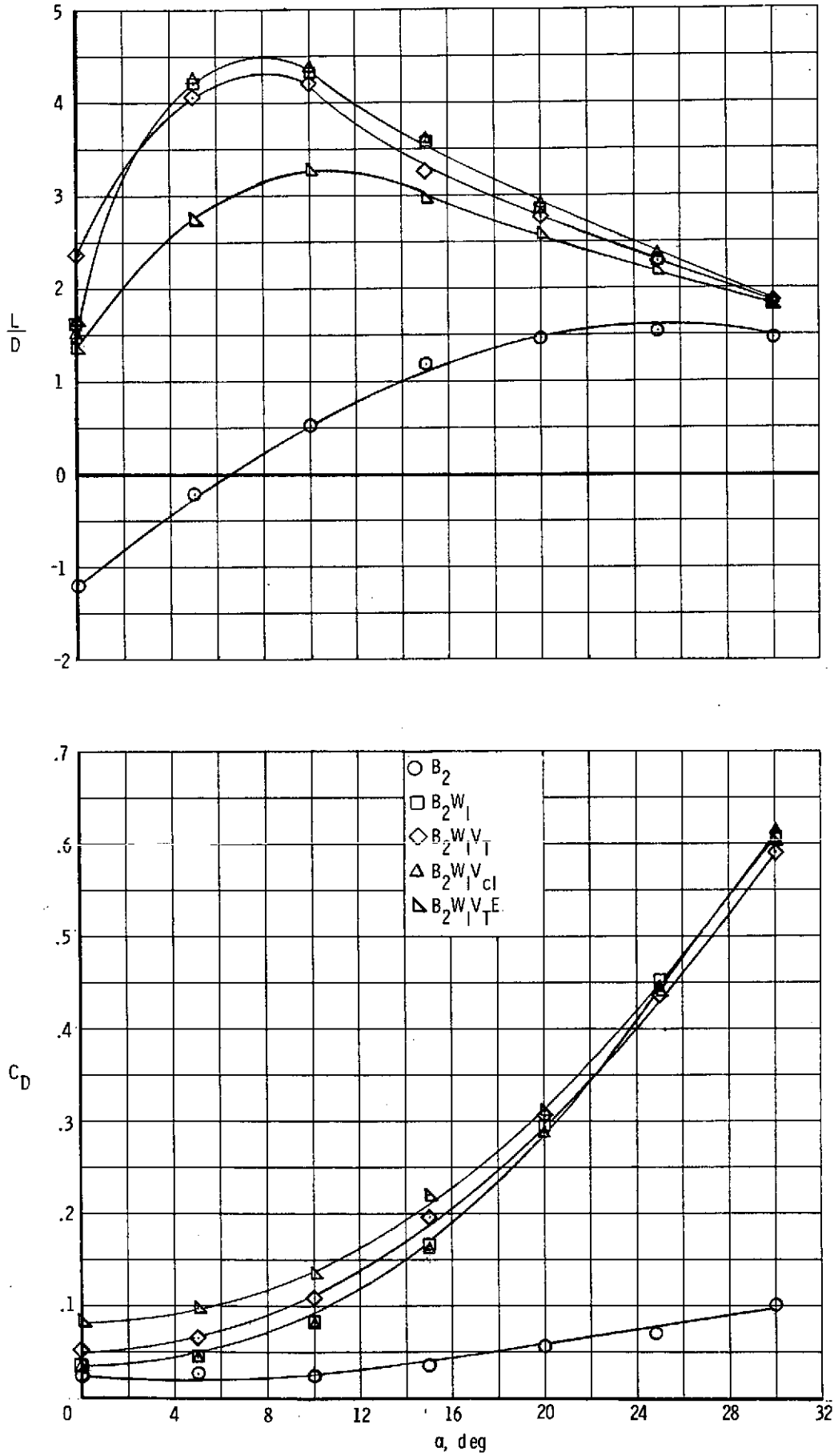

(b) Drag and lift-drag ratio

Figure 6. - Continued.

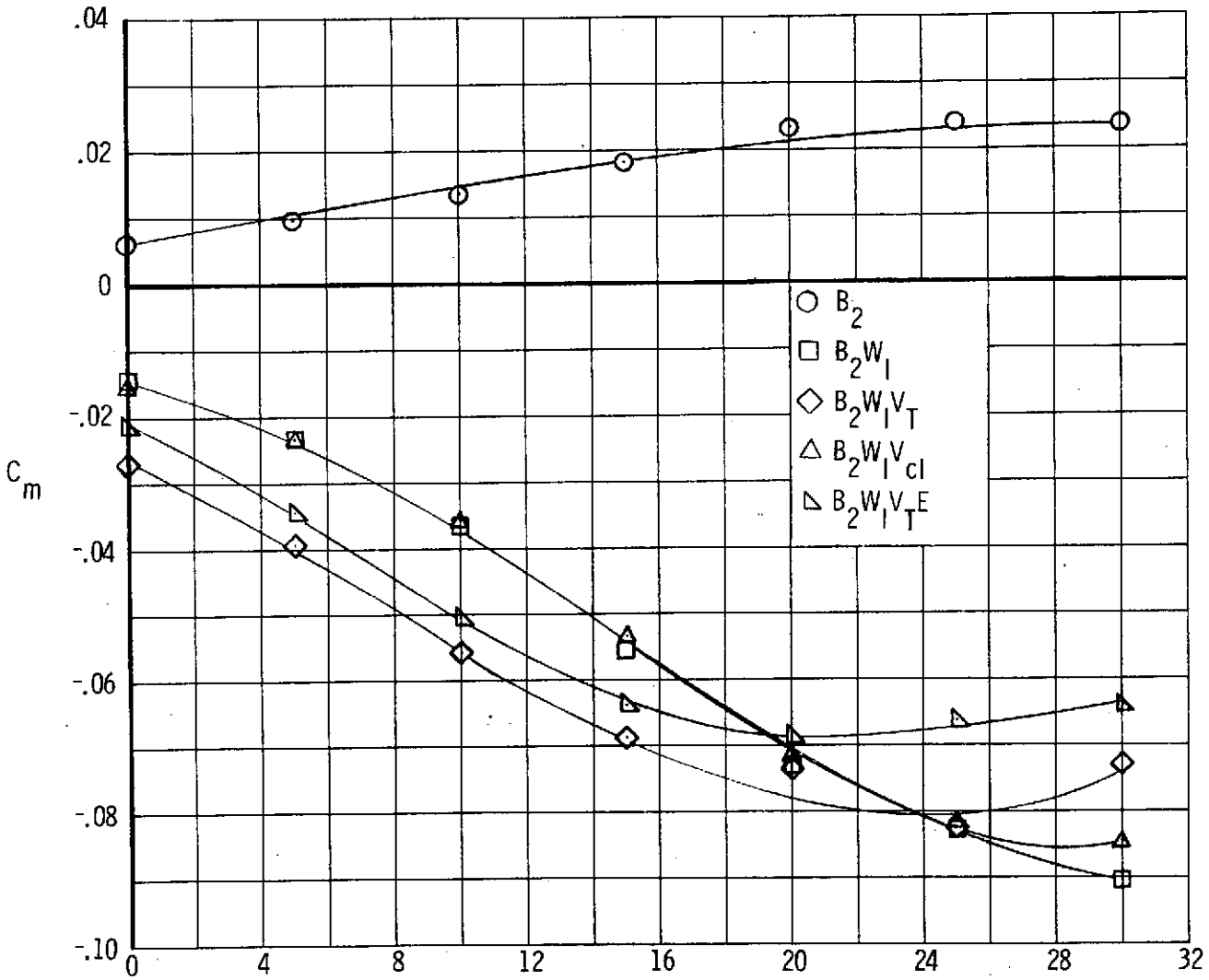

(c) Pitch

Figure 6. - Continued.

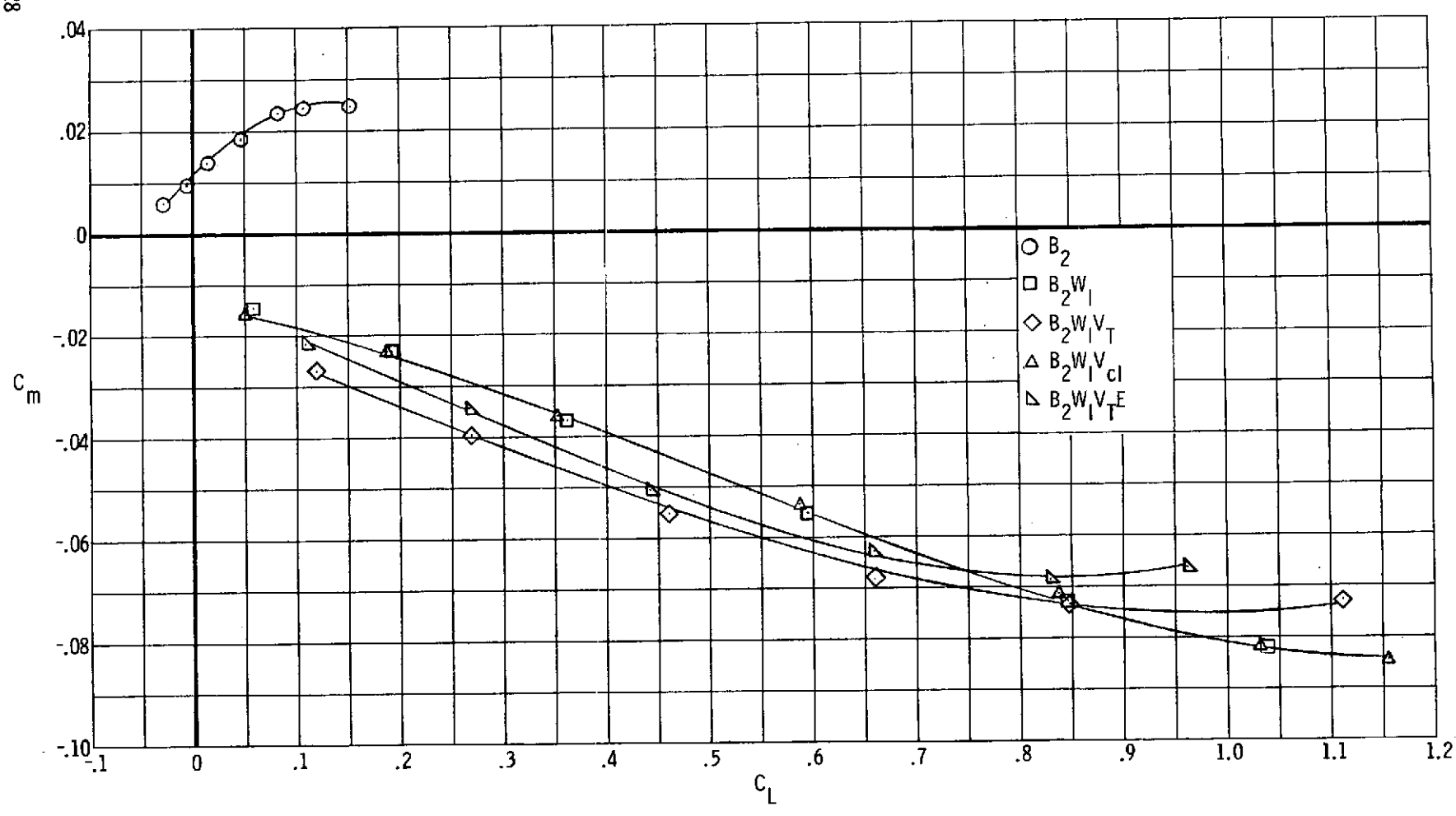

(d) Stability

Figure 6. - Concluded.

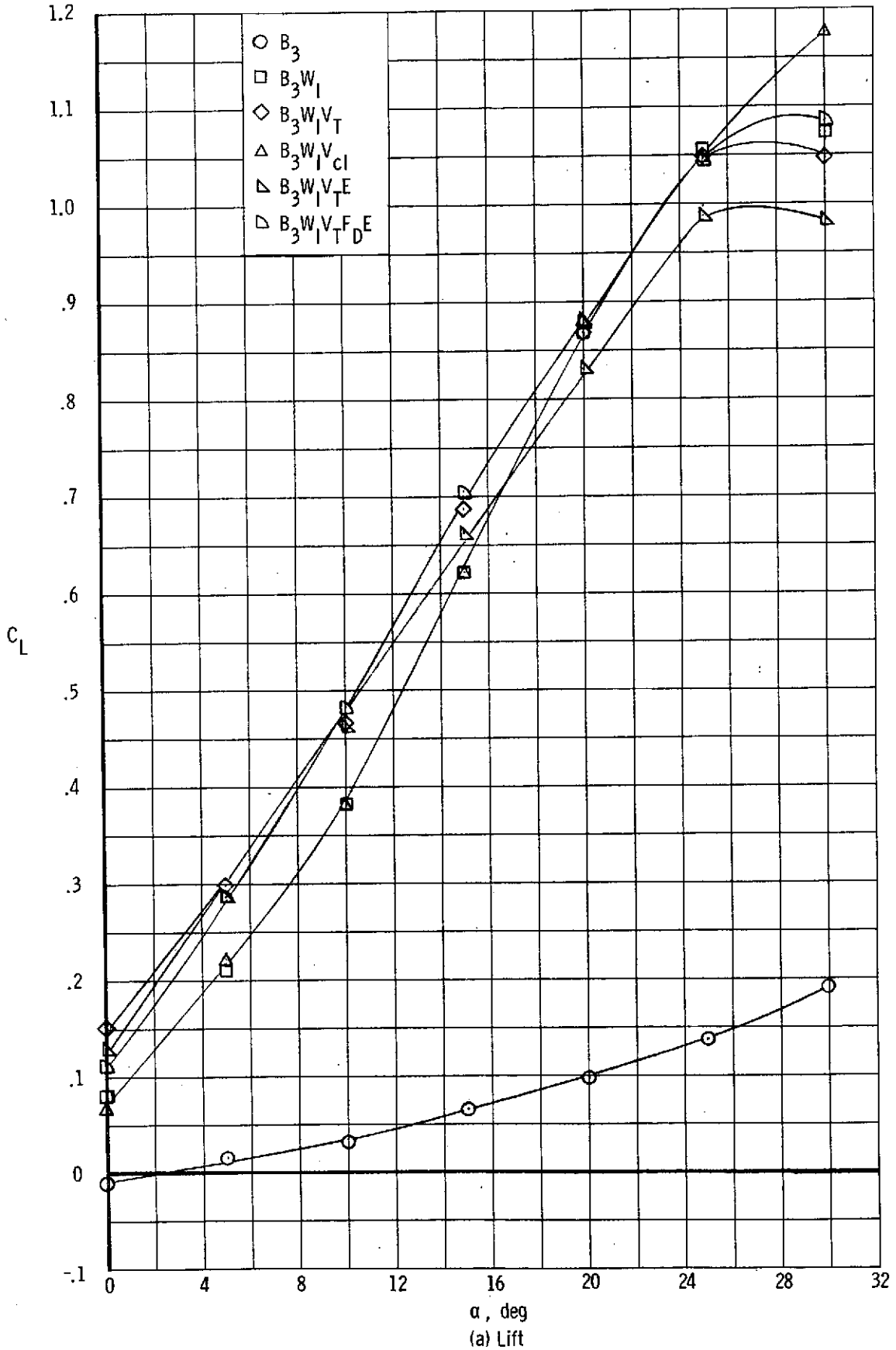

(a) Lift

Figure 7. - Longitudinal characteristics of Body 3 with various components.

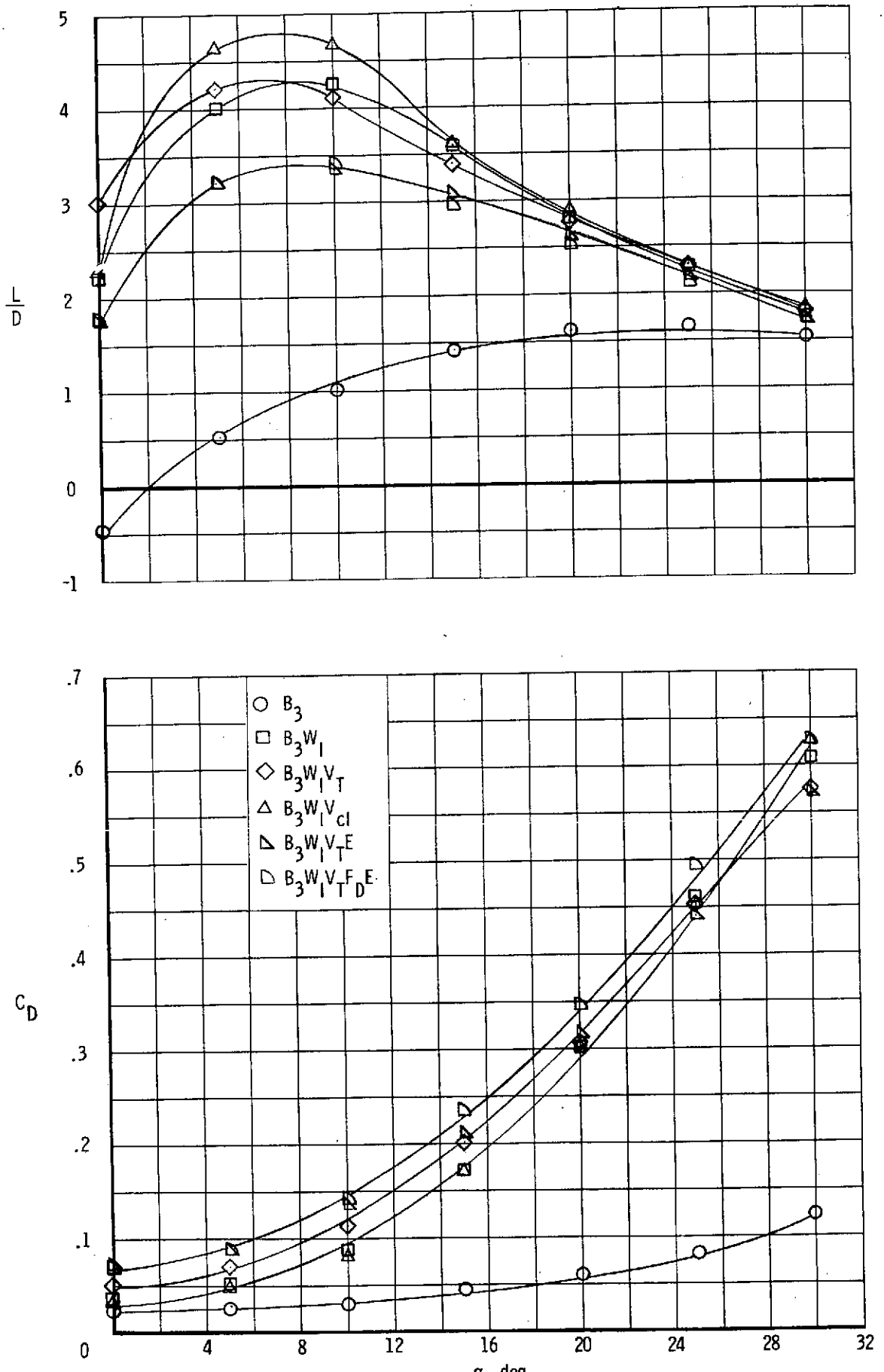

(b) Drag and lift-drag ratio

Figure 7. - Continued.

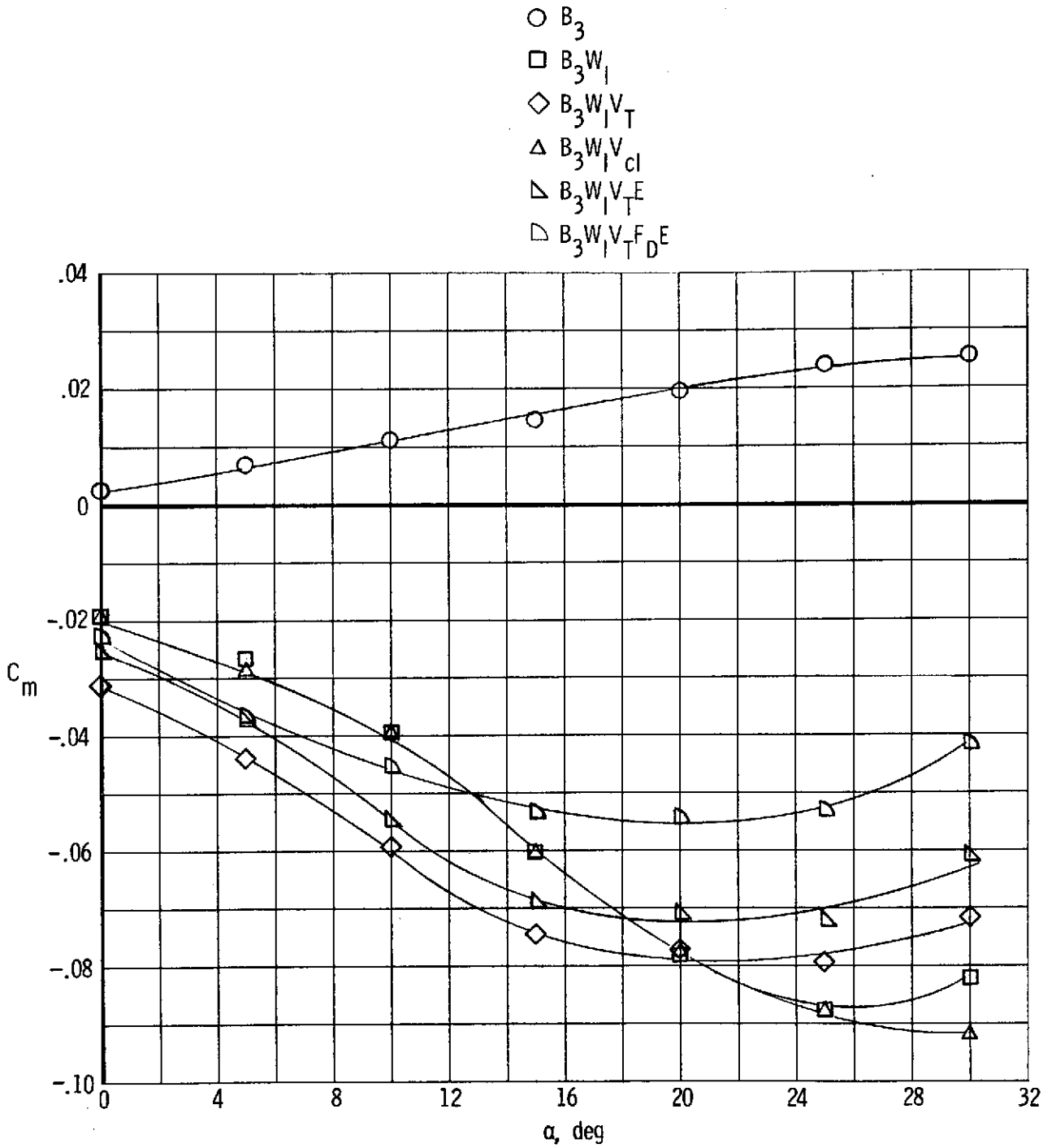

(c) Pitch

Figure 7. - Continued.

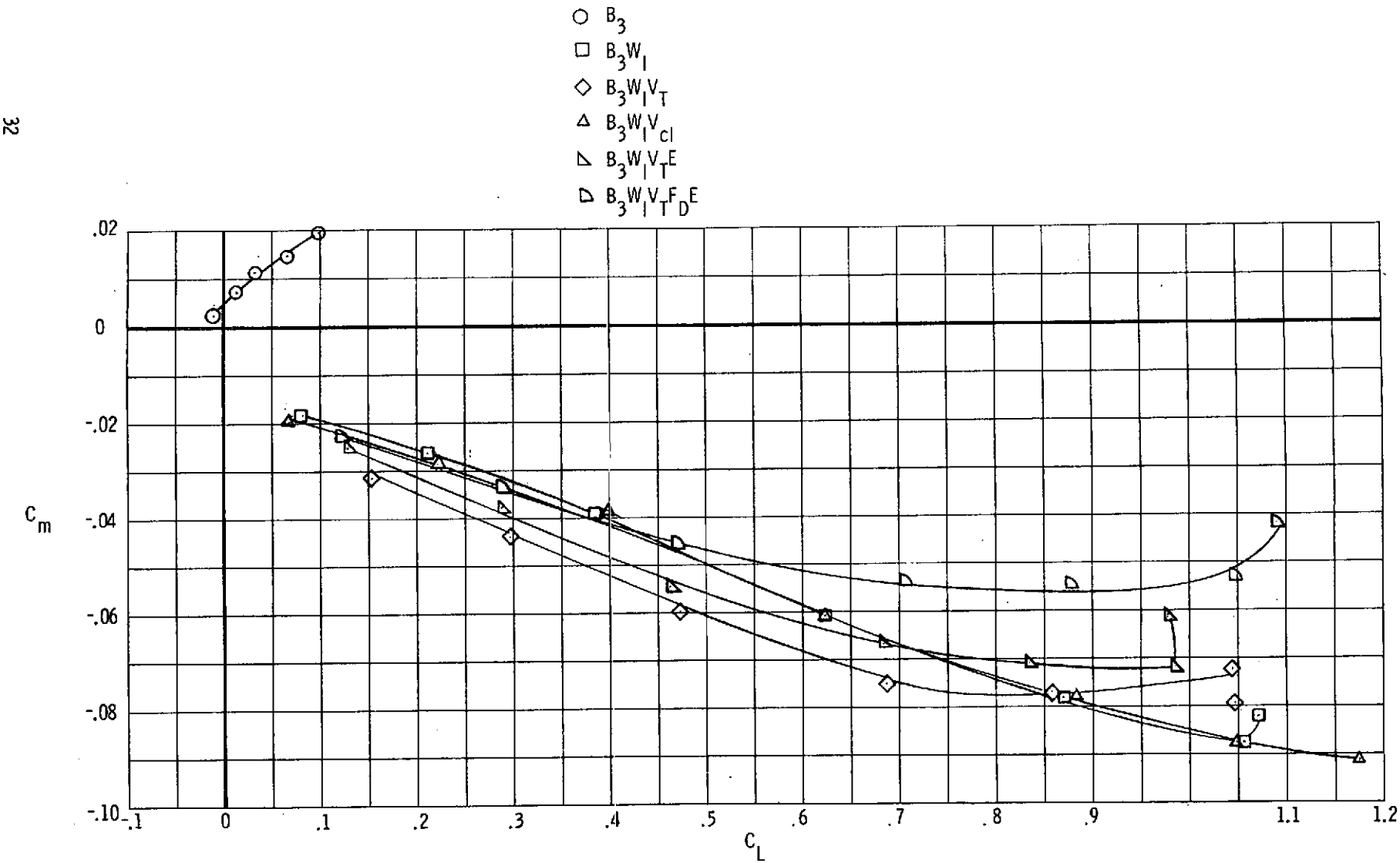

(d) Stability

Figure 7. - Concluded.

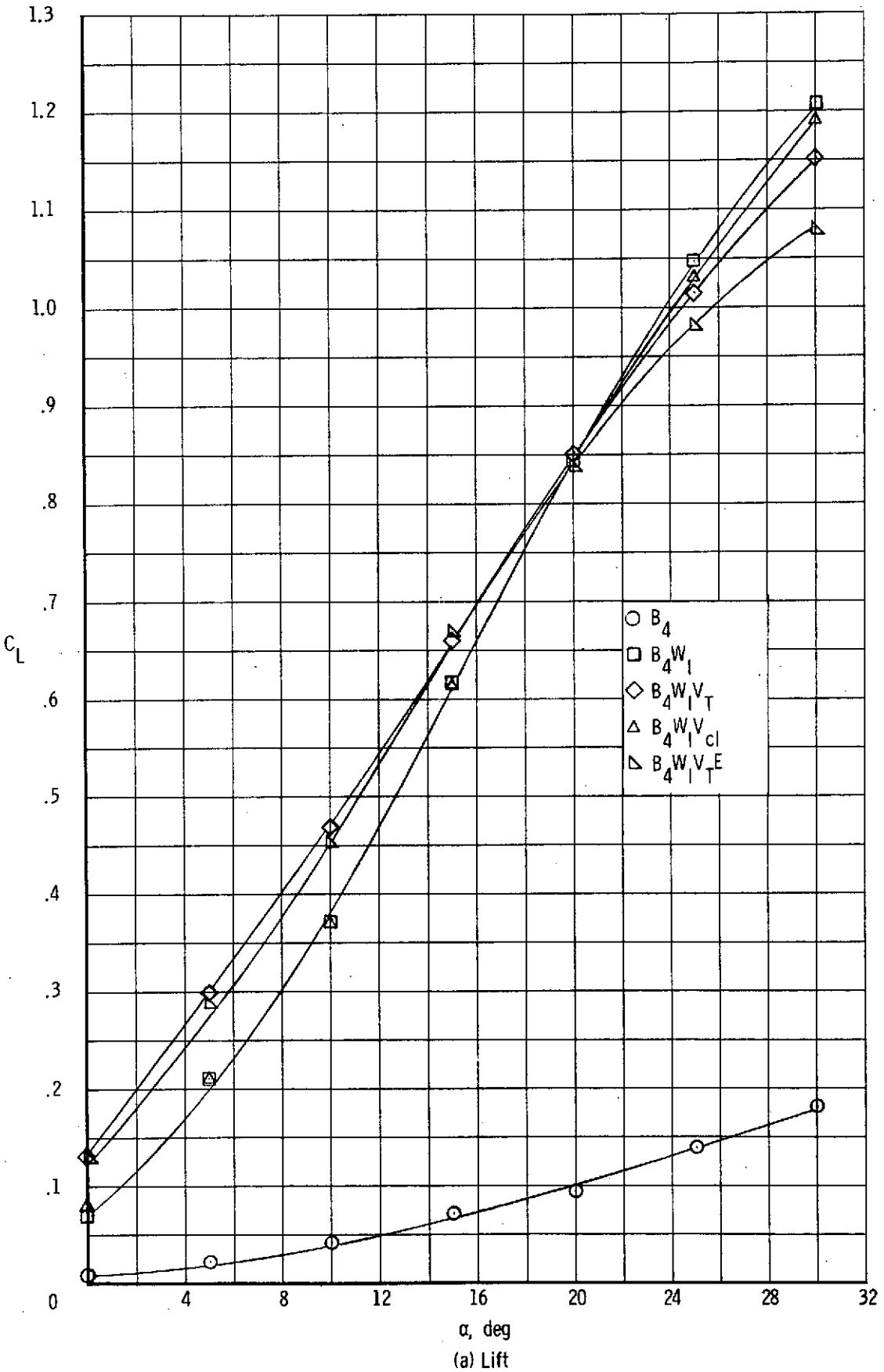

(a) Lift

Figure 8. - Longitudinal characteristics of Body 4 with various components.

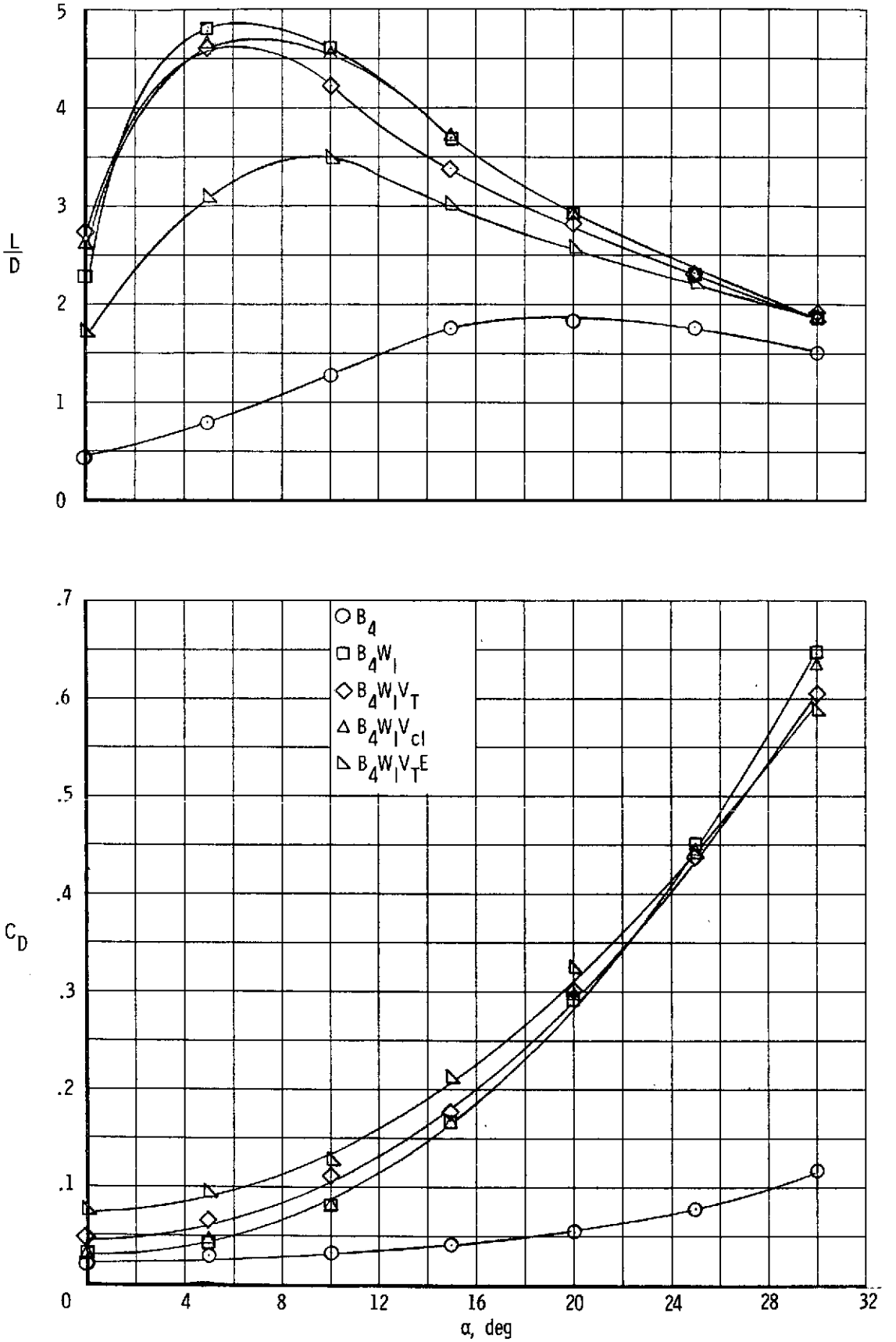

(b) Drag and lift-drag ratio

Figure 8. - Continued.

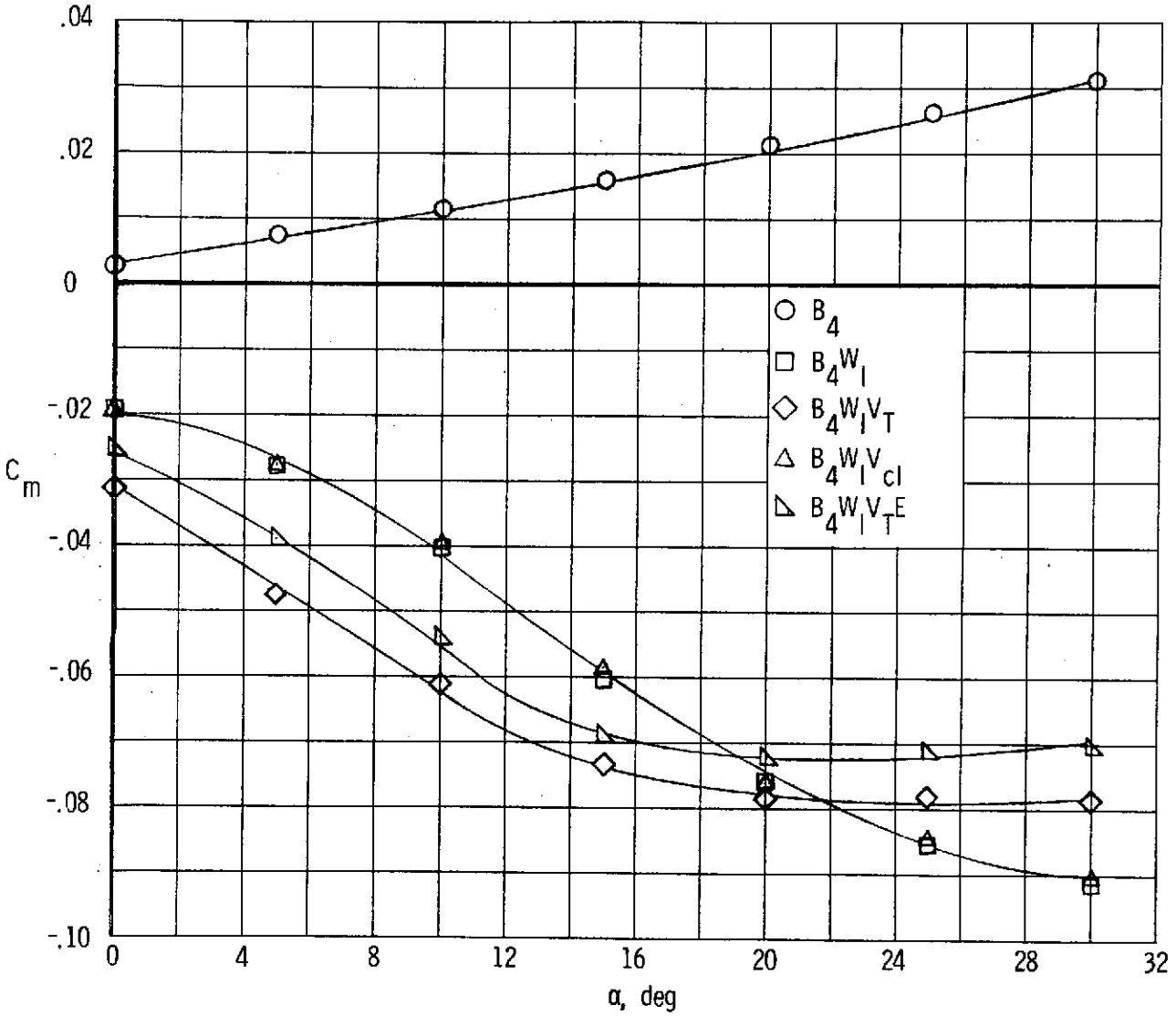

(c) Pitch

Figure 8. - Continued.

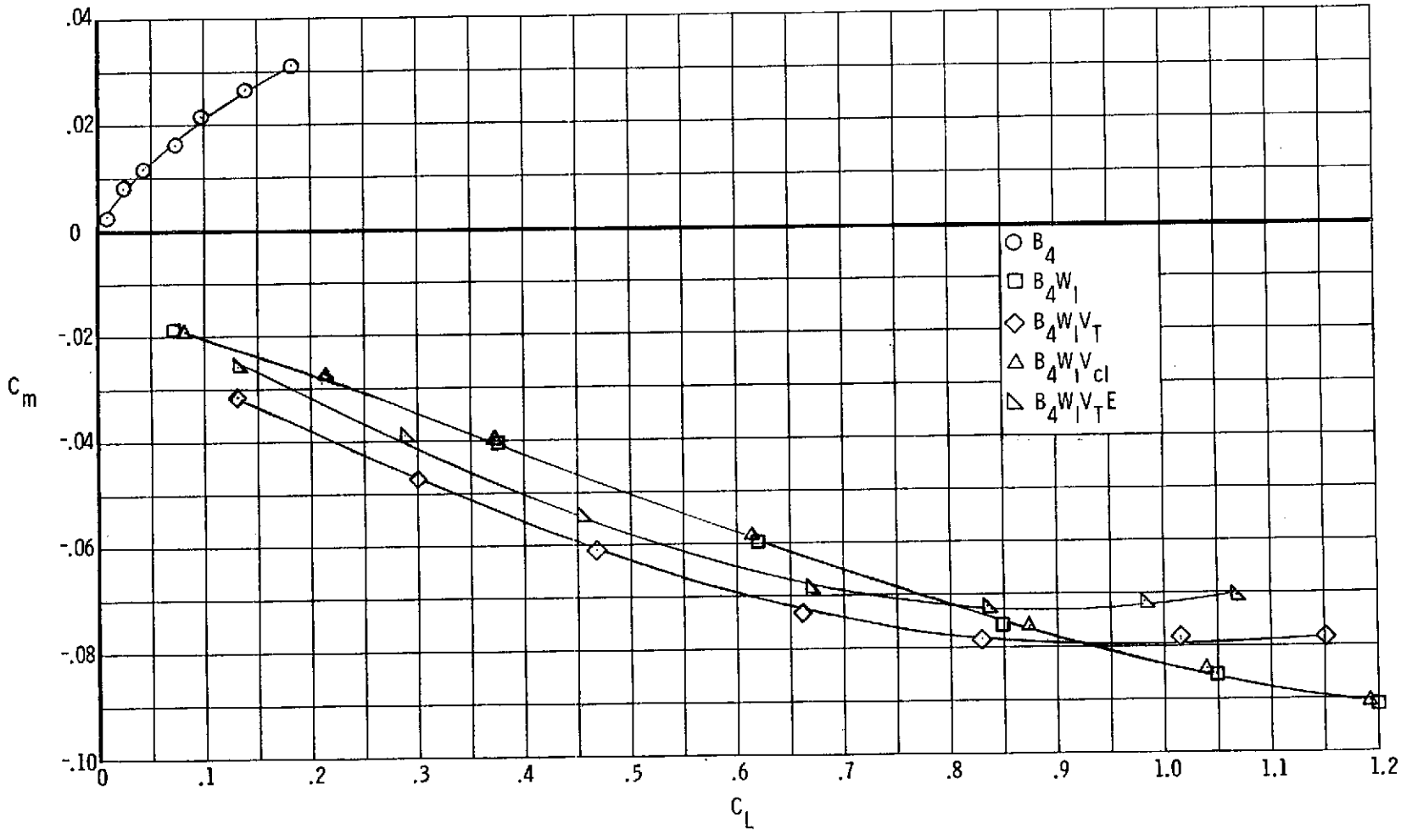

(d) Stability

Figure 8. - Concluded.

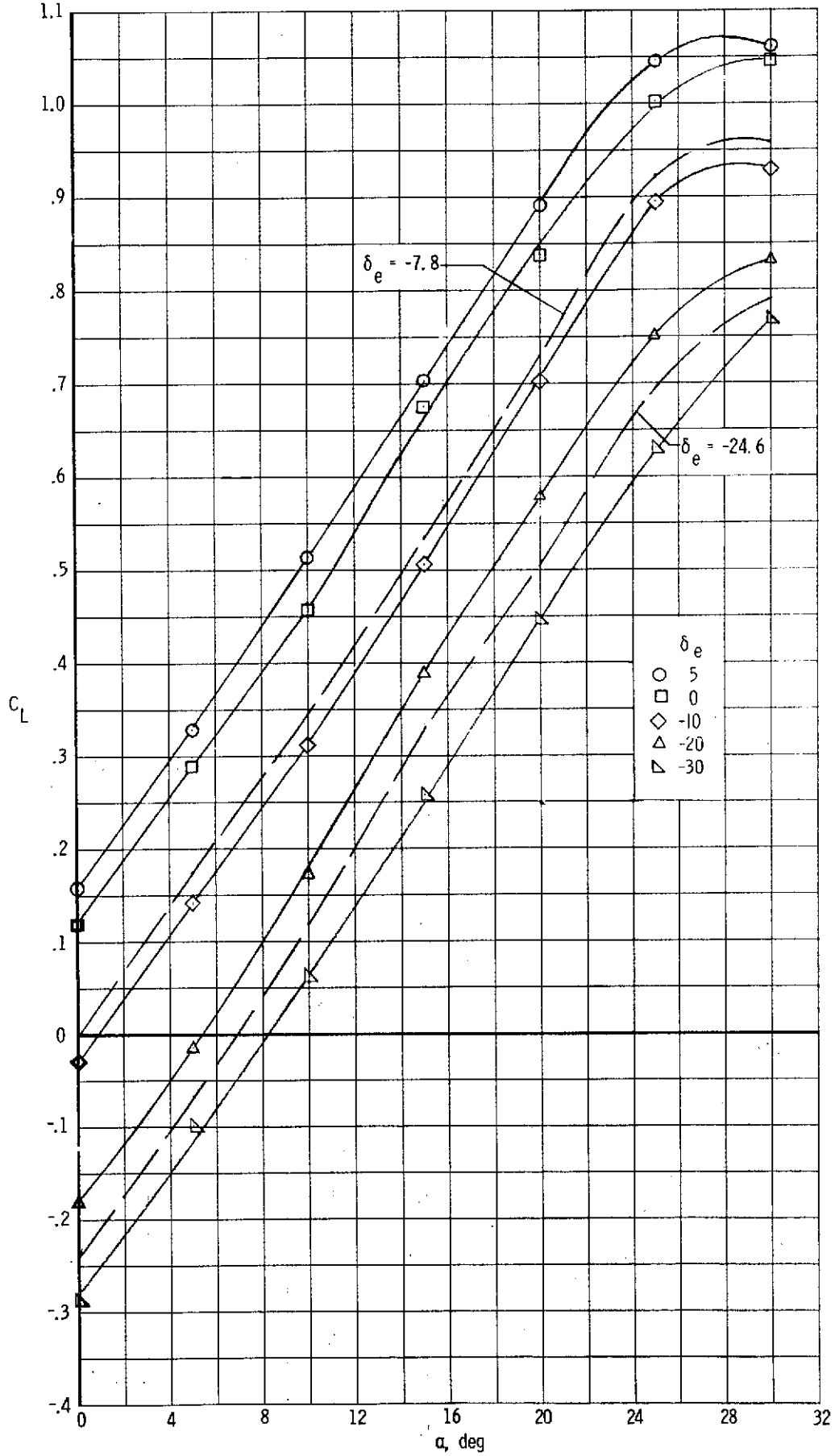

(a) Lift

Figure 9. - Longitudinal characteristics of $B_1W_1V_T$.

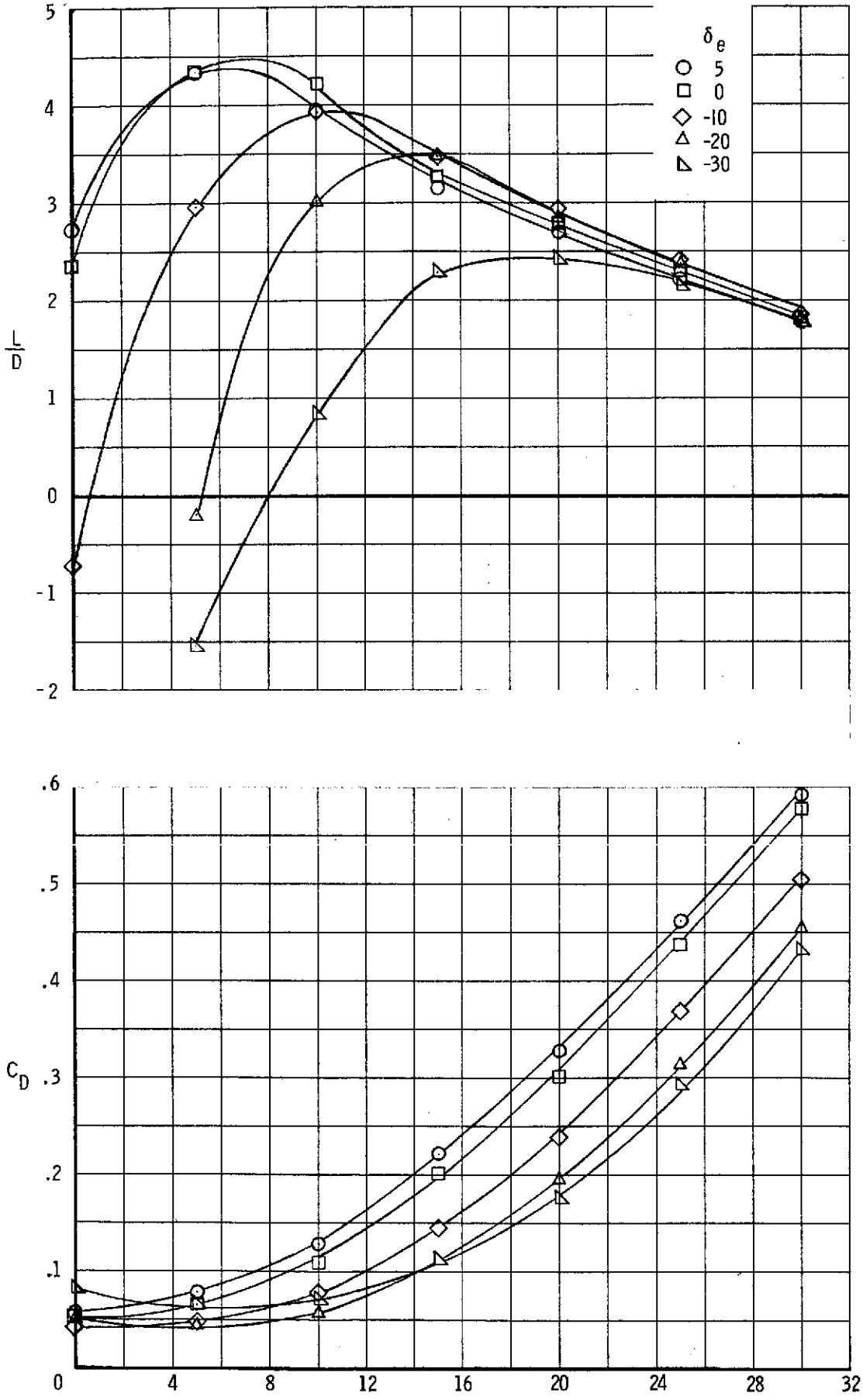

(b) Drag and lift-drag ratio

Figure 9. - Continued.

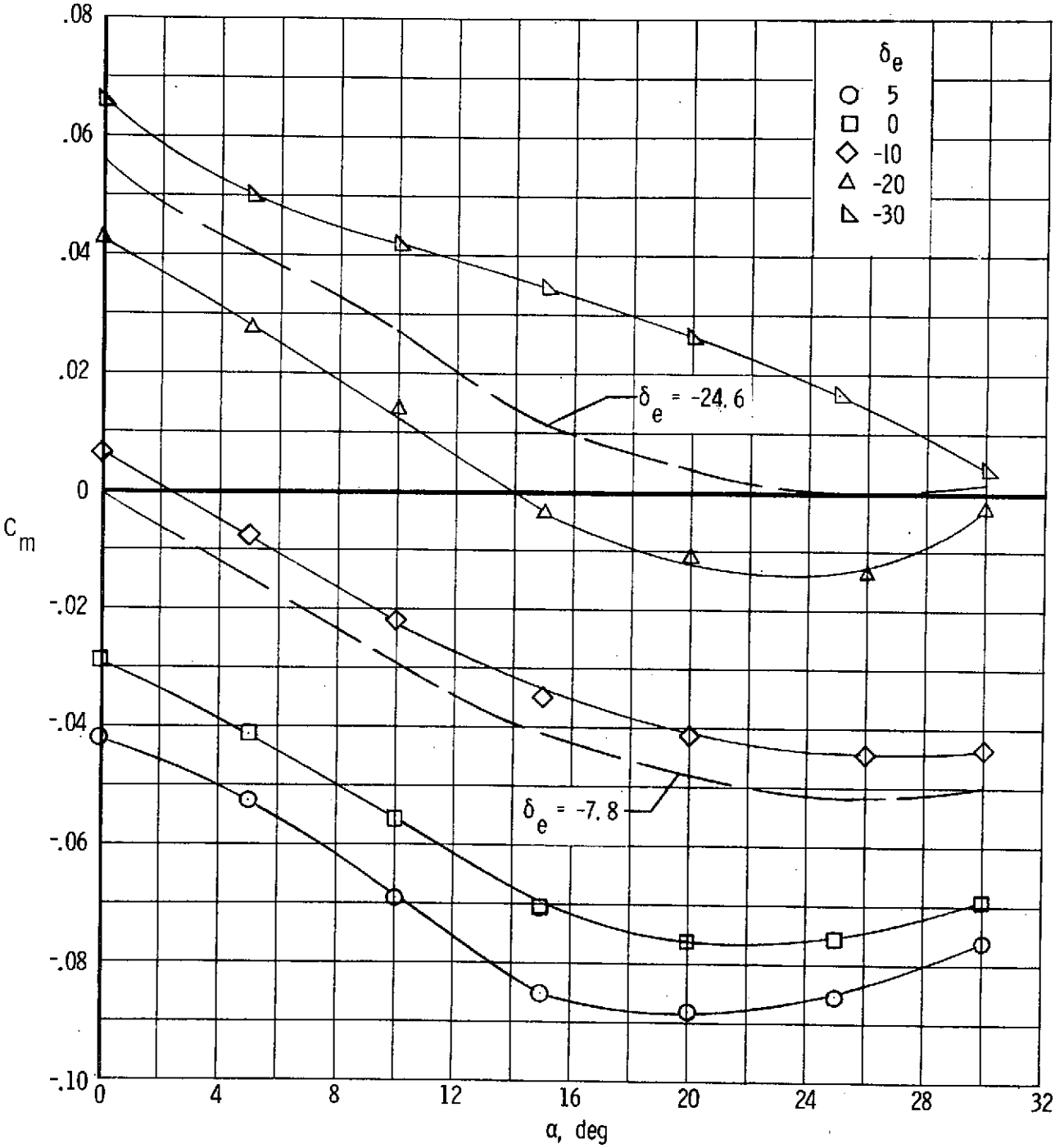

(c) Pitch

Figure 9 . - Continued.

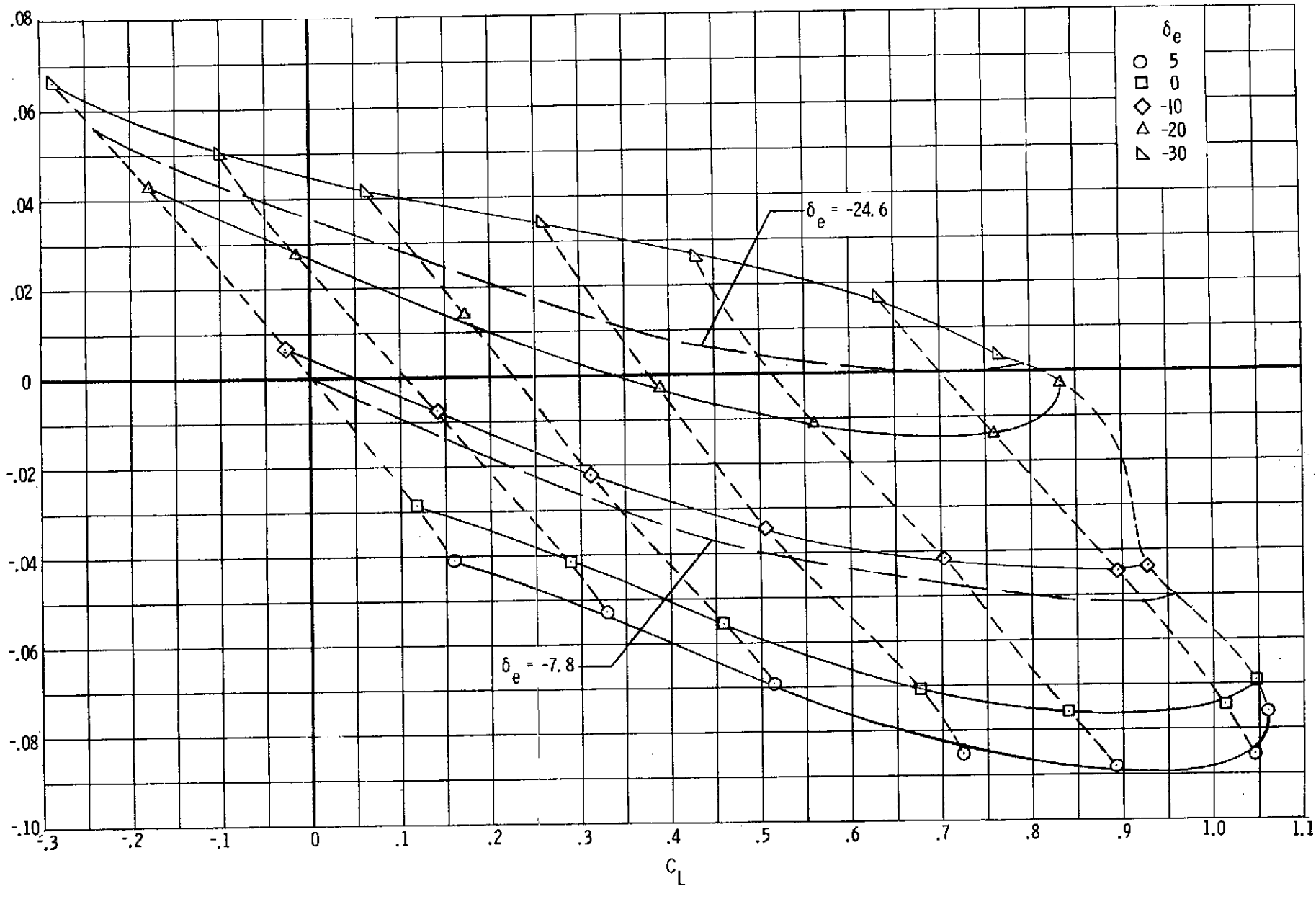

(d) Stability

Figure 9. - Concluded.

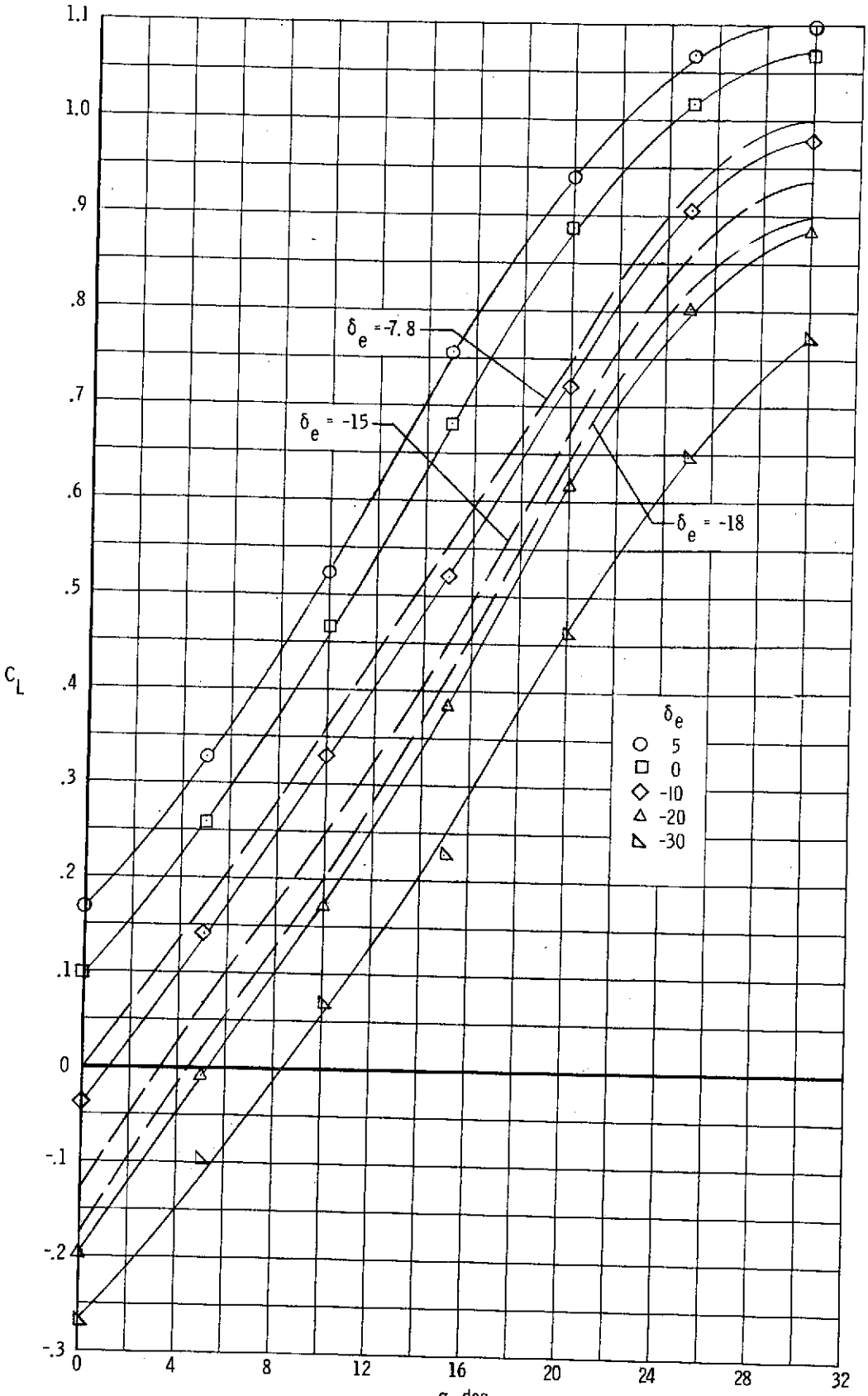

(a) Lift

Figure 10. - Longitudinal characteristics of $B_1W_1V_TF_D$.

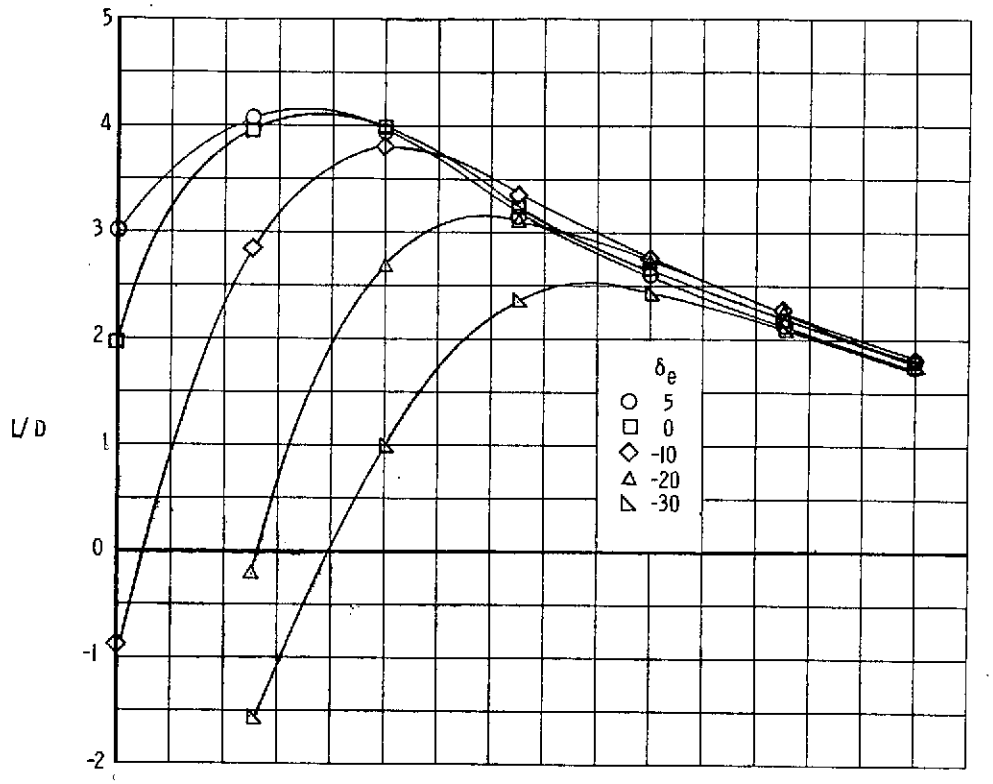

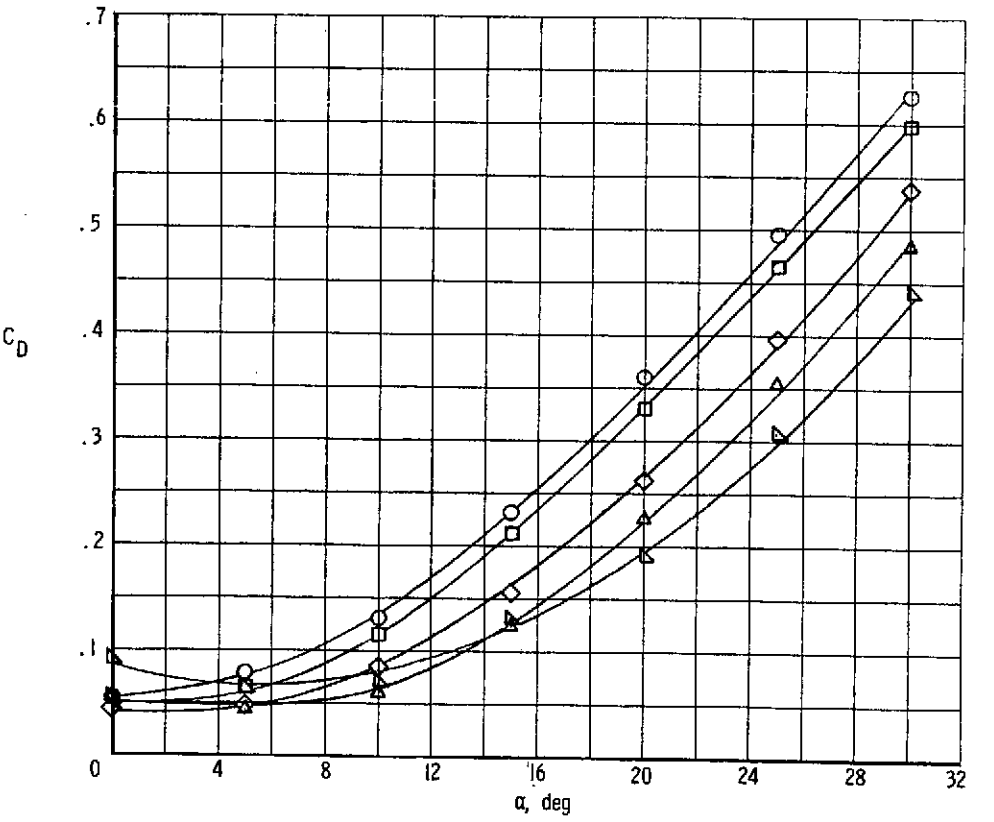

(b) Drag and lift-drag ratio

Figure 10. - Continued.

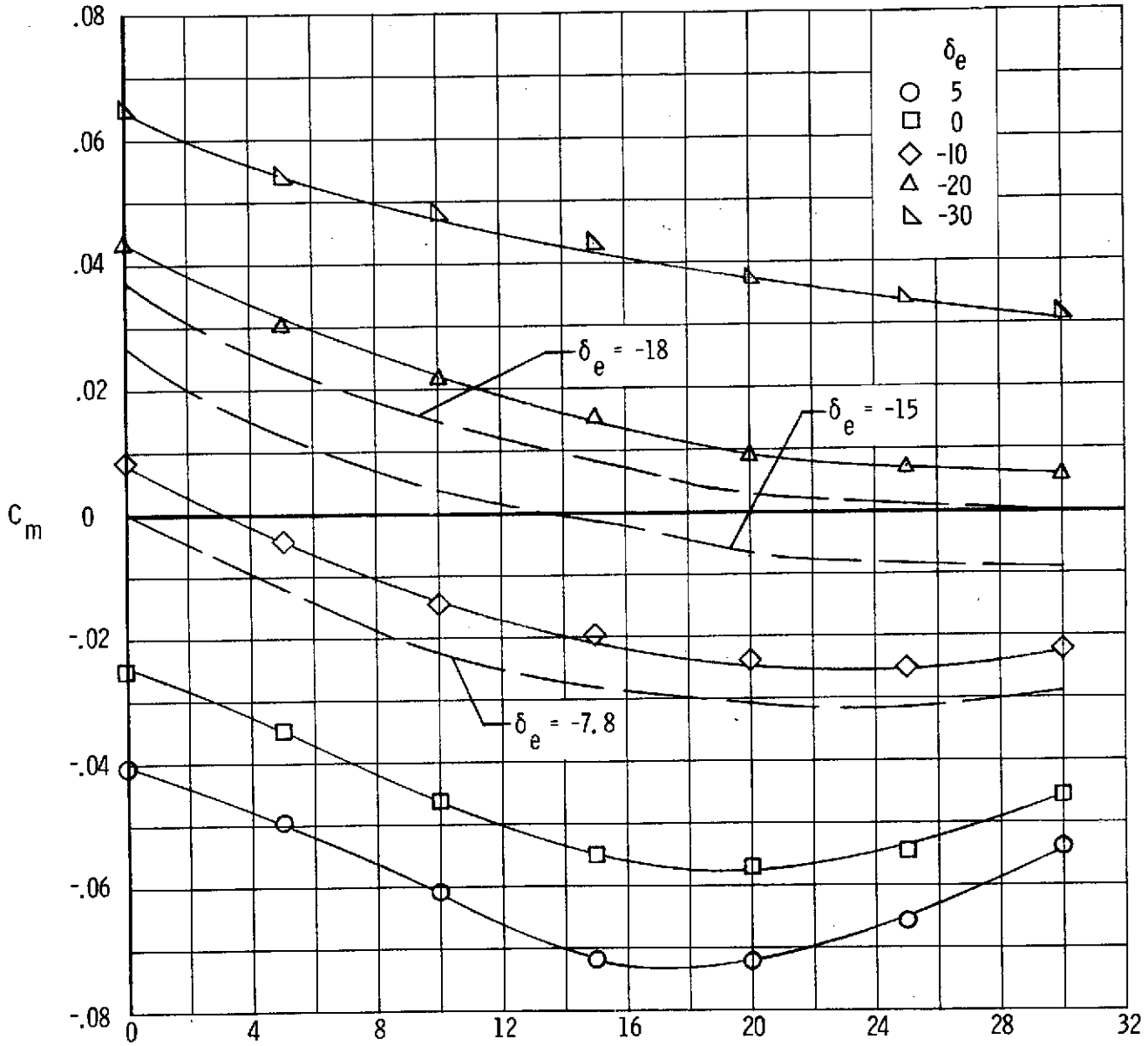

(c) Pitch

Figure 10. - Continued.

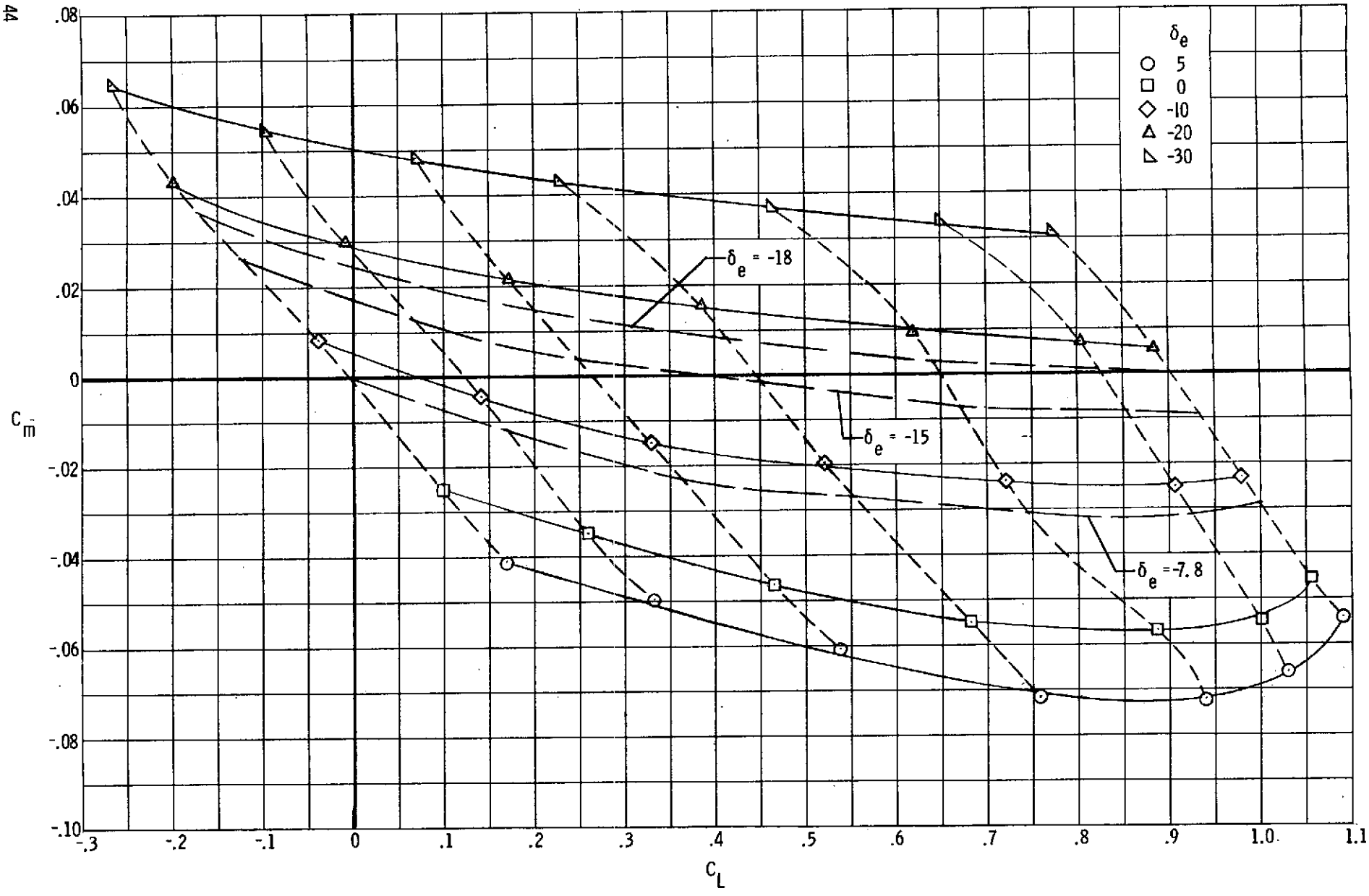

(d) Stability

Figure 10. - Concluded.

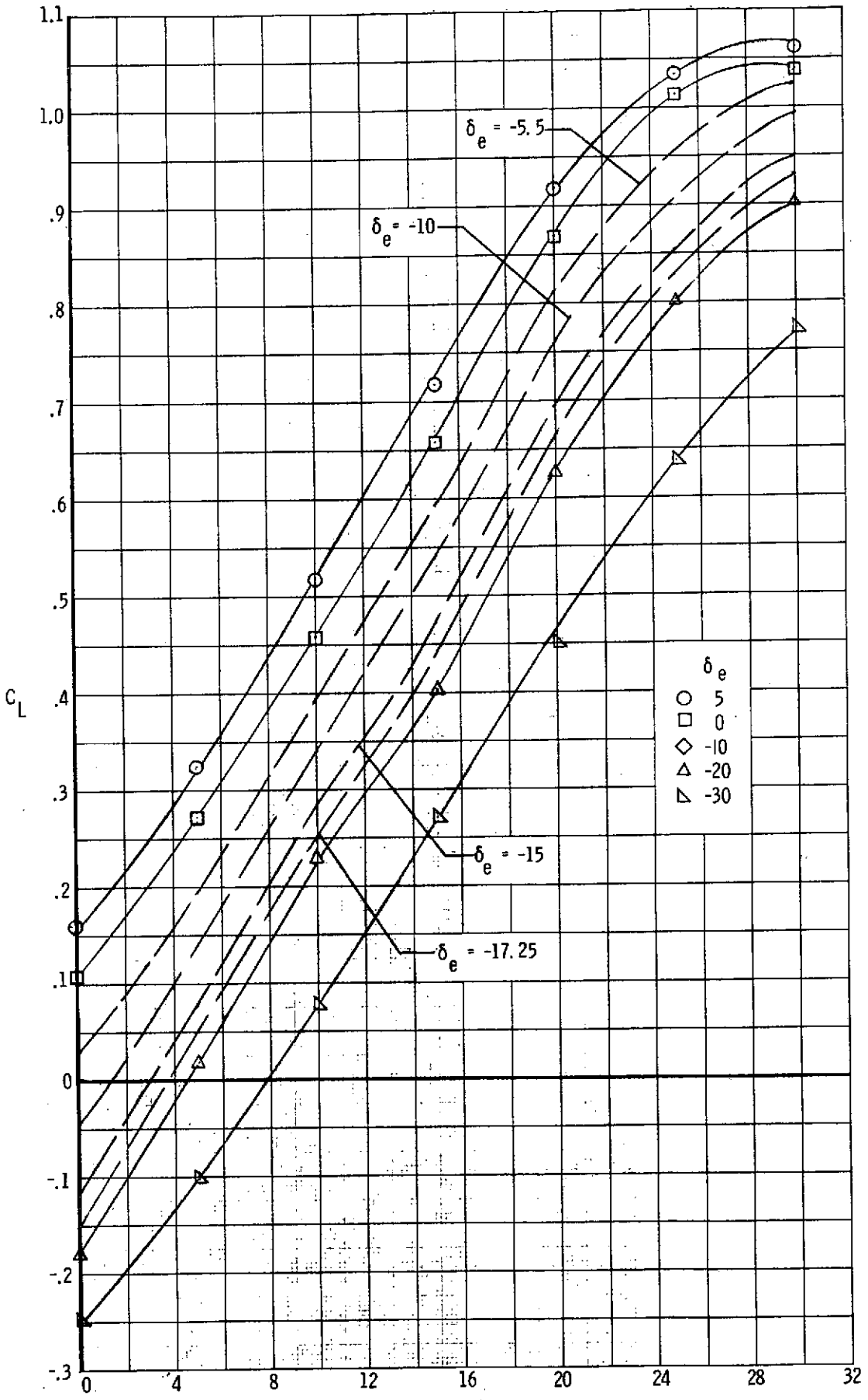

(a) Lift

Figure 11. - Longitudinal characteristics of $B_1W_1V_TF_DE$.

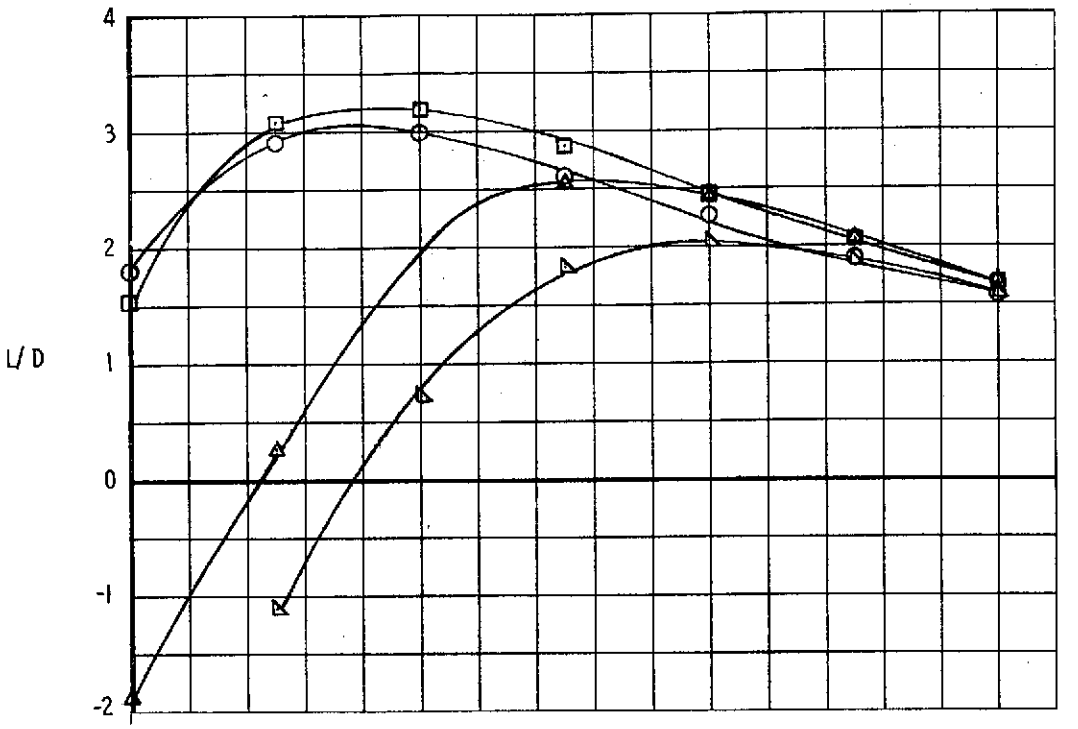

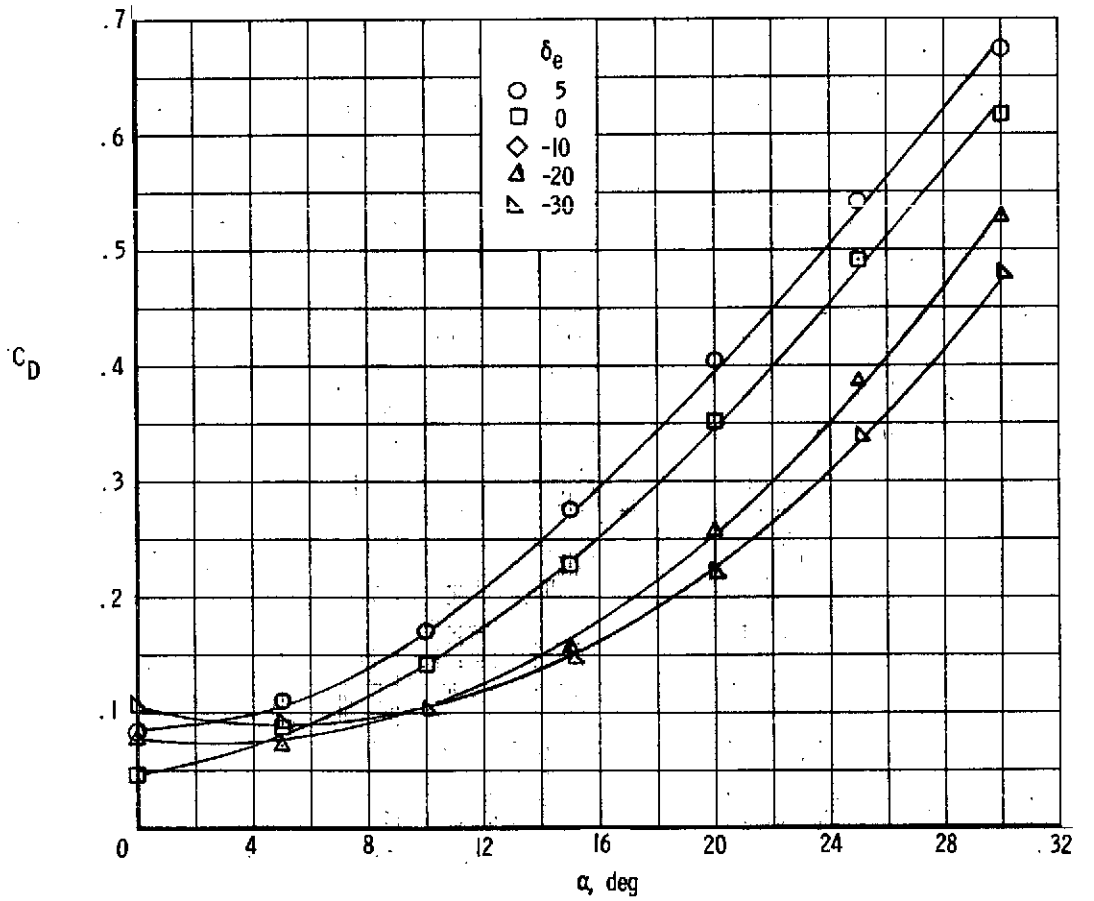

(b) Drag and lift-drag ratio

Figure 11. - Continued.

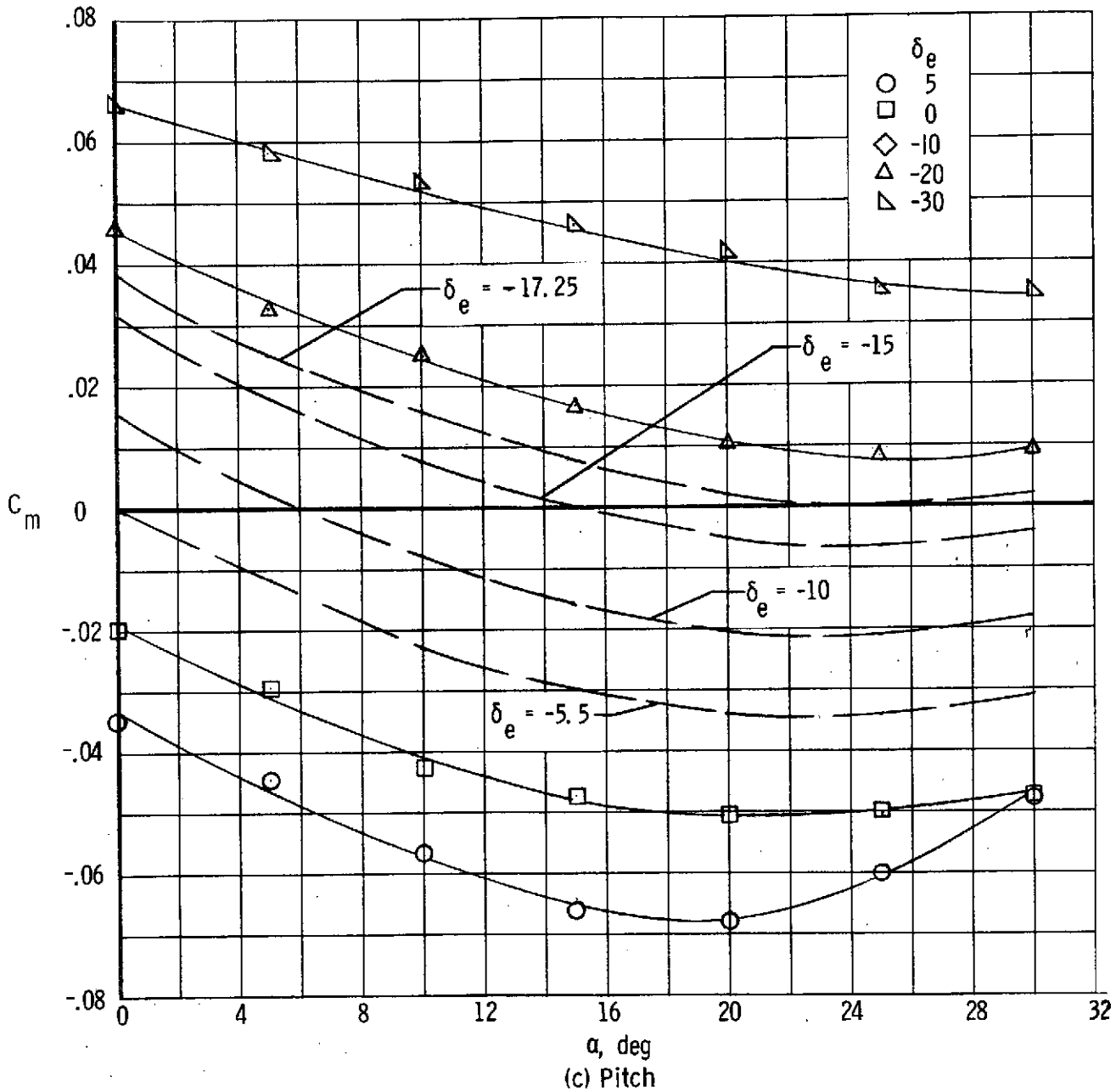

(c) Pitch

Figure 11.- Continued.

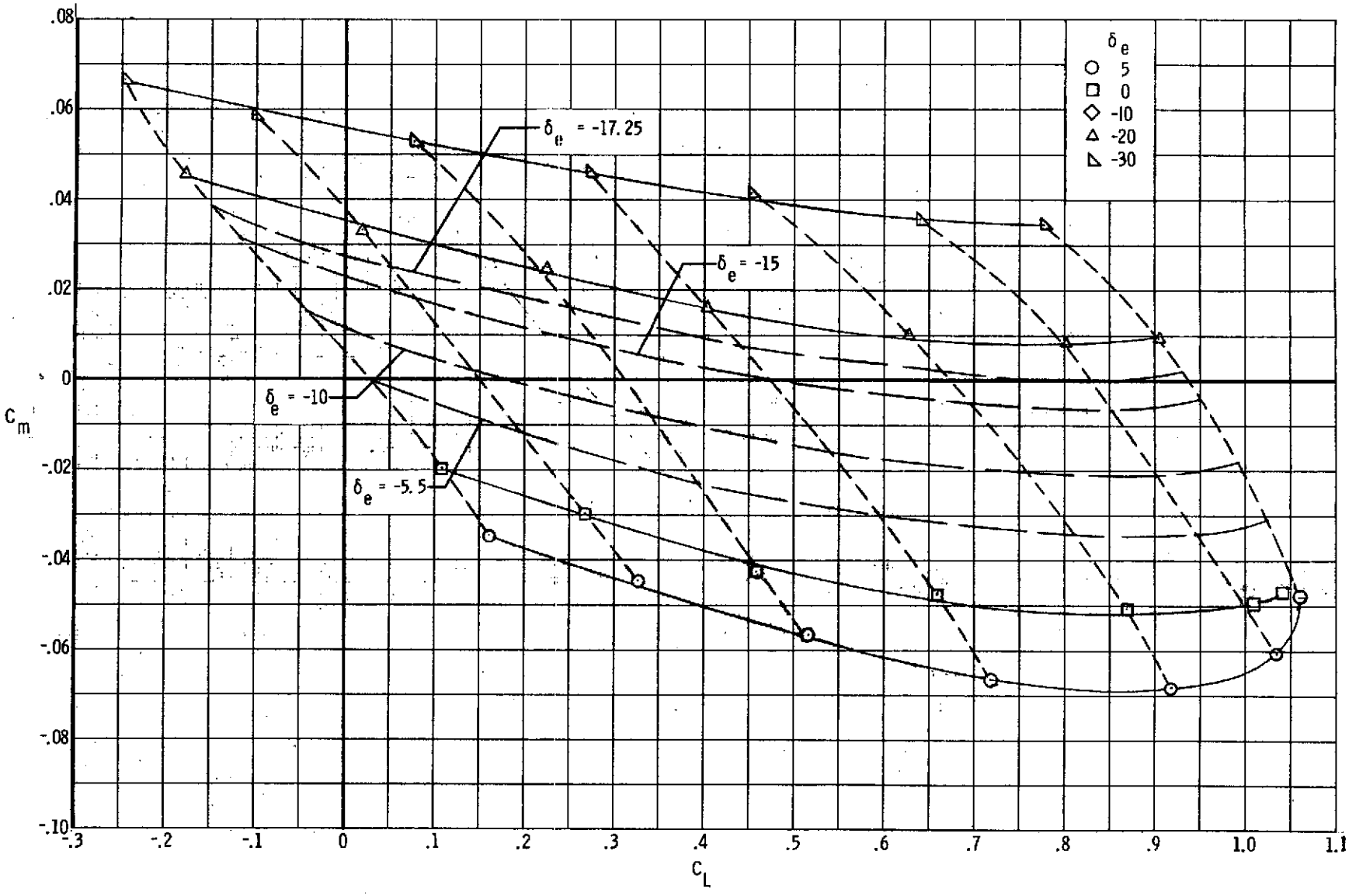

(d) Stability

Figure 11. - Concluded.

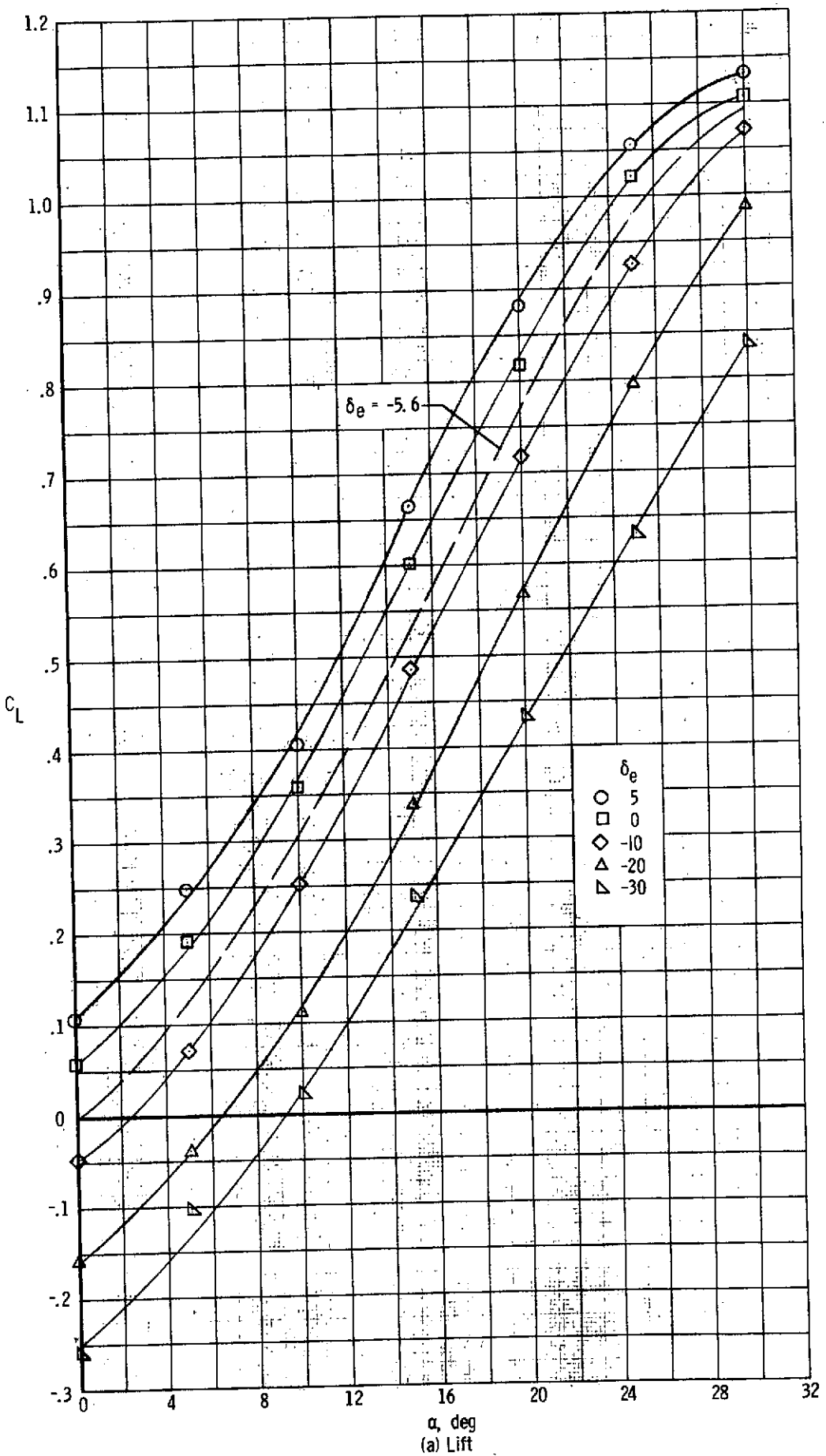

(a) Lift

Figure 12. - Longitudinal characteristics of $B_1W_1V_{c1}$.

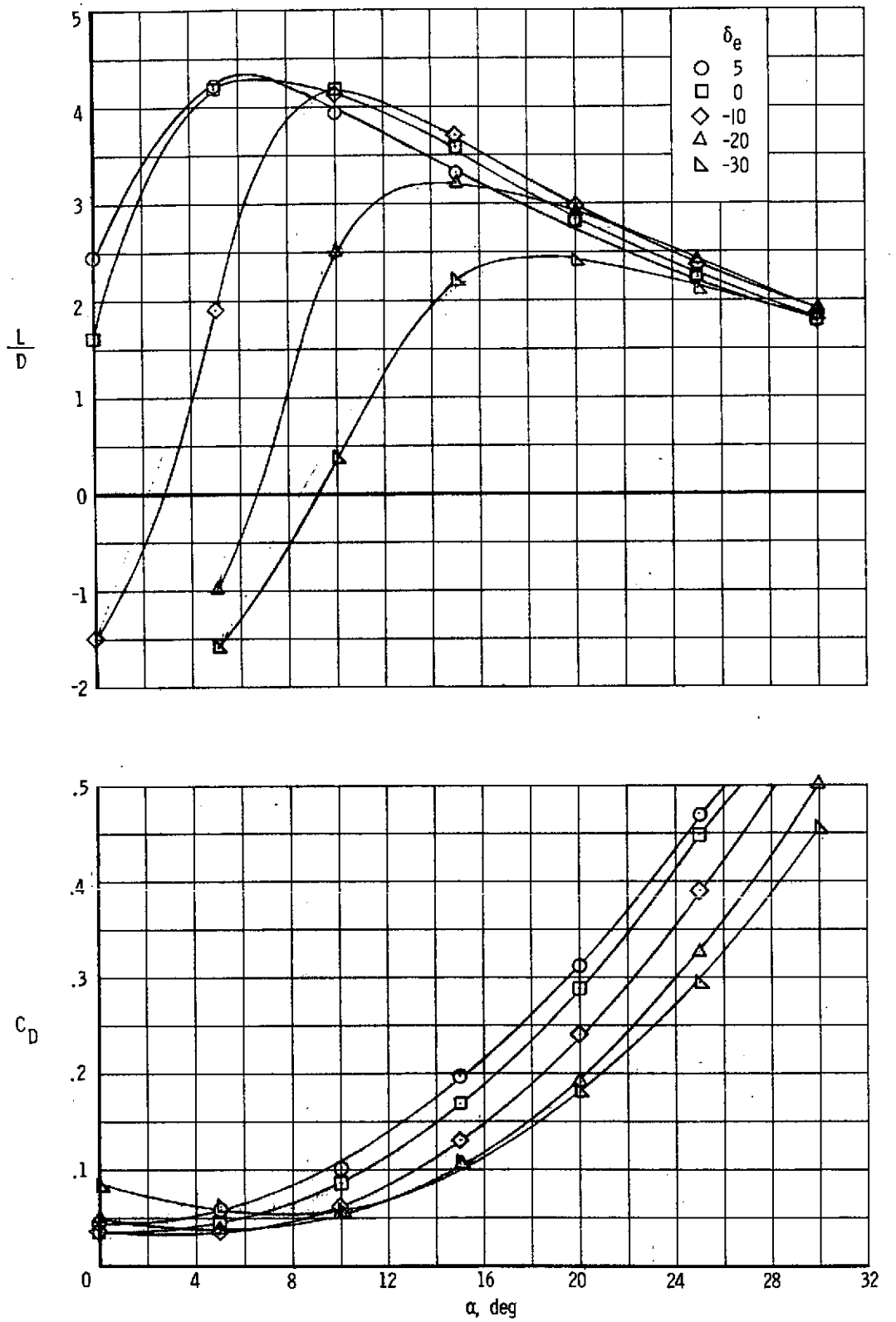

(b) Drag and lift-drag ratio.

Figure 12. - Continued.

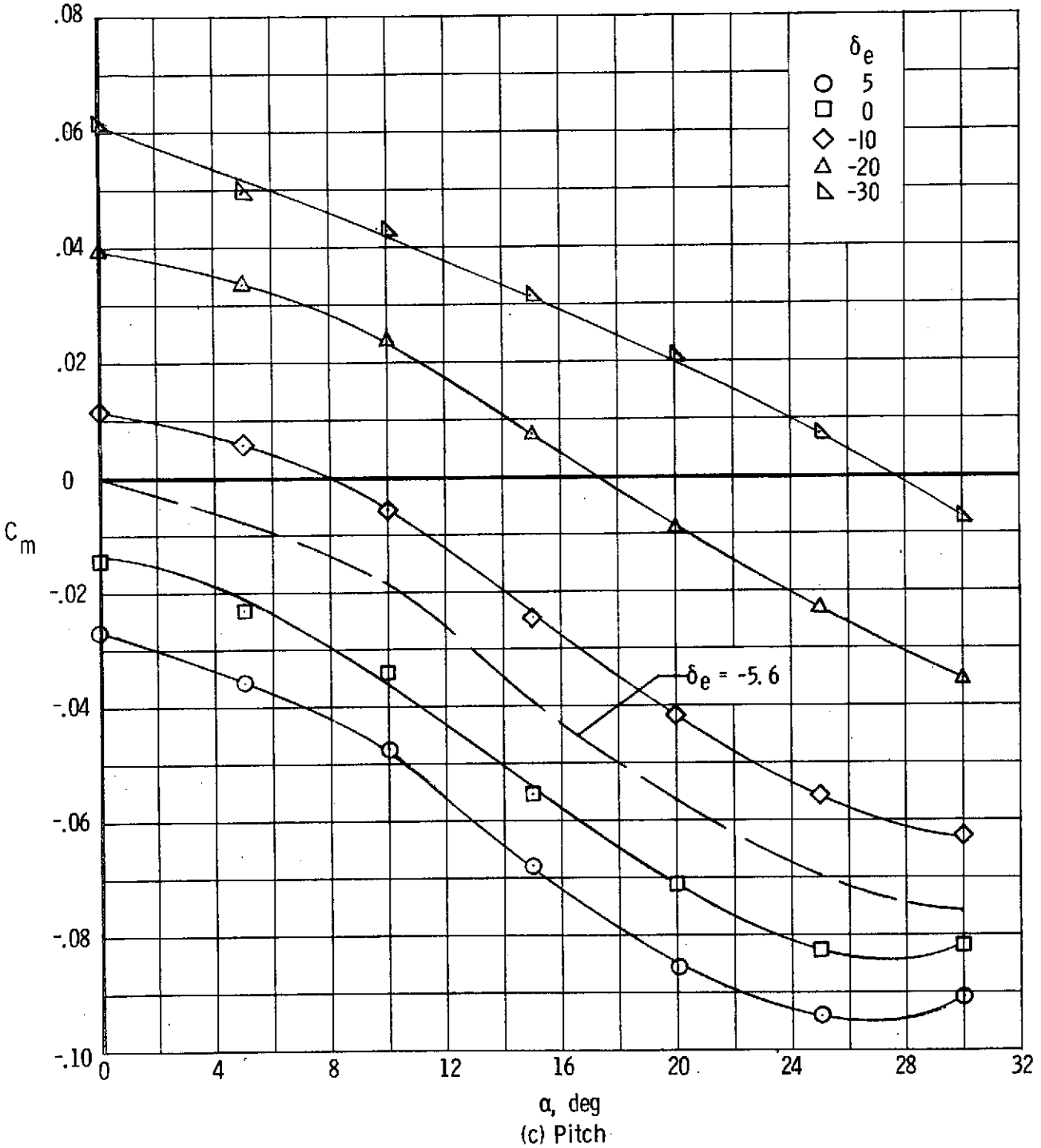

(c) Pitch

Figure 12. - Continued.

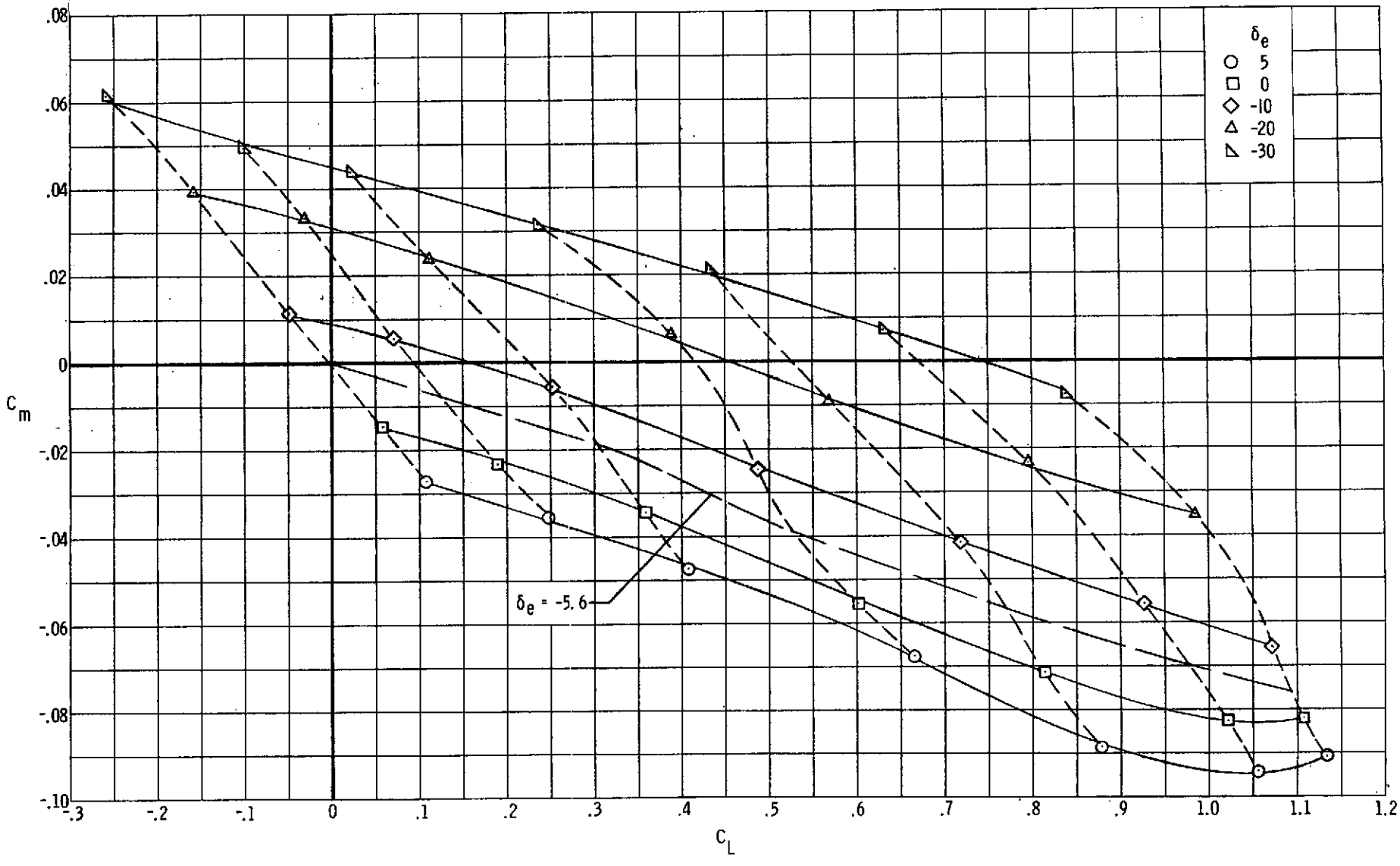

(d) Stability

Figure 12. - Concluded.

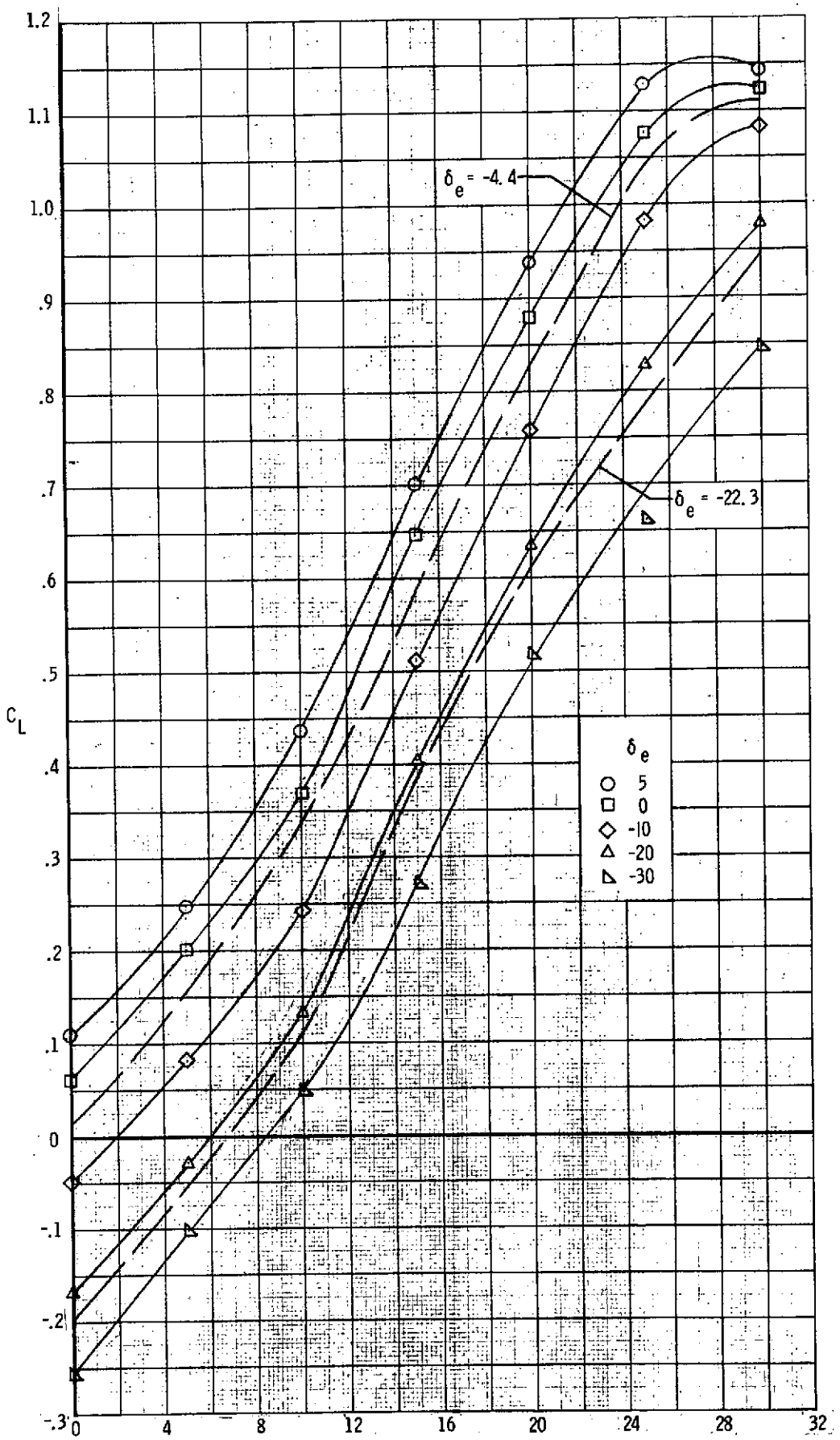

(a) Lift

Figure 13. - Longitudinal characteristics of $B_1W_1V_{c1}F_D$.

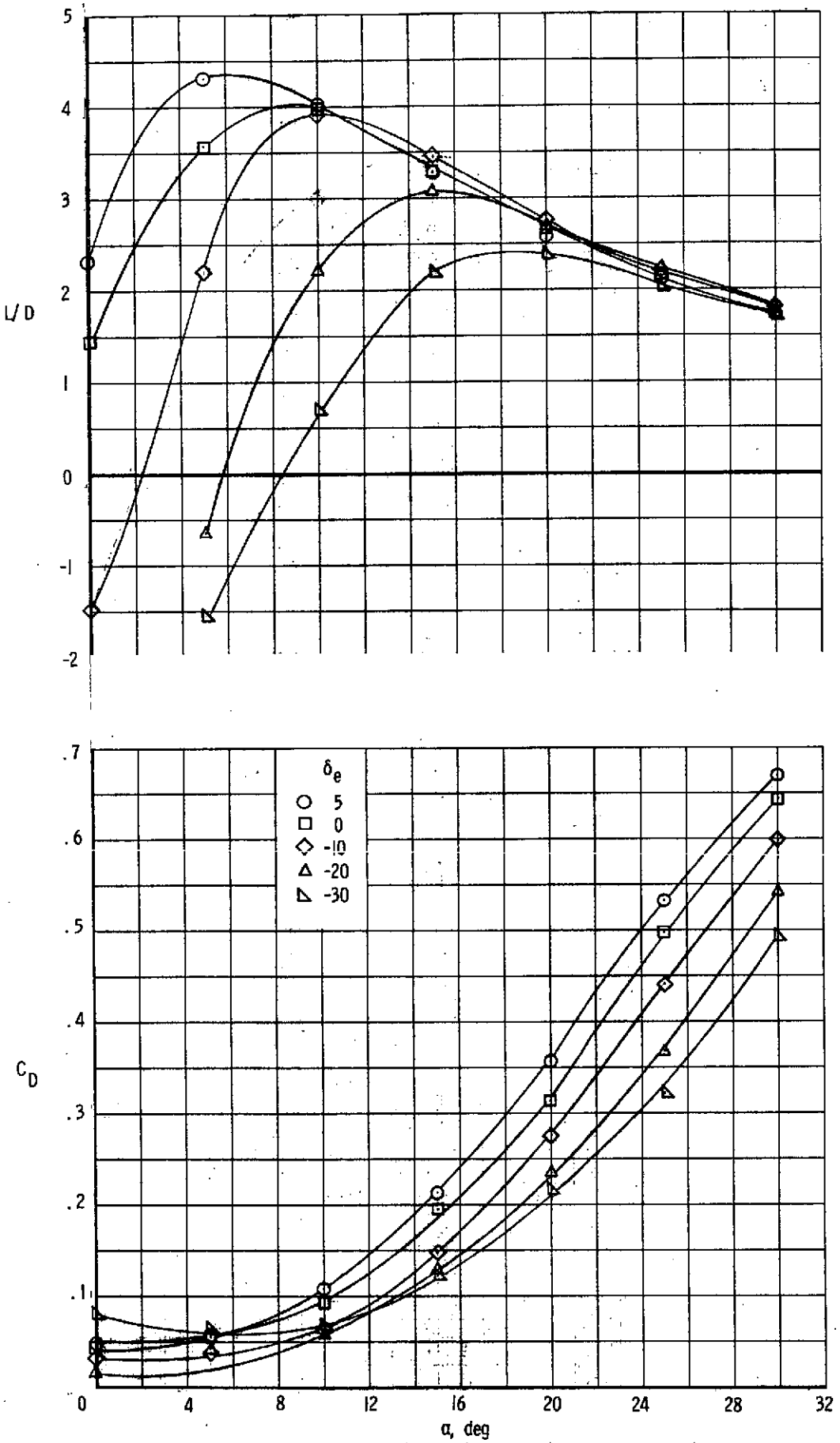

(b) Drag and lift-drag ratio

Figure 13. - Continued.

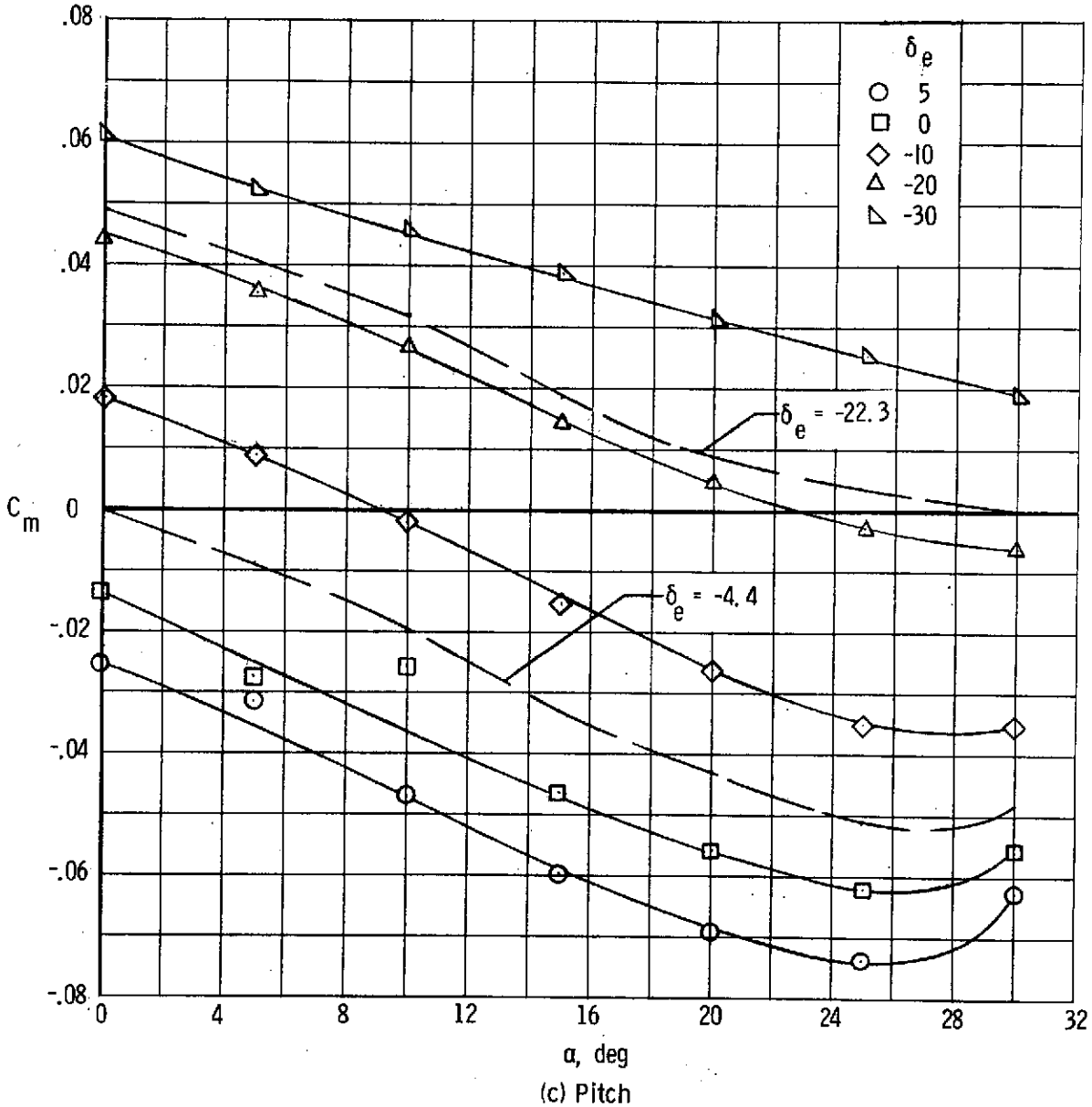

(c) Pitch

Figure 13. - Continued.

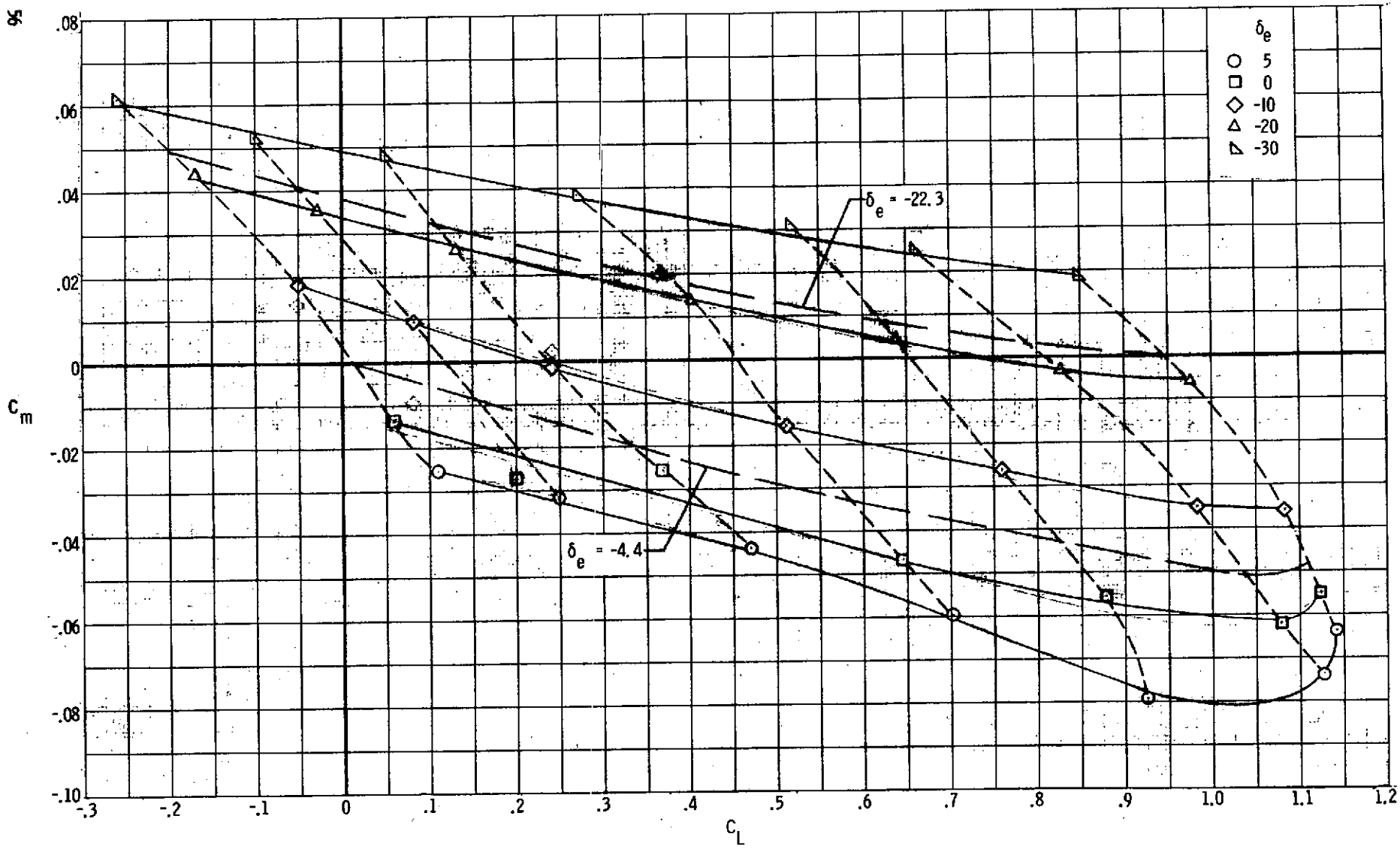

(d) Stability

Figure 13. - Concluded.

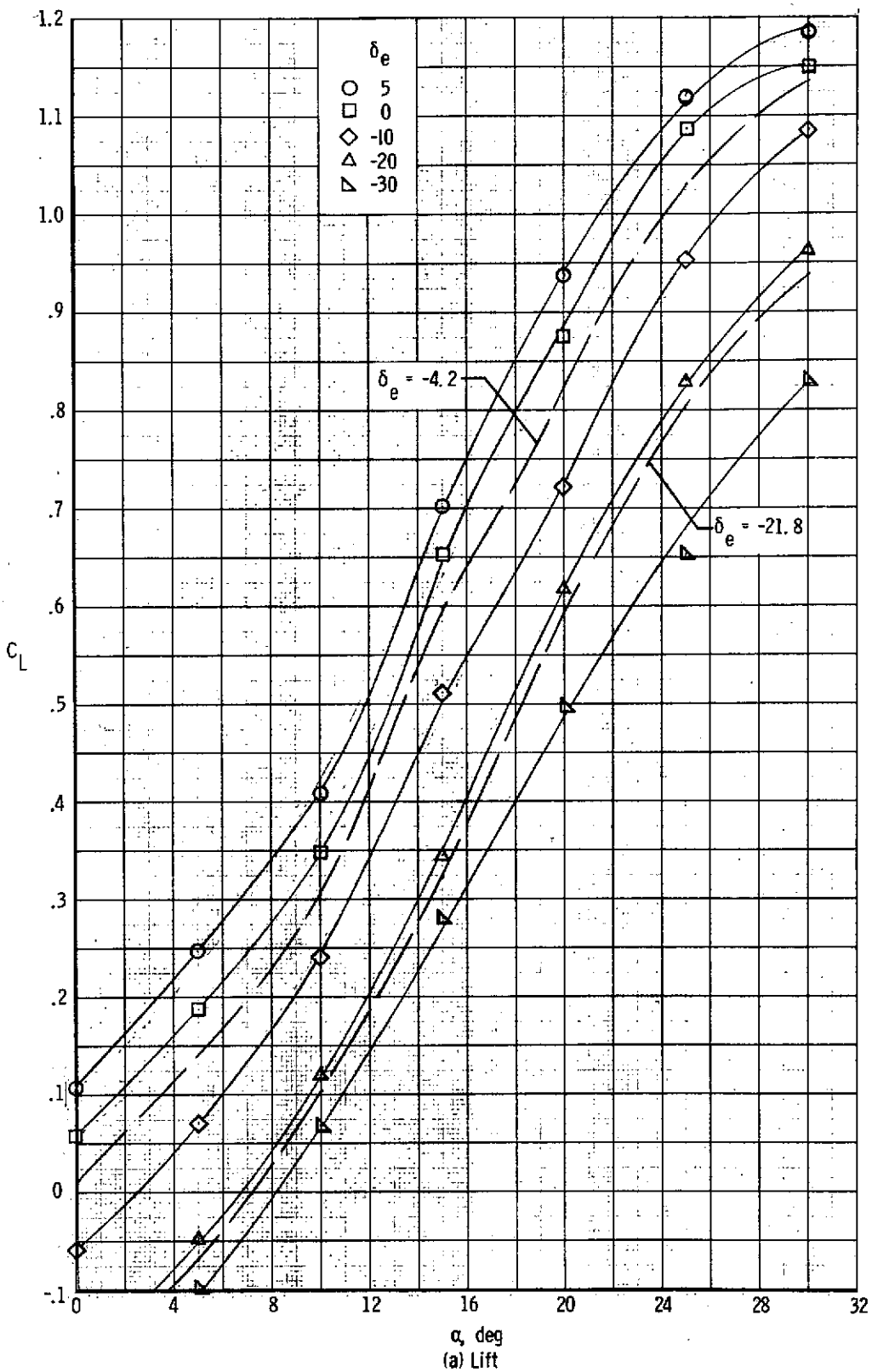

(a) Lift

Figure 14. - Longitudinal characteristics of $B_1W_1V_{c2}F_D$.

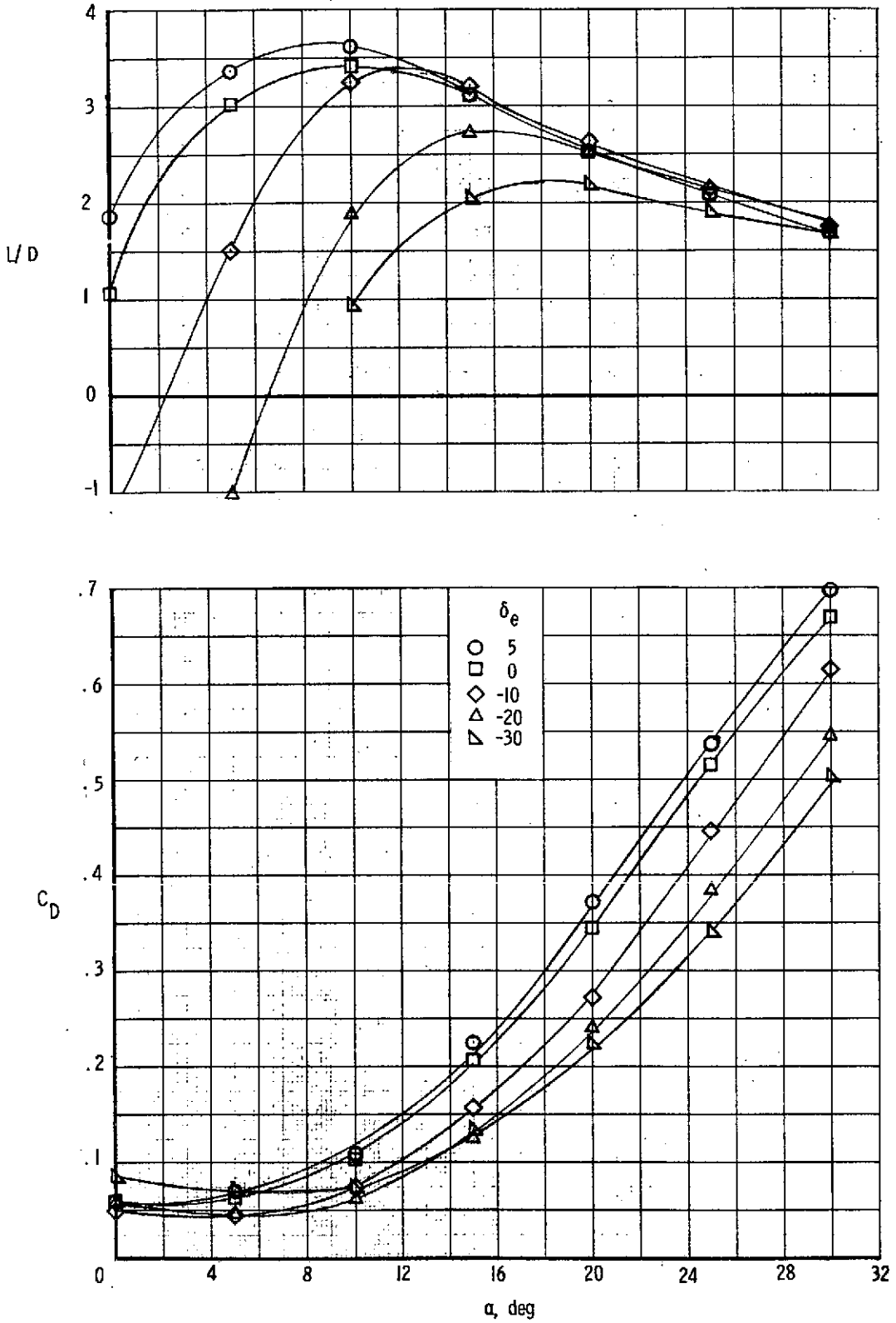

(b) Drag and lift-drag ratio

Figure 14. - Continued.

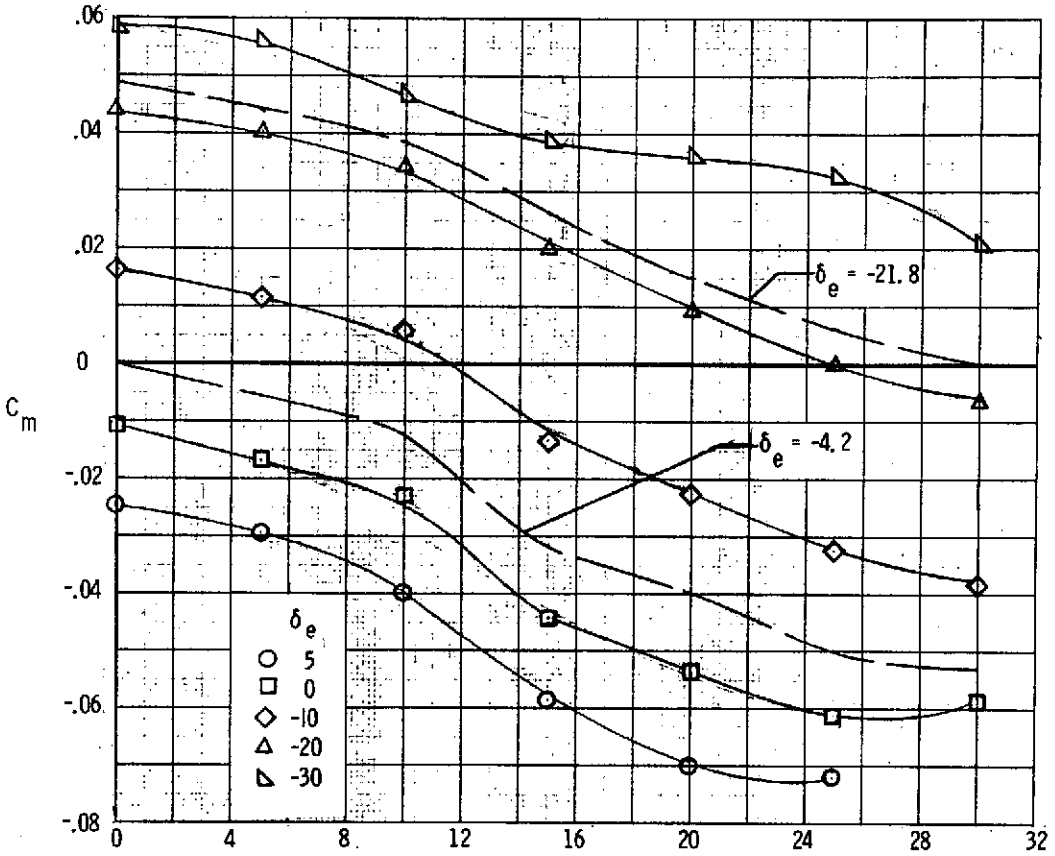

(c) Pitch

Figure 14. - Continued.

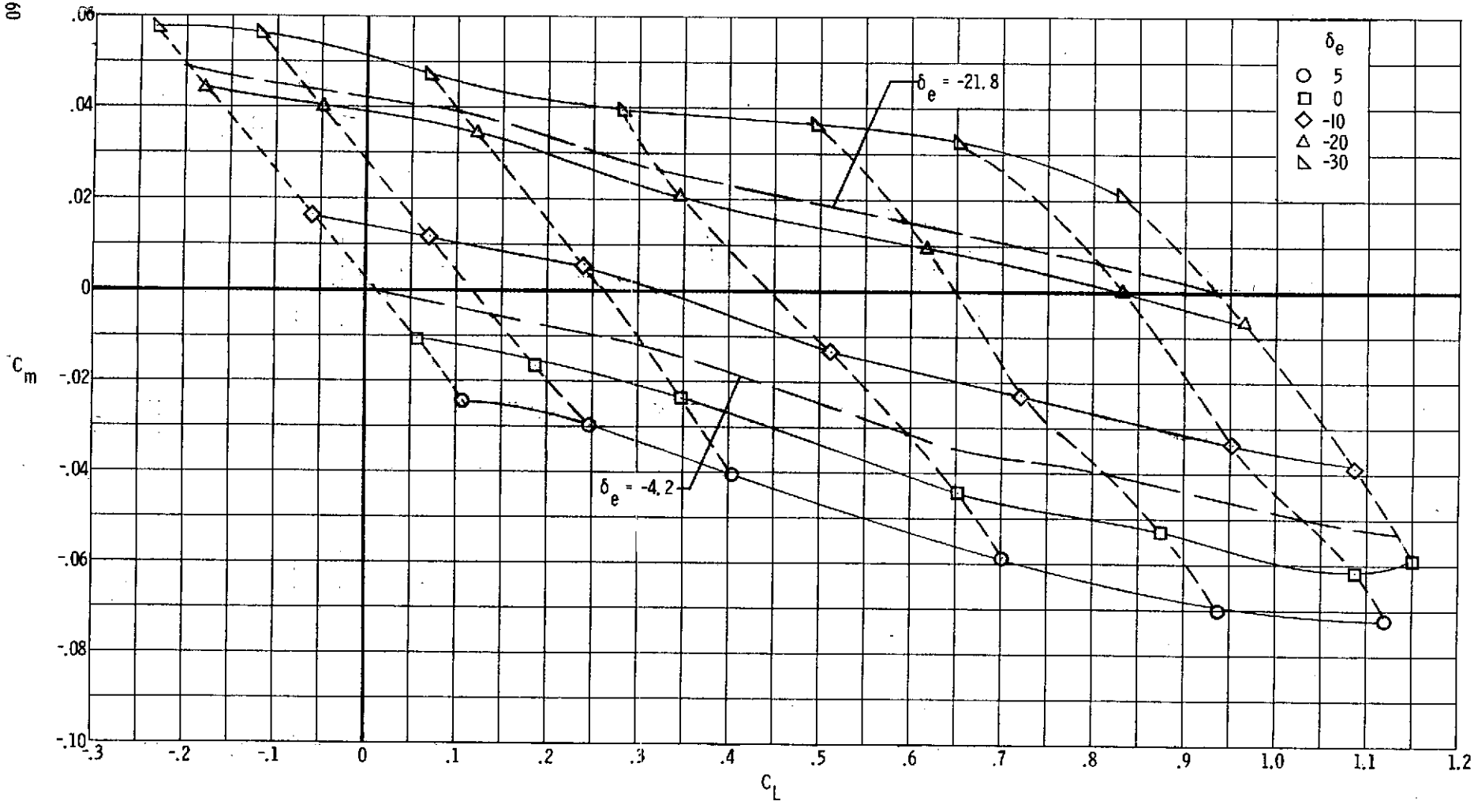

(d) Stability

Figure 14. - Concluded.

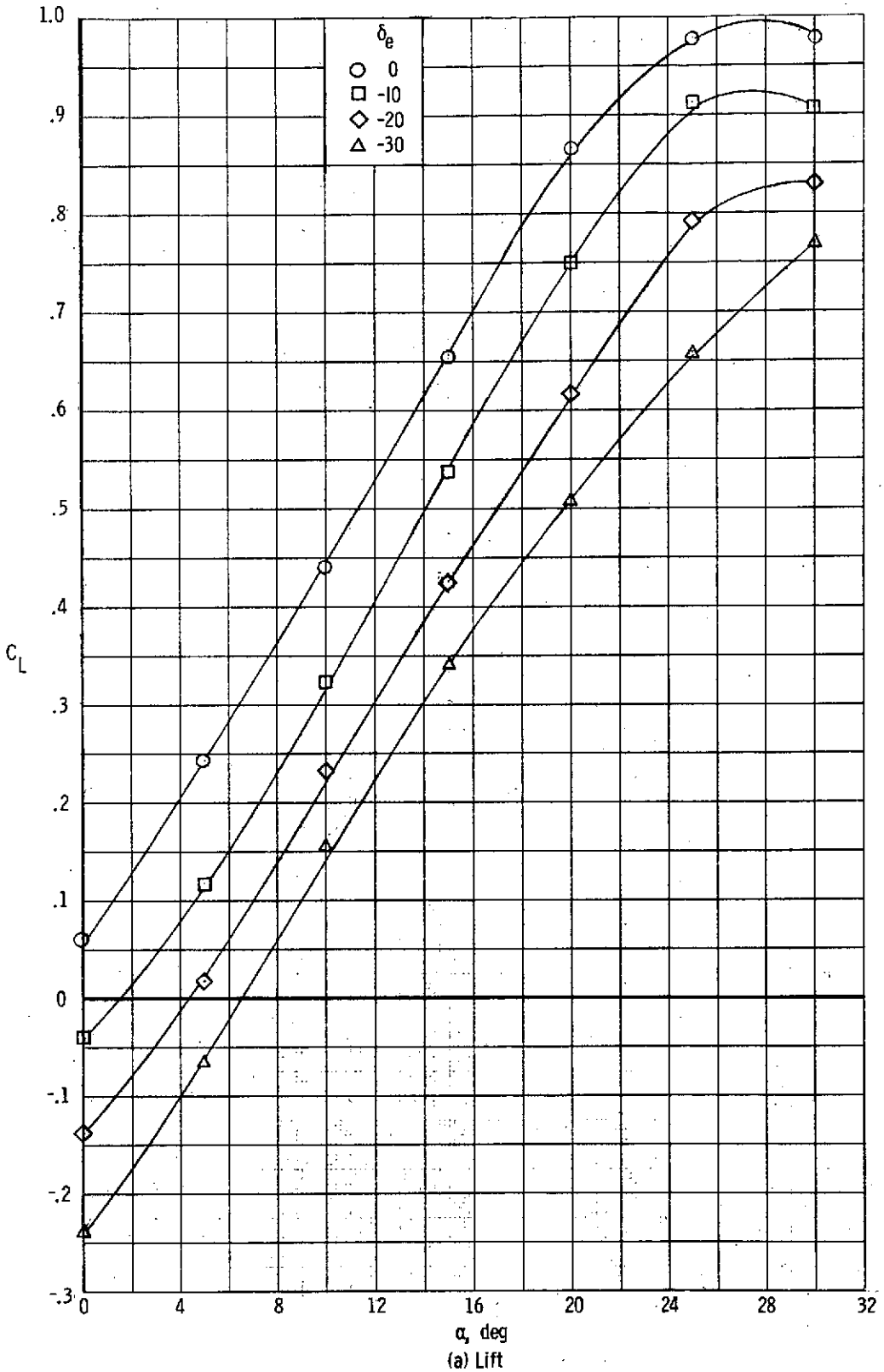

(a) Lift

Figure 15. - Longitudinal characteristics of B_1W_2E.

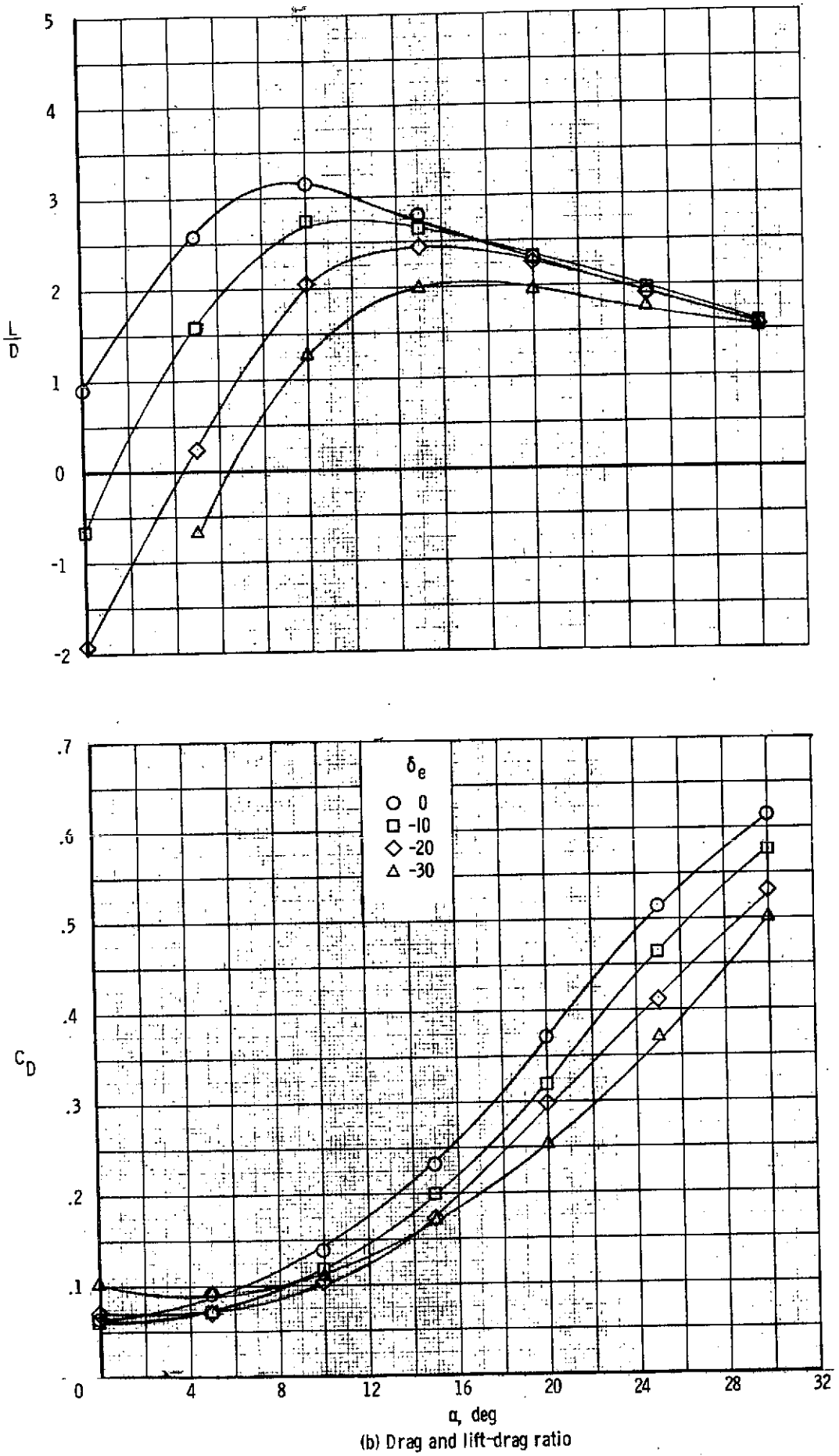

(b) Drag and lift-drag ratio

Figure 15. - Continued.

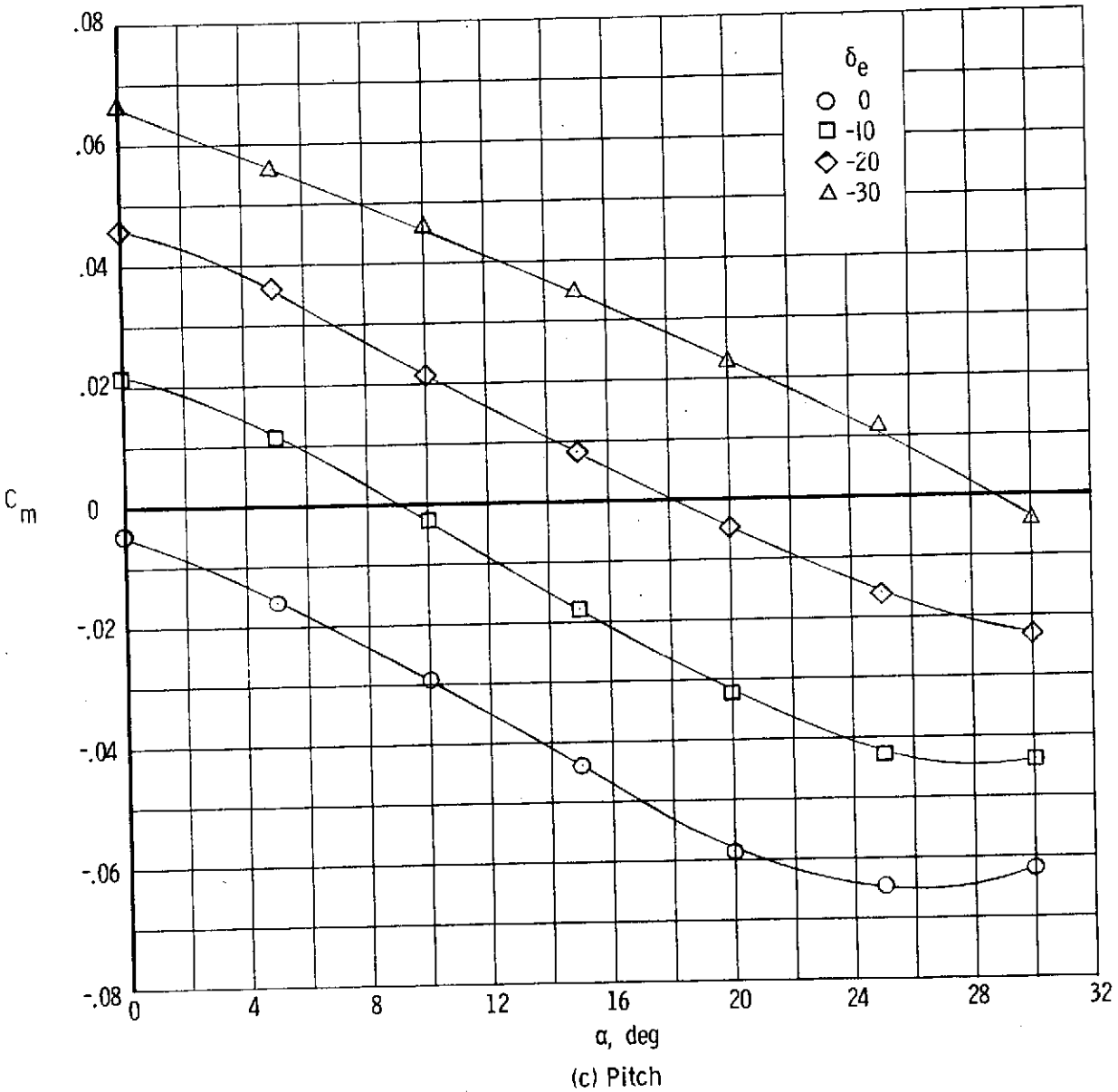

(c) Pitch

Figure 15. - Continued.

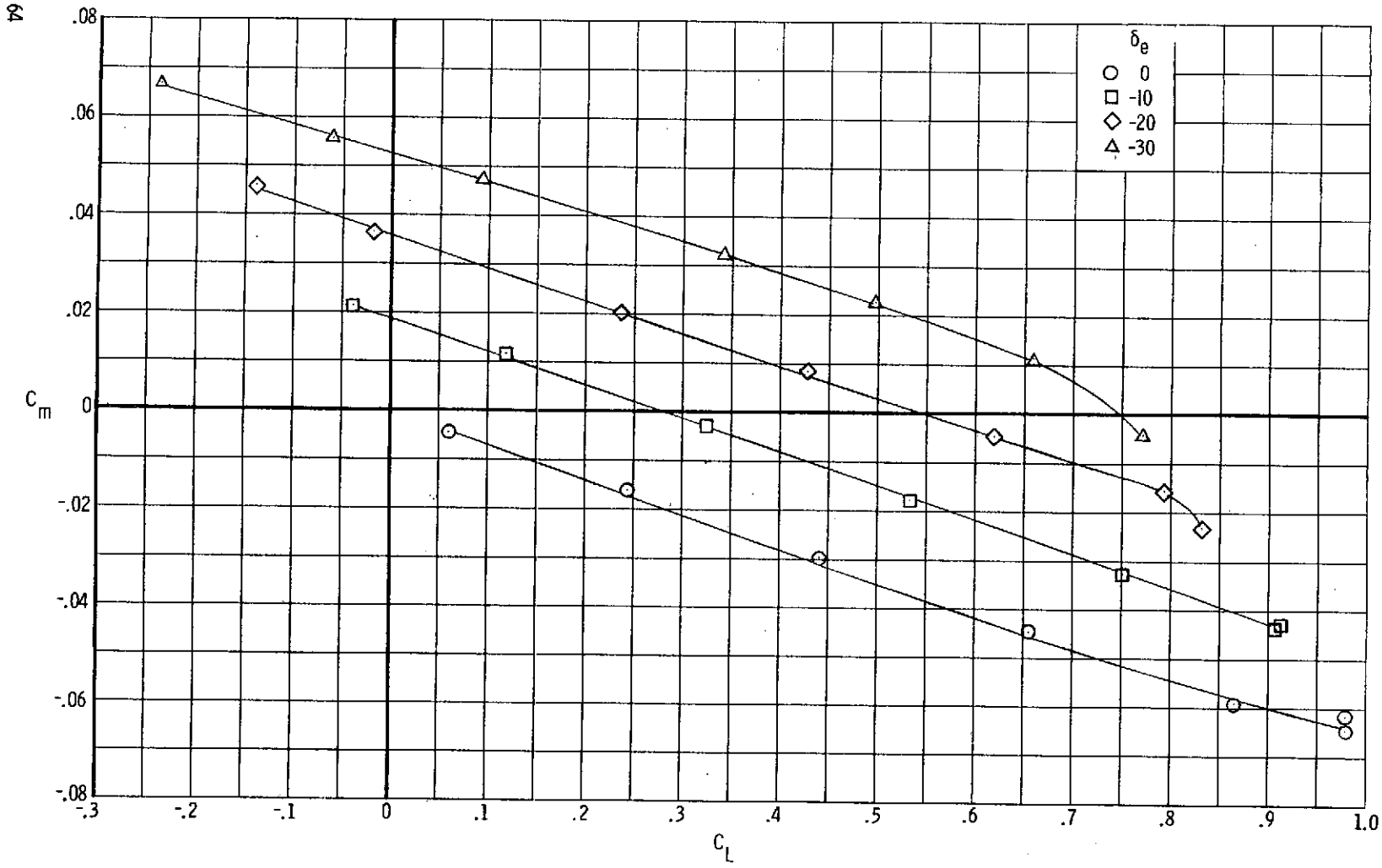

(d) Stability

Figure 15. - Concluded.

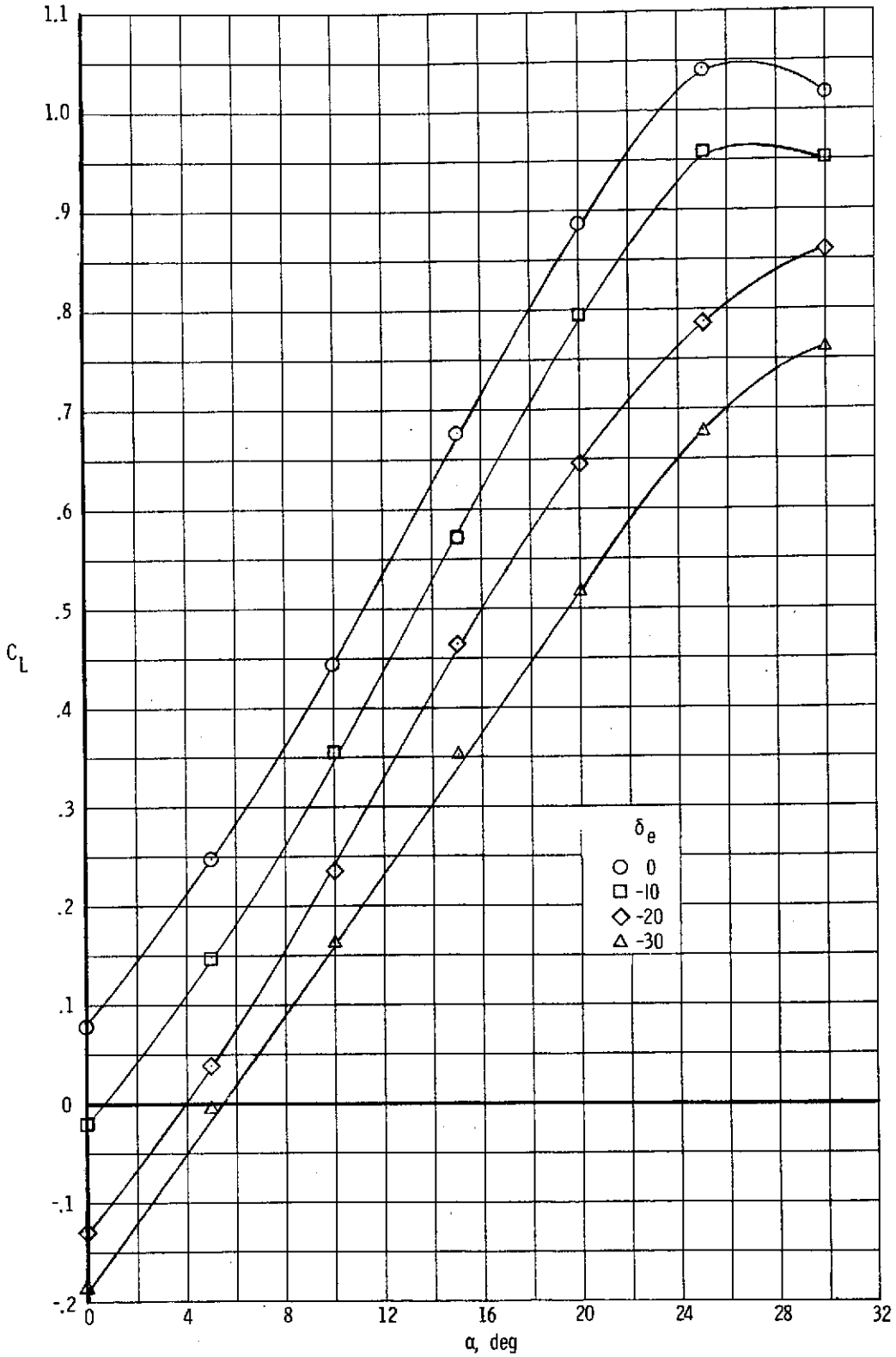

(a) Lift

Figure 16. - Longitudinal characteristics of B_3W_2E.

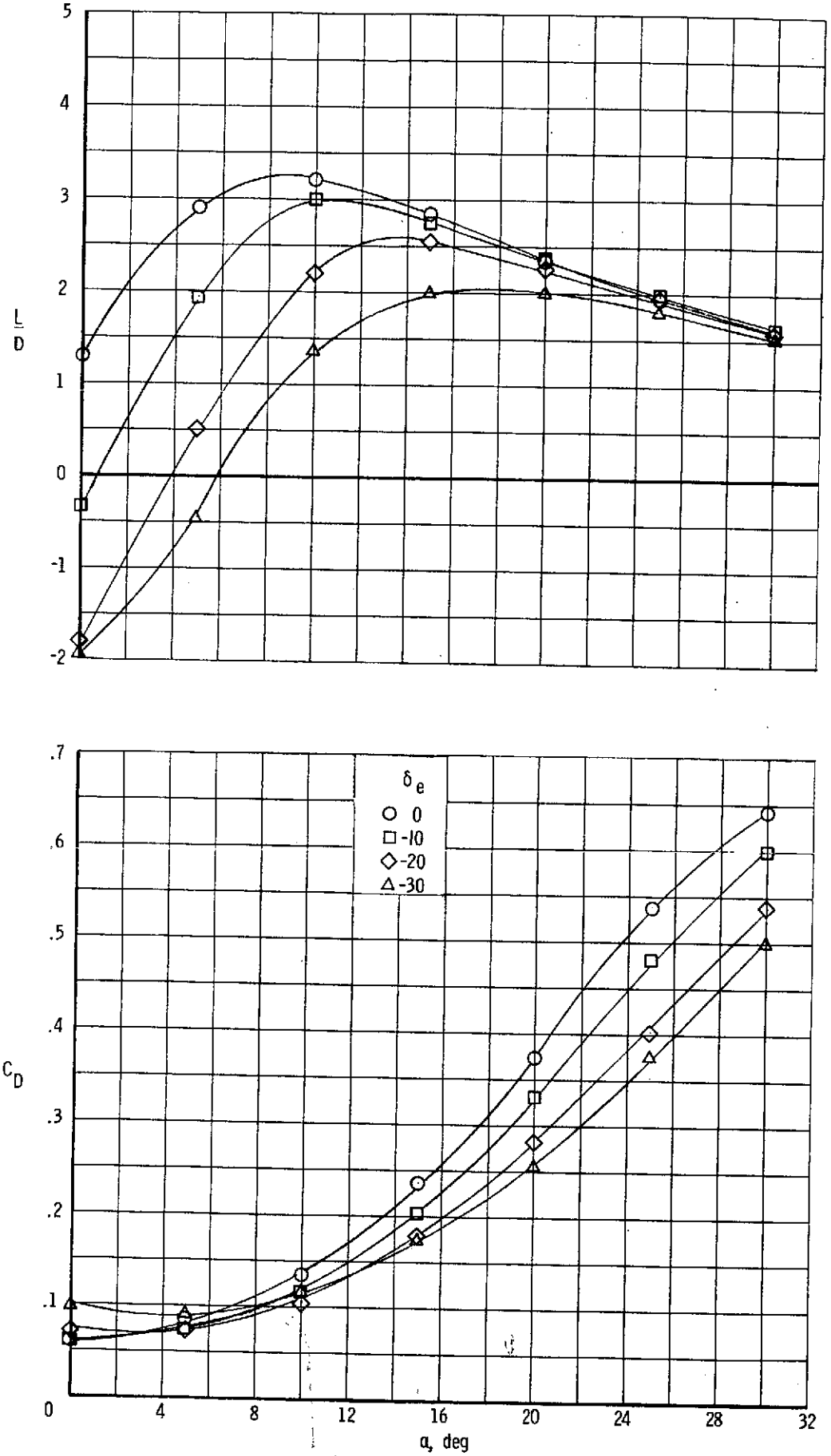

(b) Drag and lift-drag ratio

Figure 16. - Continued.

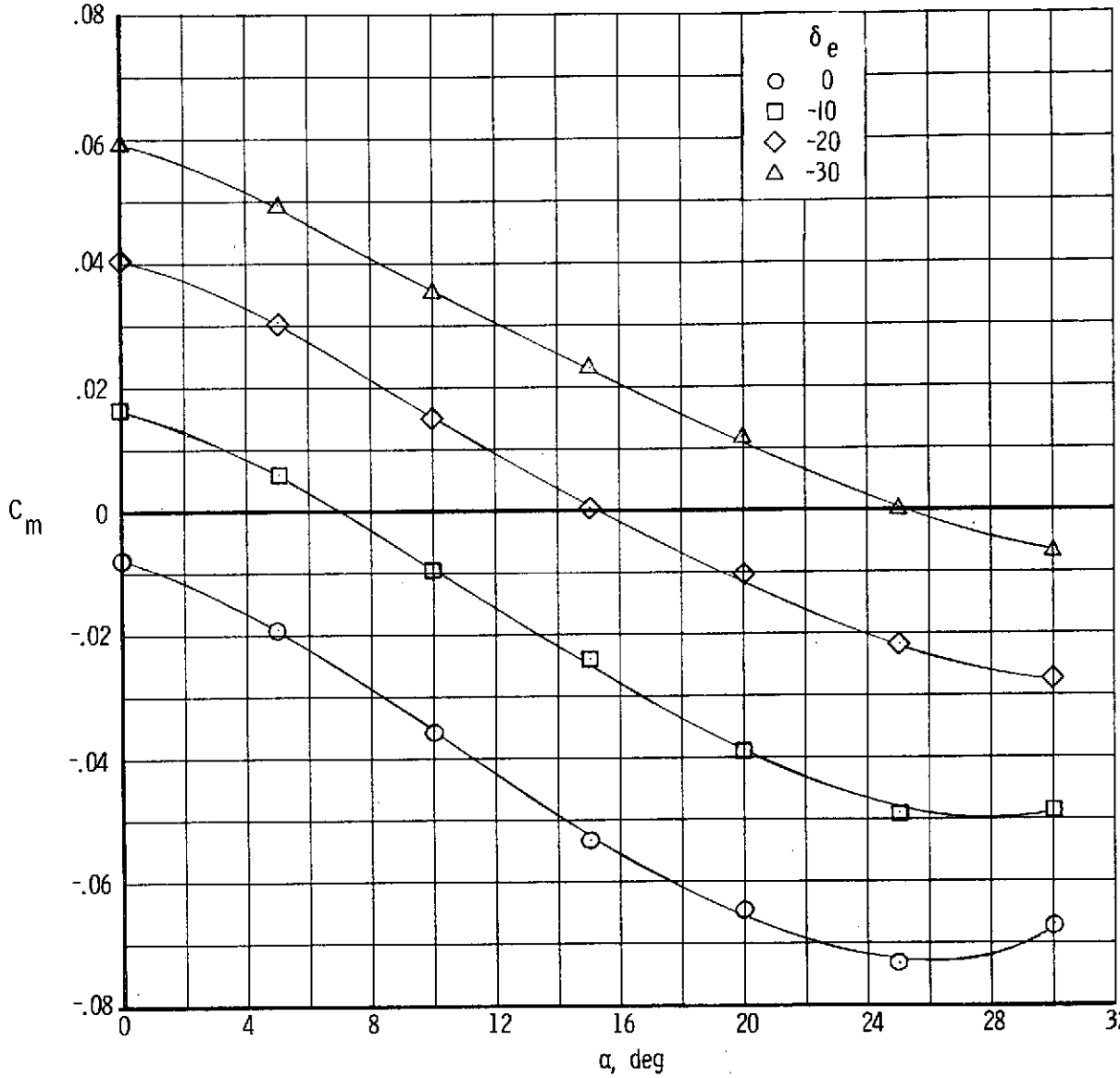

(c) Pitch

Figure 16. - Continued.

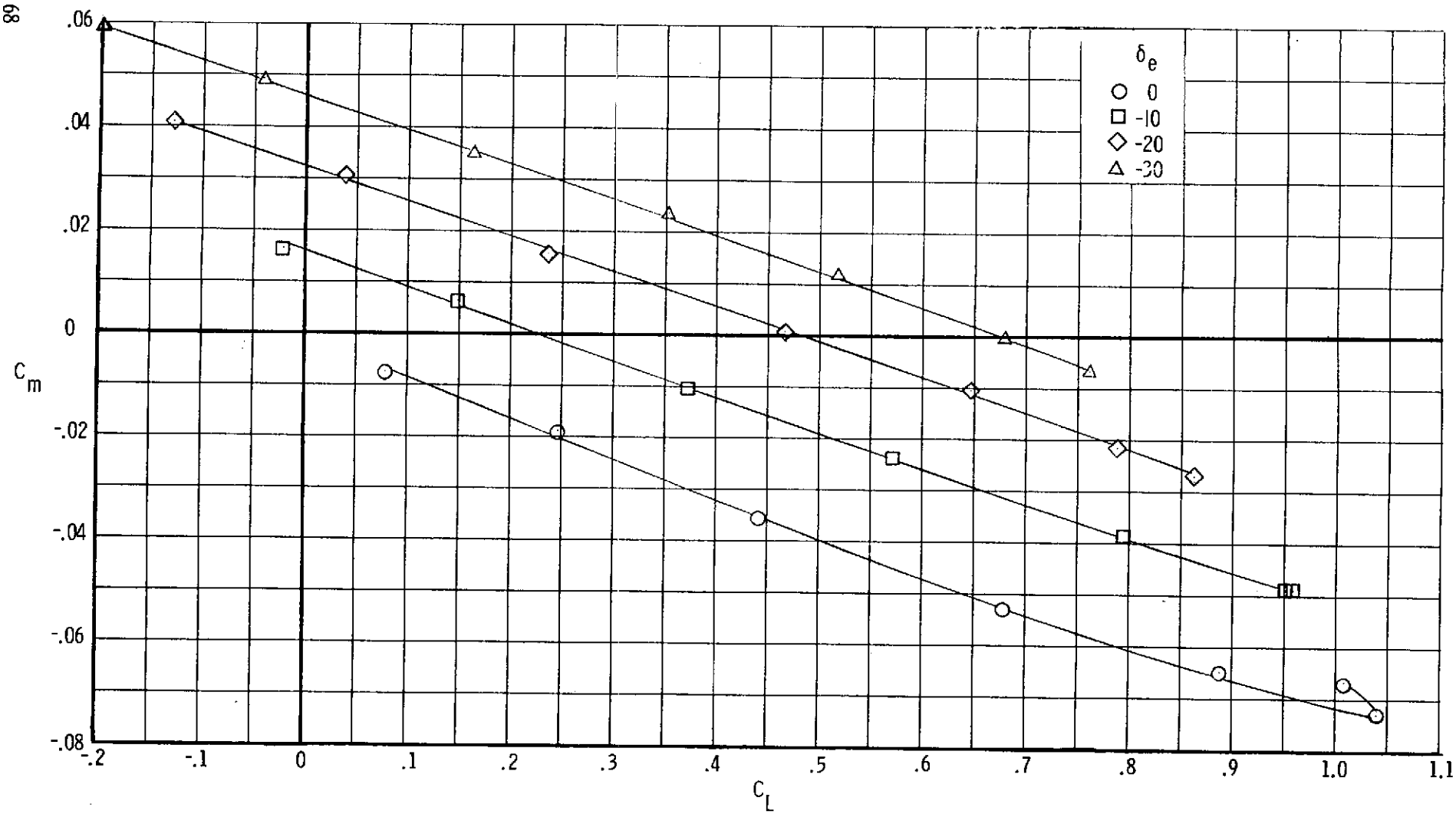

(d) Stability

Figure 16. - Concluded.

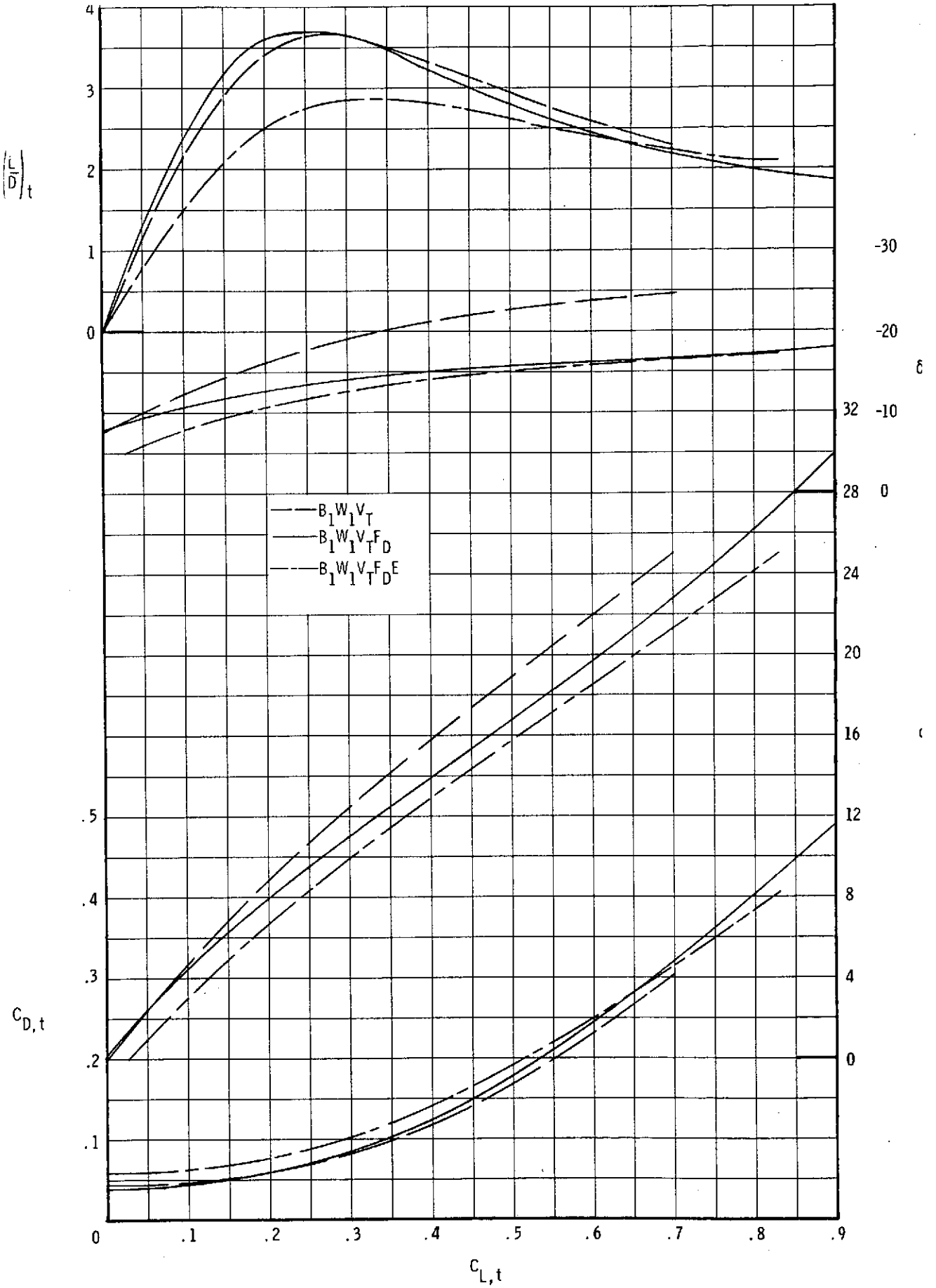

(a) Lift, drag and lift-drag ratio

Figure 17. - Longitudinal characteristics at trim of $B_1W_1V_T$, $B_1W_1V_TF_D$, and $B_1W_1V_TF_DE$.

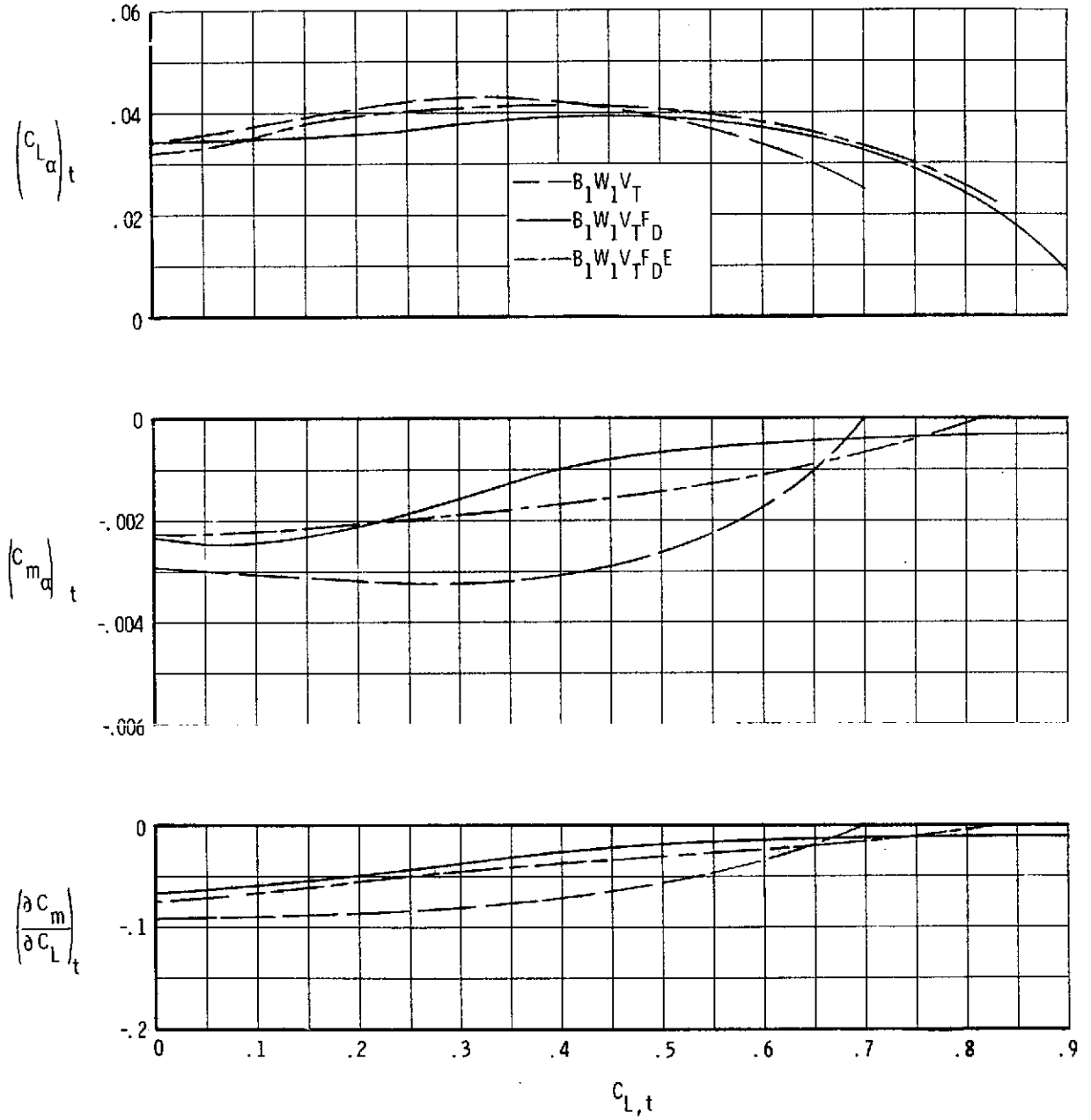

(b) Lift, pitch curve slopes and longitudinal stability

Figure 17. - Concluded.

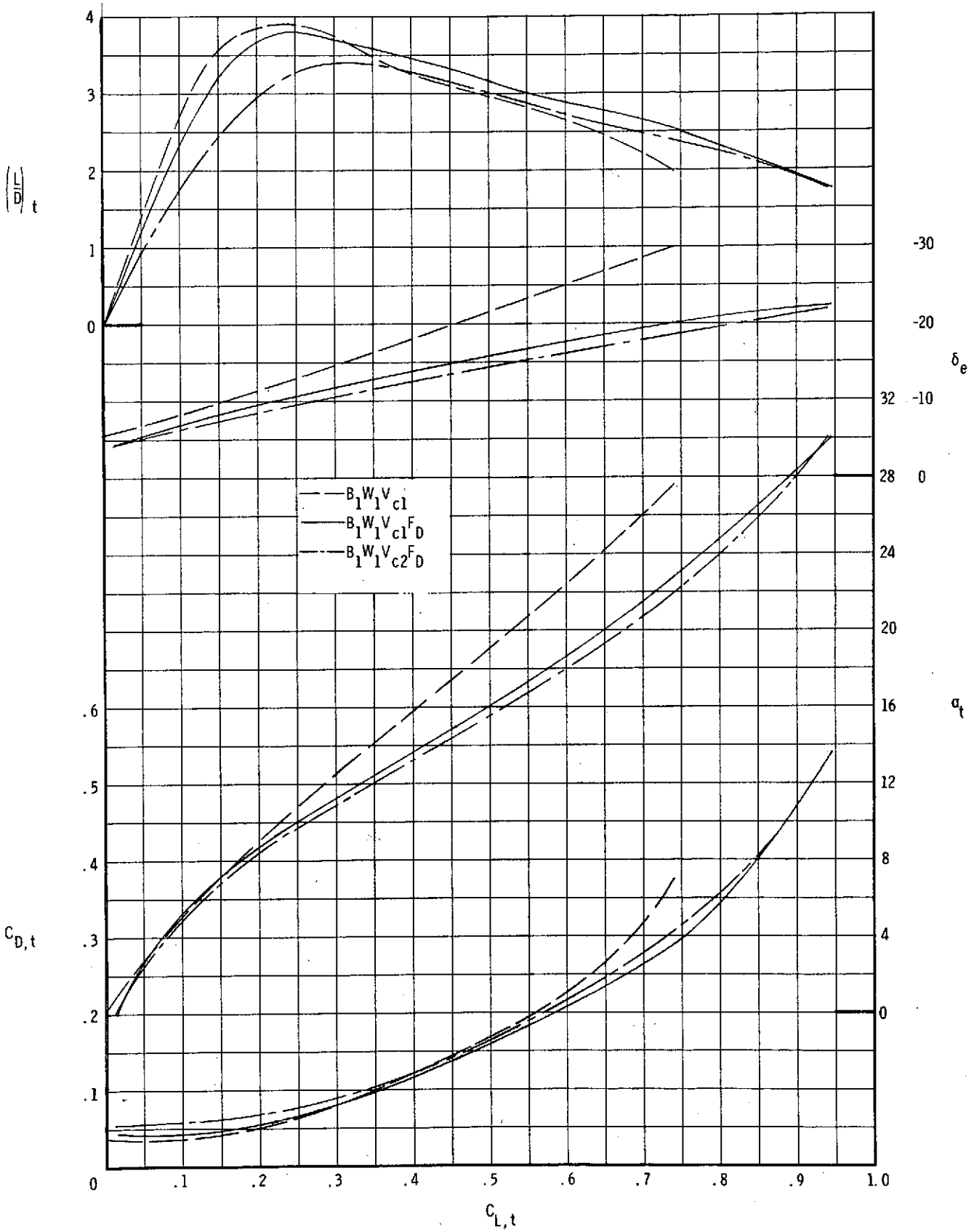

(a) Lift, drag and lift-drag ratio.

Figure 18. - Longitudinal characteristics at trim of $B_1W_1V_{c1}$, $B_1W_1V_{c1}F_D$, and $B_1W_1V_{c2}F_D$.

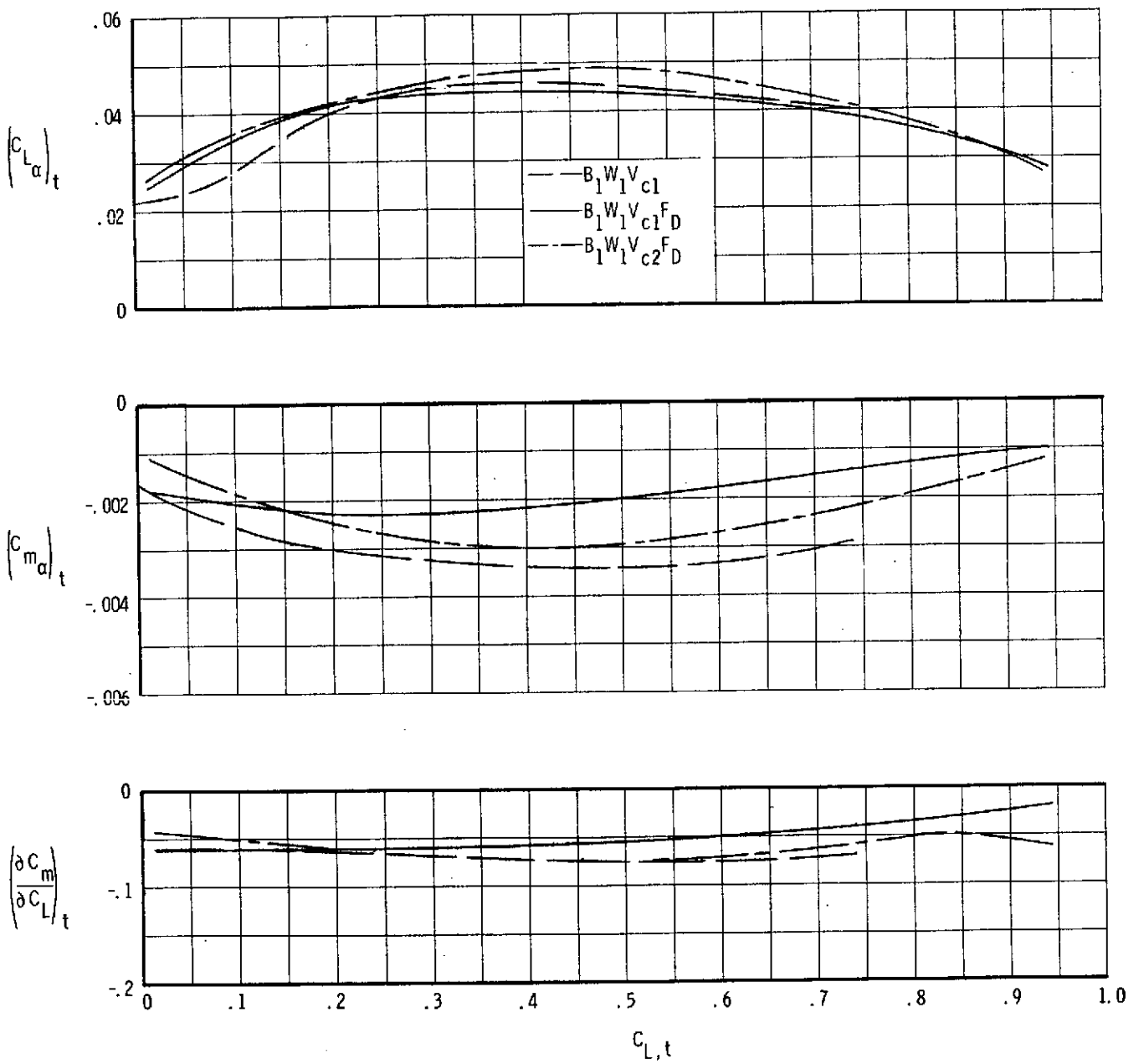

(b) Lift, pitch curve slopes and longitudinal stability.

Figure 18. - Concluded.

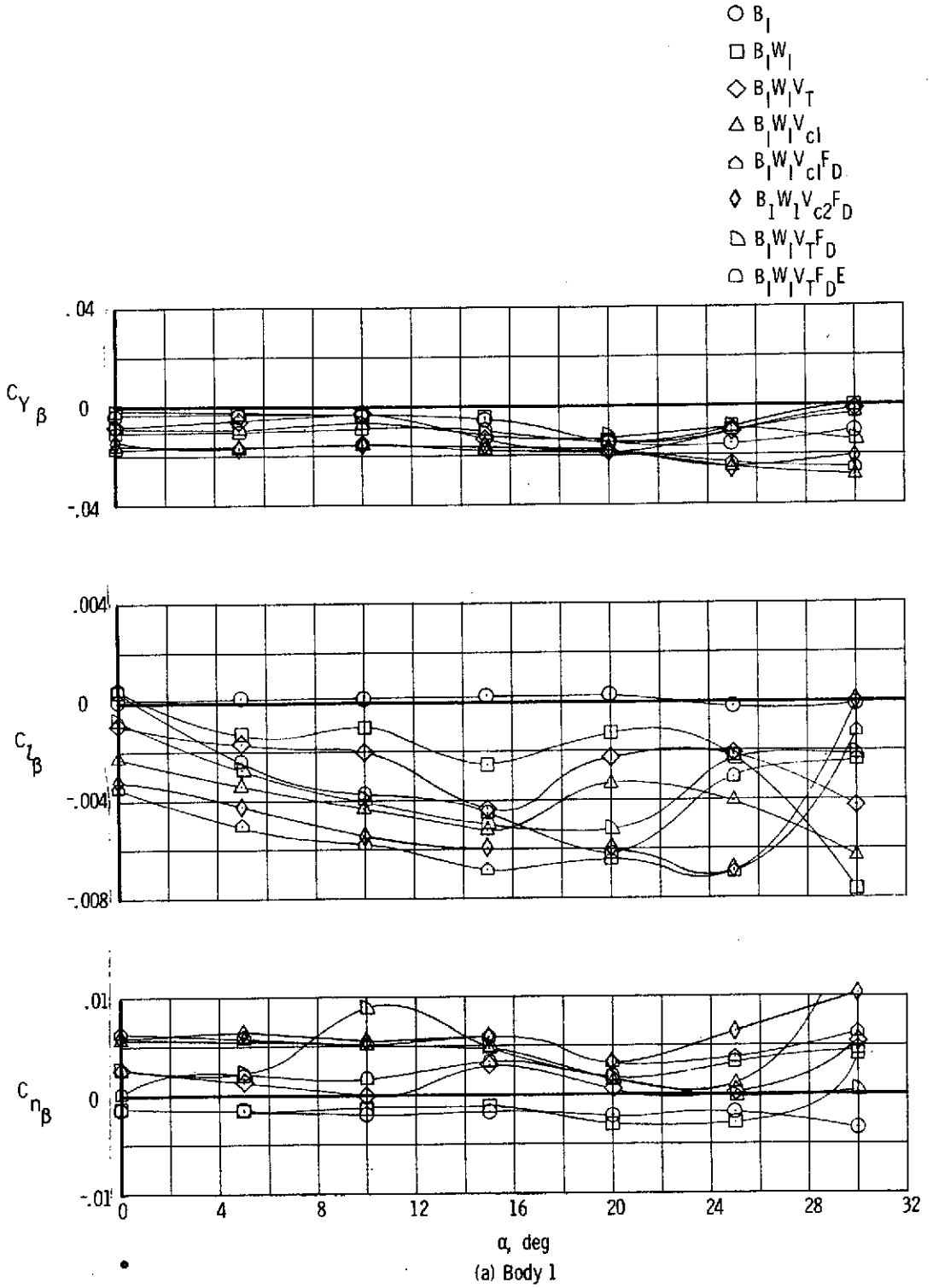

(a) Body 1

Figure 19.- Lateral and directional stability parameters for four bodies B_1, B_2, B_3, B_4.

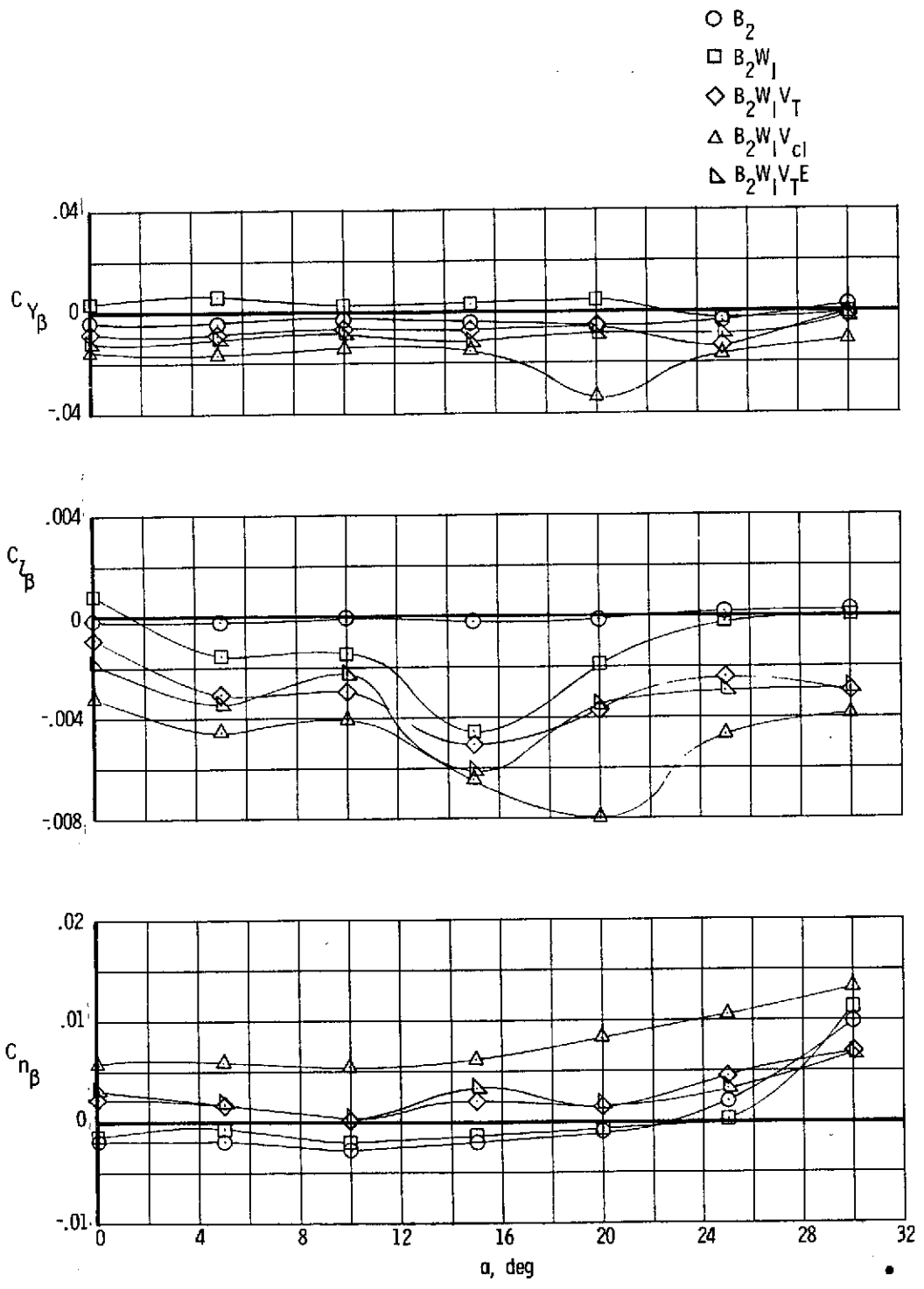

(b) Body 2

Figure 19.- Continued.

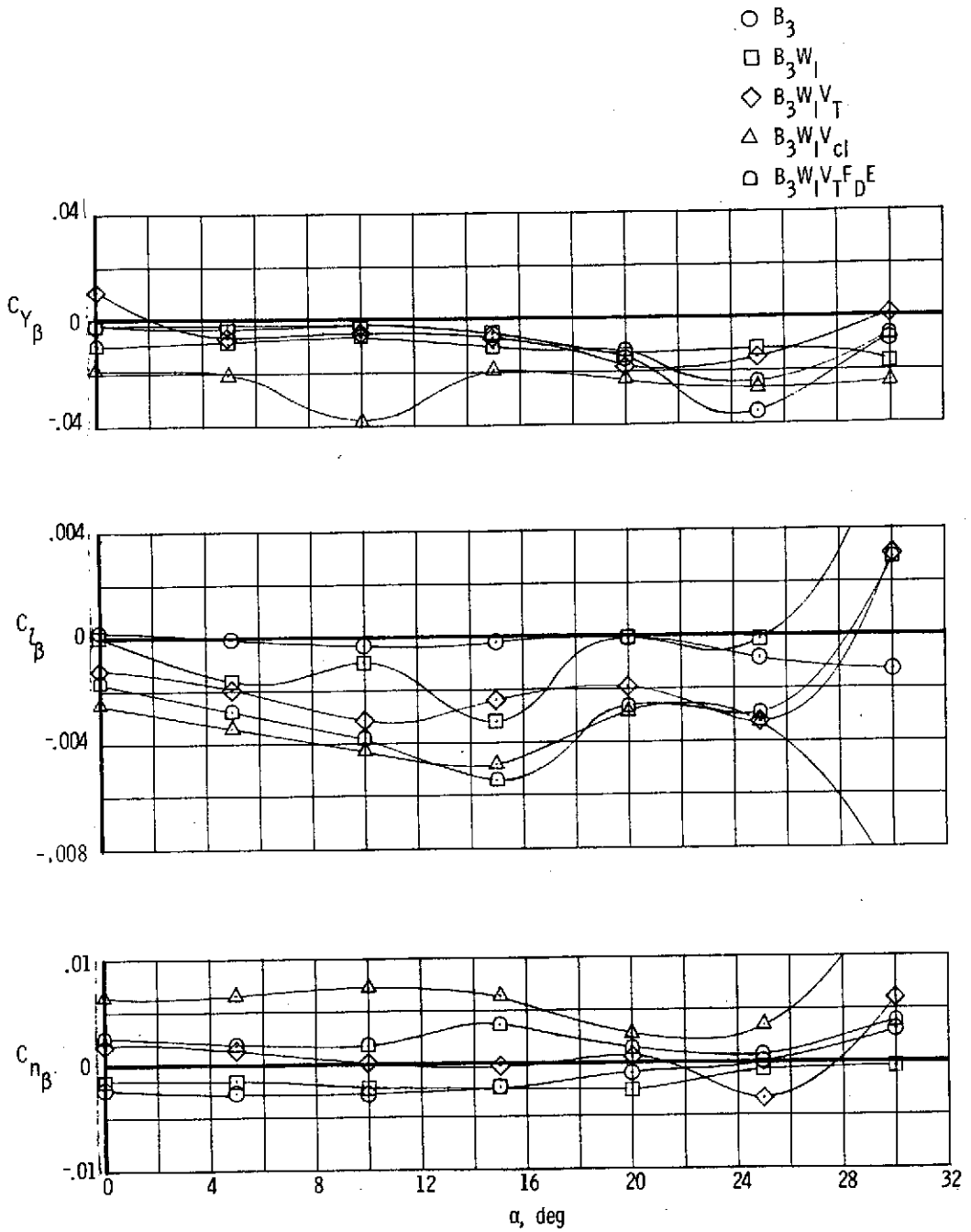

(c) Body 3

Figure 19.- Continued.

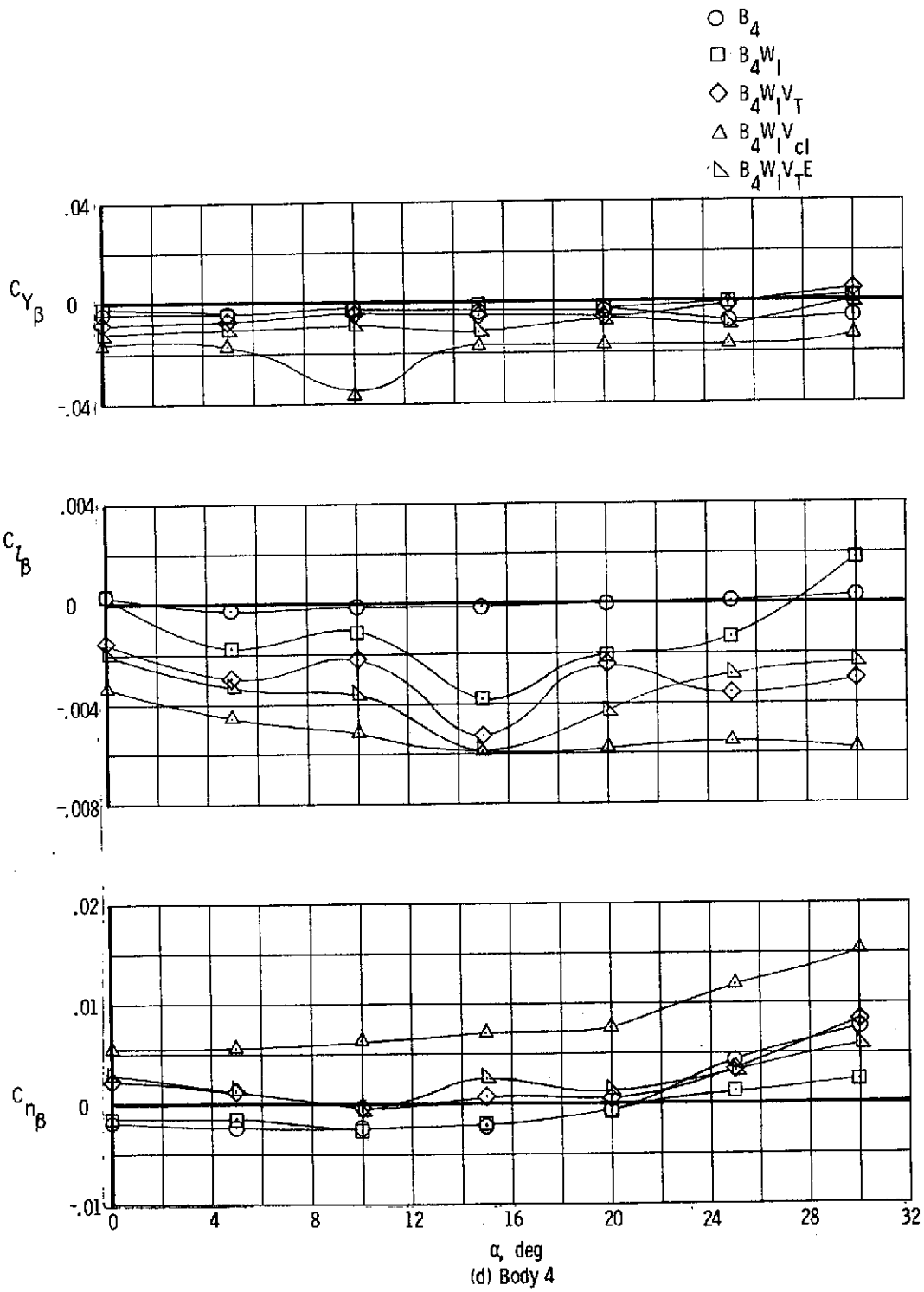

(d) Body 4

Figure 19. - Concluded.